ISSN 1063-7796, Physics of Particles and Nuclei, 2012, Vol. 43, No. 2, pp. 147–186. © Pleiades Publishing, Ltd., 2012.
Original Russian Text © L.I. Galanina, N.S. Zelenskaya, 2012, published in Fizika Elementarnykh Chastits i Atomnogo Yadra, 2012, Vol. 43, No. 2.

Mechanisms of Sequential Particle Transfer and Characteristics of Light Neutron-Excess and Oriented Nuclei

L. I. Galanina and N. S. Zelenskaya

Skobeltsyn Institute of Nuclear Physics, Moscow State University, Moscow, 119991 Russia
e-mail: galanina@nsrd.sinp.msu.ru

Abstract—The procedure for evaluating the second-order corrections to the matrix elements of the reaction $A(x, y)B$, which are obtained using the method of distorted waves with a finite radius of intercluster interaction (DWBAFR), is developed. It is based on the assumption of a virtual cluster structure of light nuclei and uses integral equations for a four-body problem in the Alt–Grassberger–Sandhas formalism. These corrections are related with the mechanisms of sequential particles transfer. The latter are represented by the quadrangle diagrams. Their matrix elements are summed up coherently with those given by the pole and triangle diagrams which were calculated by using DWBAFR. The computer code QUADRO is written for the numerical implementation of the method proposed. The statistical tensors of nucleus B formed in the reaction $A(x, y)B$ at incident particle energies of about 10 MeV/nucleon in the center of mass frame are determined. Specific calculations allowed for description of both the experimental cross sections (0-rank statistical tensors) of various reactions (including those where nucleus B has some excess neutrons) and polarized characteristics of nucleus B^* (in the case of the latter produced in the exited state). A two-neutron periphery of nuclei ^{6}He, ^{10}Be, ^{12}B (both in dineutron and cigarlike configurations) is restored by analyzing the differential cross sections of elastic alpha-^{6}He-scattering and ^{9}Be$(d, p)^{10}$Be and ^{10}B$(t, p)^{12}$B reactions. It is shown that the structure of neutron peripheries is fundamentally different for these nuclei and its feature depends on the way those neutron-excess nuclei are formed: in ^{6}He both configurations contribute to a two-neutron halo, while in ^{10}Be there is a barely noticeable one–neutron halo, and in ^{12}B there is a "dineutron skin". Orientation characteristics of nuclei B^* are calculated. Their comparison with experimental data made it possible to draw important conclusions about a contribution to the statistical tensors of nucleus B^* coming from the two-step mechanisms and its impact on the properties of oriented light nuclei, including their polarization. Finally, a simplified method for calculating the matrix elements of mechanisms, which take into account sequential particle transfer, is proposed. It is demonstrated to be correct by evaluating a contribution of the corresponding corrections to the total amplitude of the reaction.

DOI: 10.1134/S1063779612020049

INTRODUCTION

While considering a complicated problem of nuclear interaction taking place in the binary reaction $A(x, y)B$, a multinucleon nuclear system is generally reduced to the relatively simple few-body system. Such a simplified analysis for light nuclei is justified by clustering effects, caused by the Majorana exchange forces [1] in nucleon–nucleon interaction. Here, the clusters (d, t, ^{3}He, α, and protons and neutrons in some problems) inside a nucleus are only virtual formations. The probability of their existence in a particular nuclear state is determined by the nuclear structure.

An effective synthesis of the Faddeev integral equation formalism [2] for a three-body system and models that take into account a nuclear structure [1] led to the development of a consistent method of distorted waves with finite radius of interaction (DWBAFR) [3, 4]. DWBAFR considers one-step reaction mechanisms related with the dissociation of one of initial nuclei to two virtual clusters followed by particle rearrangement. In those cases when no adequate description of the process in the context of the three-body approximation is available, it is necessary to use the four-body approximation [5, 6]. In a four-body system there are two types of channels for binary reactions: channels of the type (3,1) corresponding to relative motion of one of particles and a three-particle cluster; and those of the type (2,2), which describe relative motion of two two-particle clusters. In general, we restrict ourselves to considering those reactions, which are channels of the type (3,1) in the initial and final states.

This review is concerned with a method developed to take into account those corrections to DWBAFR, which are associated with breakup of virtual clusters and independent sequential particle transfer. In the next section, the reaction $A(x, y)B$ is considered in the context of the four-body approximation, thus giving a chance to obtain analytical expressions for the amplitudes of two-step mechanisms, which are in fact second-order corrections to DWBAFR. In Sec. 2, physical criteria for the implementation of such mechanisms are obtained and the types of reactions, in which these mechanisms are most likely realized, are found.

Section 3 gives a general formalism for calculating the matrix elements of two-step mechanisms and describes the structure of QUADRO code that implements this formalism. The results of calculations of the cross sections for a number of specific reactions are given in Sec. 4. On the base of the results obtained, a spatial configuration of the neutron periphery in light nuclei with two excess neutrons (^{6}He, ^{10}Be, ^{12}B) is studied in Sec. 5. It is shown to fundamentally differ in these nuclei and its dependence on how a neutron-excess nucleus is formed is demonstrated. In Sec. 6, formulas for calculating the statistical tensors of nucleus B^*, formed in the reaction $A(x, y)B^*$, are obtained, orientation characteristics of some light oriented nuclei are calculated and compared with experimental data, and important conclusions about the impact of two-step mechanisms on the orientation characteristics are drawn. A simplified method for calculating the contribution of mechanisms, which take into account sequential particle transfer, is proposed in Sec. 7. In the concluding section, the results obtained are summarized and those aspects of the nuclear structure, in which two-step mechanisms become most clearly apparent, are discussed.

1. DWBAFR AND ITS CORRECTIONS IN THE CONTEXT OF A FOUR-BODY PROBLEM

Consider the reaction $A(x, y)B$ as an idealized problem of interaction of four virtual particles. Let us use notation from [7], where "elementary" particles are labeled by roman letters i, j, x, y (in our case these are protons, neutrons, deuterons, tritium and helium nuclei). The lowercase Greek letters α, β, γ denote three-particle channels and corresponding two-particle clusters. The capital roman letters A, B, C denote binary channels of the type (3,1) and respective three-particle clusters (i.e., sets of three elementary particles that feature bound states). Binary channels of the type (2,2) will be denoted by the letter F. The two-particle clusters of channels (2,2) will be labeled by the letters ρ and σ.

Let us consider the reaction $A(x, y)B$, in which a system proceeds from an initial $A = \underbrace{(ijy)}_{A} + x$ to a final $B = \underbrace{(ijx)}_{B} + y$ state. Such an approach corresponds to the transfer of two particles (ij) from three-particle cluster A to a particle x. The case when these two particles bind to form a virtual cluster are transferred as a whole, reduces to the three-body approximation. In other words, the one-step mechanisms embodied in DWBAFR correspond to the first terms of iterative series of integral equations for a four-body problem. The subsequent terms of iterative series stem from breakup of this pair and independent transfer of particles i and j.

Let us prove this latter statement by using the Alt–Grassberger–Sandhas method (AGS) [6] developed for the scattering amplitudes in a four-body system. It is based on a consistent reduction from a four-body system down to those of three and two bodies.

Let us write down the total Hamiltonian for four bodies in their center-of-mass frame:

$$\mathbf{H} = \mathbf{H}_0 + \mathbf{V}, \tag{1}$$

where $\mathbf{V} = V_{ij} + V_{iy} + \mathrm{V_{jy}} + V_{ix} + V_{yx} + V_{jx}$ is a complete two-particle interaction in a system, and $\mathbf{H}_0$ stands for a kinetic energy operator.

At the first stage of the reduction let us consider a system transiting from three-particle channel α to three-particle channel β. The indices α, β can assume the values (ij), (ix), (iy), (jx), (jy), (xy). In addition to the total Hamiltonian (1) we introduce the channel Hamiltonians $\mathbf{H}_\alpha = \mathbf{H}_0 + V_\alpha$, respective Green's functions $\mathbf{g}_\alpha = (\mathbf{H}_\alpha - E)^{-1}$ (E is the total energy of a four-body system), and eigenfunctions $|\phi_\alpha\rangle$. The operator, describing a transition from α to β channel in a four-body system, satisfies the Faddeev–Yakubovsky type equation [5]:

$$\mathbf{U}_{\beta\alpha} = -(1 - \delta_{\beta\alpha})(\mathbf{H}_0 - E) - \sum_{\lambda\neq\beta} \mathbf{T}_\lambda \mathbf{g}_0 \mathbf{U}_{\lambda\alpha}, \tag{2}$$

where $\mathbf{g}_0 = (\mathbf{H}_0 - E)^{-1}$, $\mathbf{T}_\lambda$ are two-particle transition operators which are determined by the equation $\mathbf{T}_\lambda = V_\lambda - V_\lambda \mathbf{g}_\lambda V_\lambda$.

Using the Weinberg–Schmidt quasiparticle method [8, 9], divide the two-particle matrices into separable part, including bound states and resonances of the cluster λ, and a nonseparable component:

$$\mathbf{T}_\lambda = -\sum_l |\lambda l\rangle \mathbf{t}^{\lambda l} \langle \lambda l| + \mathbf{T}'_\lambda. \tag{3}$$

Define $\mathbf{U}'_{\beta\alpha}$ as part of the complete transition operator $\mathbf{U}_{\beta\alpha}$ that satisfies an equation similar to (2):

$$\mathbf{U}'_{\beta\alpha} = -(1 - \delta_{\beta\alpha})(\mathbf{H}_0 - E) - \sum_{\lambda\neq\beta} \mathbf{T}'_\lambda \mathbf{g}_0 \mathbf{U}'_{\lambda\alpha}. \tag{4}$$

Then, for the operator $\mathbf{U}_{\beta\alpha}$ we obtain an equation analogous to the Faddeev one in a three-particle system, where the role of two-particle $\mathbf{T}$-matrices is played by the generalized potential—$\mathbf{U}'_{\beta\alpha}$ operator:

$$\mathbf{U}_{\beta\alpha} = \mathbf{U}'_{\beta\alpha} - \sum_{\lambda\neq\beta} \sum_l \mathbf{U}'_{\beta\lambda}\, \mathbf{g}_0 |\lambda l\rangle \mathbf{t}^{\lambda l} \langle \lambda l| \mathbf{g}_0 \mathbf{U}_{\lambda\alpha}. \tag{5}$$

Now, average the operators $\mathbf{U}_{\beta\alpha}$ and $\mathrm{U}'_{\beta\alpha}$ over the functions $\mathbf{g}_0|\alpha m\rangle$ and $\mathbf{g}_0|\beta n\rangle$, where $|\alpha m\rangle$ and $|\beta n\rangle$

are form factors of the corresponding bound states, and denote

$$(\bar{\mathbf{G}}_0)^{\beta\alpha} = \mathbf{t}^{\alpha m}\delta_{\beta n,\alpha m}$$
$$(\bar{\mathbf{V}})^{\beta\alpha} = \langle\beta n|\mathbf{g}_0\mathbf{U}'_{\beta\alpha}\mathbf{g}_0|\alpha m\rangle, \quad (6)$$
$$(\bar{\mathbf{T}})^{\beta\alpha} = \langle\beta n|\mathbf{g}_0\mathbf{U}_{\beta\alpha}\mathbf{g}_0|\alpha m\rangle.$$

The operator $(\bar{\mathbf{T}})^{\beta\alpha}$ coincides with the operator corresponding to the transition from α to β states, if the form factors $|\alpha m\rangle$ and $|\beta n\rangle$ are taken in the form: $|\alpha m; E = \varepsilon_{\alpha m}\rangle = -V_\alpha|\phi_{\alpha m}\rangle$ and $|\beta n; E = \varepsilon_{\beta n}\rangle = -V_\beta|\phi_{\beta n}\rangle$, where $|\phi_{\alpha m}\rangle, |\phi_{\beta n}\rangle$ are eigenfunctions of α and β channels. Equation (5) can be written in the operator form

$$\bar{\mathbf{T}} = \bar{\mathbf{V}} - \bar{\mathbf{V}}\bar{\mathbf{G}}_0\bar{\mathbf{T}}, \quad (7)$$

which formally coincides with a three-particle Lippmann–Schwinger equation. As a matter of fact, Eq. (7) defines a transition operator in a system of three particles, with one of the latter being a bound two-particle cluster (Green's function describes the free motion of a two-particle cluster and two remaining particles).

At the next stage of the reduction in the AGS method, they proceed to two-particle virtual channels of the type (3,1) and (2,2). In a considered system of four particles *i*, *j*, *x*, *y*the following two-particle channels are possible:

$A = (ijy) + x$; $B = (ijx) + y$; $C_1 = (jxy) + i$; $C_2 = (ixy) + j$—channels of the type (3,1);

$F_1 = (ij) + (xy)$, $F_2 = (ix) + (jy)$, $F_3 = (jx) + (iy)$—channels of the type (2,2).

A reference frame corresponding to different channels in the reaction $A(x, y)B$ is depicted in Fig. 1.

The generalized potential elements are represented via an internal interaction, which forms a three-particle or a couple of two-particle clusters, and external one:

$$(\bar{\mathbf{V}})^{\beta\alpha} = \sum_{Z=C,\,F}\bar{\mathbf{V}}_Z^{\beta\alpha} + \bar{\mathbf{V}}_{out}^{\beta\alpha}.$$

The interaction $\bar{\mathbf{V}}_Z^{\beta\alpha}$ (or $\mathbf{U}'_{\beta\alpha,z}$ according to (6)) in the channel (3,1) satisfies an equation similar to (4), provided only three internal interactions, which form a *Z* cluster, are taken into account:

$$\mathbf{U}'_{\alpha\beta;Z} = -(1-\delta_{\alpha\beta})(\mathbf{H}_0 - E) - \sum_{\substack{\lambda\neq\beta,\\ \lambda\in Z}}\mathbf{T}'_\lambda\mathbf{g}_0\mathbf{U}'_{\lambda\beta,Z}. \quad (8)$$

Define now a "free three-body" Hamiltonian $\bar{\mathbf{H}}_0 = \left(\bar{\mathbf{G}}_0^{-1} + E\mathbf{I}\right)$, channel "Hamiltonians" $\bar{\mathbf{H}}_C = \bar{\mathbf{H}}_0 + \bar{\mathbf{V}}_C$ and their eigenfunctions $\bar{\mathbf{H}}_C|\Psi_C\rangle = E_C|\Psi_C\rangle$, where $|\Psi_C\rangle$ is a column of three elements $\left|\Psi_C^{\alpha m}\right\rangle, \alpha\in C$. Introduce "two-particle"

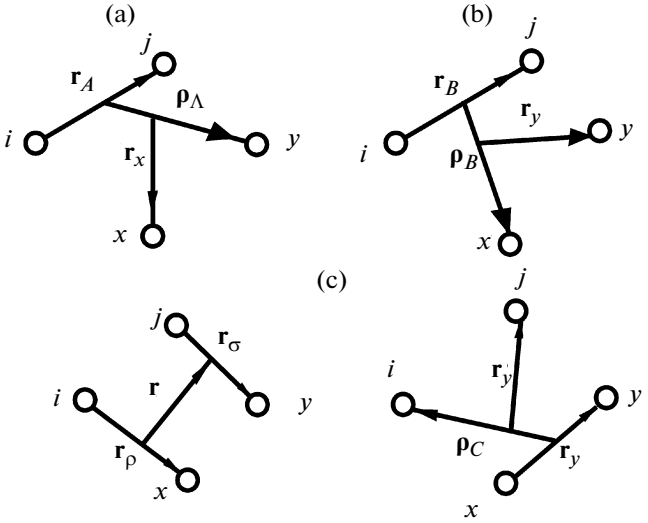

Fig. 1. A reference frame for a four-body problem in the initial (a), final (b), and virtual (c) channels (2,2) and (3,1) of the reaction $A(x, y)B$.

$\bar{\mathbf{T}}_C$-matrices: $\bar{\mathbf{T}}_C = \bar{\mathbf{V}}_C - \bar{\mathbf{V}}_C\bar{\mathbf{G}}_0\bar{\mathbf{T}}_C$, where $\bar{\mathbf{V}}_C$ denotes an interaction that binds a three-particle cluster and is defined by Eqs. (6) and (8).

By once again applying the quasiparticle method, we divide matrices into separable and non-separable parts:

$$\bar{\mathbf{T}}_C = -\sum_\eta|C\eta\rangle\bar{\mathbf{T}}_C^s\langle C\eta| + \bar{\mathbf{T}}'_C. \quad (9)$$

where $\bar{\mathbf{T}}_C^s(E) = \dfrac{1}{E_{C\eta} - E}$ corresponds to a "free two-particle propagator" and describes the motion of a fourth particle with respect to a bound system *C*.

As we have done at the first stage of the reduction, let us further introduce

$$\bar{\mathbf{U}}'^{BA} = -(1-\delta_{BA})(\bar{\mathbf{H}}_0 - E) - \sum_{Z\neq B}\bar{\mathbf{T}}'_C\bar{\mathbf{G}}_0\bar{\mathbf{U}}'^{ZA}. \quad (10)$$

Then, for the operator $\bar{X}^{BA} = \sum_{\beta\alpha}\left\langle\begin{matrix}B\\ \beta n\end{matrix}\middle|\left(\bar{\mathbf{G}}_0\bar{\mathbf{U}}^{BA}\bar{\mathbf{G}}_0\right)^{\beta\alpha}\middle|\begin{matrix}A\\ \alpha m\end{matrix}\right\rangle$ that gives the on-energy-shell operator for a transition from *A* to *B* channel, we find the equation

$$\bar{\mathbf{X}}^{BA} = \bar{\mathbf{Z}}^{BA} - \sum_{Z\neq B}\bar{\mathbf{Z}}^{BZ}\bar{\mathbf{T}}_Z^s\bar{\mathbf{X}}^{ZA}. \quad (11)$$

In (11) $\bar{\mathbf{Z}}^{BA}$ represents a generalized potential:

$$\bar{\mathbf{Z}}^{BA} = \sum_{\beta\alpha}\left\langle\begin{matrix}B\\ \beta n\end{matrix}\middle|\left(\bar{\mathbf{G}}_0\bar{\mathbf{U}}'^{BA}\bar{\mathbf{G}}_0\right)^{\beta\alpha}\middle|\begin{matrix}A\\ \alpha m\end{matrix}\right\rangle.$$

Equation (11) relates the scattering operators $\bar{\mathbf{X}}^{AA}$ and $\bar{\mathbf{X}}^{BB}$ in entrance and exit channels of the reaction $A(x, y)B$ with the transition operators $\bar{\mathbf{X}}^{BA}$. In [4, 10] it is shown that these equations can be transformed to take the form similar to DWBAFR:

$$\bar{\mathbf{X}}^{BA} = (1 + \bar{\mathbf{X}}^{BB}\mathbf{T}_B^s)\bar{\mathbf{Z}}^{BA}(1 + \mathbf{T}_A^s\bar{\mathbf{X}}^{AA}) + \mathbf{R}, \qquad (12)$$

where a remainder $\mathbf{R}$ contains the terms with at least triple rearrangements of a four-body system, which are neglected in specific calculations. In relationship (12) the term $(1 + \mathbf{T}_A^s\bar{\mathbf{X}}^{AA})\left\{(1 + \bar{\mathbf{X}}^{BB}\mathbf{T}_B^s)\right\}$ is an operator that takes a plane wave of the relative motion of particles in initial (final) channels of the reaction into a distorted one $\chi_x^{(+)}(\mathbf{p}_x\mathbf{r}_x)\left\{\chi_y^{(-)}(\mathbf{p}_y\mathbf{r}_y)\right\}$, while $\bar{\mathbf{Z}}^{BA}$ can be viewed as an interaction operator that defines transition of a system from initial to final channel. Thus,

$$\bar{\mathbf{X}}^{BA} \approx \left\langle \chi_y^{(-)}(\mathbf{p}_y\mathbf{r}_y)\varphi_y \right| \times \sum_{\beta\alpha} \left\langle \begin{matrix} B \\ \beta n \end{matrix} \right| \left(\bar{\mathbf{G}}_0\,\bar{\mathbf{U}}'^{BA}\,\bar{\mathbf{G}}_0\right)^{\beta\alpha} \left| \begin{matrix} A \\ \alpha m \end{matrix} \right\rangle \left| \varphi_x\chi_x^{(+)}(\mathbf{p}_x\mathbf{r}_x) \right\rangle, \qquad (13)$$

where $\varphi_x\,(\varphi_y)$ is an internal function of particle x (y).

Let the form factors of initial and final nuclei in (13) correspond to the bound states of nuclei A and B:

$$\left| \begin{matrix} A \\ \alpha m \end{matrix} \right\rangle = \bar{\mathbf{G}}_0{}^{-1}\Psi_A^{\alpha m}; \quad \left| \begin{matrix} B \\ \beta n \end{matrix} \right\rangle = \bar{\mathbf{G}}_0{}^{-1}\Psi_B^{\beta n}. \qquad (14)$$

Then,

$$\bar{\mathbf{X}}^{BA} \approx \left\langle \chi_y^{(-)}(\mathbf{p}_y\mathbf{r}_y)\varphi_y \right| \times \sum_{\beta\alpha} \left\langle \Psi_B^{\beta n} \right| \left(\mathbf{U}'^{BA}\right)^{\beta\alpha} \left| \Psi_A^{\alpha m} \right\rangle \left| \varphi_x\chi_x^{(+)}(\mathbf{p}_x\mathbf{r}_x) \right\rangle \qquad (15)$$

Since $\bar{\mathbf{U}}'^{BA}$ contains only non-separable parts of T-matrices, we can approximate $\bar{\mathbf{U}}'^{BA}$ by iterating Eq. (10) [6]. Two first iterations of this equation yield $\bar{\mathbf{U}}'^{BA} = -\bar{\mathbf{G}}_0^{-1} - \sum_{Z\neq B,A}\bar{\mathbf{T}}'$. Substitute this expression into (15). The transition operator assumes the form:

$$\bar{\mathbf{X}}^{BA} \approx \sum_{\beta\alpha}\left\{-\left\langle \chi_y^{(-)}(\mathbf{p}_y\mathbf{r}_y)\cdot\varphi_y \right| \left\langle \Psi_B^{\beta n} \right| \left(\bar{\mathbf{G}}_0^{-1}\right)^{\beta\alpha} \left| \Psi_A^{\alpha m} \right\rangle \times \left| \varphi_x\cdot\chi_x^{(+)}(\mathbf{p}_x\mathbf{r}_x) \right\rangle + \left\langle \chi_y^{(-)}(\mathbf{p}_y\mathbf{r}_y)\cdot\varphi_y \right| \times \left\langle \Psi_B^{\beta n} \right| \sum_{Z\neq B,A} \left(\bar{\mathbf{T}}_Z\right)^{\beta\alpha} \left| \Psi_A^{\alpha m} \right\rangle \left| \varphi_x\cdot\chi_x^{(+)}(\mathbf{p}_x\mathbf{r}_x) \right\rangle \right\} \qquad (16)$$

Taking into account that the following conditions should be fulfilled for indices α and β, $\begin{cases}\alpha\in A\\ \alpha\in Z\end{cases}$ and $\begin{cases}\beta\in B\\ \beta\in Z\end{cases}$, only the following terms in sums taken over α and β remain in (16):

$$\begin{aligned}\bar{\mathbf{X}}^{BA} \approx\ & \underbrace{\left\langle \chi_y^{(-)}(\mathbf{p}_y\mathbf{r}_y)\cdot\varphi_y \right| \left\langle \Phi_B^{ij} \right| \left(\bar{\mathbf{G}}_0{}^{-1}\right)^{ij} \left| \Psi_A^{ij} \right\rangle \left| \varphi_x\cdot\chi_x^{(+)}(\mathbf{p}_x\mathbf{r}_x) \right\rangle}_{M_{BA}^0} + \underbrace{\left\langle \chi_y^{(-)}(\mathbf{p}_y\mathbf{r}_y)\cdot\varphi_x \right| \left\langle \psi_B^{ij} \right| \left(\mathbf{T}'_{F_{1=(ij)(xy)}}\right)^{ij,ij} \left| \psi_A^{ij} \right\rangle \left| \varphi_x\cdot\chi_x^{(+)}(\mathbf{p}_x\mathbf{r}_x) \right\rangle}_{M_{BA}^{F_1}} \\ & + \underbrace{\left\langle \chi_y^{(-)}(\mathbf{p}_y\mathbf{r}_y)\cdot\varphi_y \right| \left\langle \Psi_B^{ix} \right| \left(\mathbf{T}'_{F_{2=(ix)(jy)}}\right)^{ix,jy} \left| \Psi_A^{jy} \right\rangle \left| \varphi_x\cdot\chi_x^{(+)}(\mathbf{p}_x\mathbf{r}_x) \right\rangle}_{M_{BA}^{F_2}} + \underbrace{\left\langle \chi_y^{(-)}(\mathbf{p}_y\mathbf{r}_y)\cdot\varphi_y \right| \left\langle \Psi_B^{jx} \right| \left(\mathbf{T}'_{F_{3=(jx)(iy)}}\right)^{jx,iy} \left| \Psi_A^{iy} \right\rangle \left| \varphi_x\cdot\chi_x^{(+)}(\mathbf{p}_x\mathbf{r}_x) \right\rangle}_{M_{BA}^{F_3}} \\ & + \underbrace{\left\langle \chi_y^{(-)}(\mathbf{p}_y\mathbf{r}_y)\cdot\varphi_y \right| \left\langle \Psi_B^{ix} \right| \left(\mathbf{T}'_{C_{2=(jxy)}}\right)^{ix,iy} \left| \Psi_A^{iy} \right\rangle \left| \varphi_x\cdot\chi_x^{(+)}(\mathbf{p}_x\mathbf{r}_x) \right\rangle}_{M_{BA}^{C_1}} + \underbrace{\left\langle \chi_y^{(-)}(\mathbf{p}_y\mathbf{r}_y)\cdot\varphi_y \right| \left\langle \Psi_B^{jx} \right| \left(\mathbf{T}'_{C_{2=(jxy)}}\right)^{jx,jy} \left| \Psi_A^{jy} \right\rangle \left| \varphi_x\cdot\chi_x^{(+)}(\mathbf{p}_x\mathbf{r}_x) \right\rangle}_{M_{BA}^{C_2}}. \end{aligned} \qquad (17)$$

Let us transform the terms in expression (17).

(1) Term M_{BA}^0. The operator $\bar{\mathbf{G}}_0^{ij}$ was defined as $\left(\bar{\mathbf{G}}_0\right)^{ij} = t^{ij} = \dfrac{1}{E_{ij} - E} + \ldots$, which is a "free" Hamiltonian in a three-body system $\lambda = (ij)$, $x$and y. Considering that $\left(\bar{\mathbf{G}}_0^{-1}\right)^{ij}\left|\Psi_A^{ij}\right\rangle = -\bar{\mathbf{V}}_A^{ij}\left|\Psi_A^{ij}\right\rangle$ and, according to (8), $\bar{\mathbf{V}}_A^{ij} = -\sum_{\gamma\neq ij}\mathbf{T}'_\gamma = -V_{ij,y}$ we find for M_{BA}^0:

$$M_{BA}^0 = \left\langle \chi_y^{(-)}(\mathbf{p}_y\mathbf{r}_y)\cdot\varphi_y \right| \left\langle \Psi_B^{ij} \right| V_{ij,y} \left| \Psi_A^{ij} \right\rangle \left| \varphi_x\cdot\chi_x^{(+)}(\mathbf{p}_x\mathbf{r}_x) \right\rangle. \qquad (18)$$

(2) The term $M_{BA}^{F_1}$ for F-type channels with two-particle virtual clusters we transform by using Eq. (8):

$$\left(\mathbf{T}'_{F_1=ij,xy}\right)^{ij,ij} = \mathbf{U}'_{ij,ij;F_1=ij,xy} = -\mathbf{T}'_{xy} \approx -V_{xy}.$$

In further calculations, the generalized potentials with real parts defined in the framework of a three-body problem will be used instead of $\mathbf{T}'$-matrices. A detailed discussion on whether such an exchange is legitimate is given in [4].

Then,

$$M_{BA}^{F_1} = \left\langle \chi_y^{(-)}(\mathbf{p}_y\mathbf{r}_y)\cdot\varphi_y \right| \left\langle \Psi_B^{ij} \right| V_{xy} \left| \Psi_A^{ij} \right\rangle \left| \varphi_x\cdot\chi_x^{(+)}(\mathbf{p}_x\mathbf{r}_x) \right\rangle. \qquad (19)$$

(3) In order to compute two other terms $M_{BA}^{F_2}$, $M_{BA}^{F_3}$ for F-type channels let us write down the matrix elements $\left(\bar{\mathbf{T}}'_{F_2=ix,jy}\right)^{ix,jy}$ and $\left(\bar{\mathbf{T}}'_{F_3=jx,iy}\right)^{jx,iy}$ following [7]:

$$\left(\bar{\mathbf{T}}'_{F_2=ix,jy}\right)^{ix,jy} = -g_0^{-1} - T'_{jy}g_{ix,jy}T'_{ix},$$

$$\left(\bar{\mathbf{T}}'_{F_3=ix,jy}\right)^{ix,jy} = -g_0^{-1} - T'_{iy}g_{jx,iy}T'_{jx}.$$

As a result, the term for a F_2-type channel is found to be of the following form:

$$M_{BA}^{F_2} = -\left\langle\chi_y^{(-)}(\mathbf{p}_y\mathbf{r}_y)\cdot\varphi_y\left|\left\langle\Psi_B^{ix}\left|g_0^{-1}\right|\Psi_A^{jy}\right\rangle\right|\varphi_x\cdot\chi_x^{(+)}(\mathbf{p}_x\mathbf{r}_x)\right\rangle \tag{20}$$

$$-\left\langle\chi_y^{(-)}(\mathbf{p}_y\mathbf{r}_y)\cdot\varphi_y\left|\left\langle\Psi_B^{ix}\left|T'_{jy}g_{ix,jy}T'_{ix}\right|\Psi_A^{jy}\right\rangle\right|\varphi_x\cdot\chi_x^{(+)}(\mathbf{p}_x\mathbf{r}_x)\right\rangle.$$

The operator g_0 in the first term of (20) is defined in space of eigenfunctions of four interacting particles, which are orthogonal to eigenfunctions of both initial and final channels so that the first term in (20) turns to zero. Therefore, Eq. (20) reduces to the form

$$M_{BA}^{F_2} = -\left\langle\chi_y^{(-)}(\mathbf{p}_y\mathbf{r}_y)\cdot\varphi_y\right| \times \left\langle\Psi_B^{ix}\left|T'_{jy}g_{ix,jy}T'_{ix}\right|\Psi_A^{jy}\right\rangle\left|\varphi_x\cdot\chi_x^{(+)}(\mathbf{p}_x\mathbf{r}_x)\right\rangle. \tag{21a}$$

The term for the F_3-type channel transforms analogously:

$$M_{BA}^{F_3} = -\left\langle\chi_y^{(-)}(\mathbf{p}_y\mathbf{r}_y)\cdot\varphi_y\right| \times \left\langle\Psi_B^{jx}\left|T'_{iy}g_{jx,iy}T'_{jx}\right|\Psi_A^{iy}\right\rangle\left|\varphi_x\cdot\chi_x^{(+)}(\mathbf{p}_x\mathbf{r}_x)\right\rangle. \tag{21b}$$

(4) The terms $M_{BA}^{C_1}$, $M_{BA}^{C_2}$ for C-type channels transform by using the following definitions:

$$\bar{\mathbf{T}}'_{C_i} = \bar{\mathbf{V}}_{C_i} - \bar{\mathbf{V}}_{C_i}\bar{\mathbf{G}}_{C_i}\bar{\mathbf{V}}_{C_i};$$

$$\bar{\mathbf{V}}_{C_1} = \mathbf{V}_{(iy),x} = \mathbf{V}_{(ix),y};\ \bar{\mathbf{V}}_{C_2} = \mathbf{V}_{(jy),x} = \mathbf{V}_{(jx),y}.$$

Then, for the term $M_{BA}^{C_1}$ one obtains the expression

$$M_{BA}^{C_1} = \left\langle\chi_y^{(-)}(\mathbf{p}_y\mathbf{r}_y)\cdot\varphi_y\left|\left\langle\Psi_B^{ix}\left|V_{(iy)x}\right|\Psi_A^{iy}\right\rangle\right|\varphi_x\cdot\chi_x^{(+)}(\mathbf{p}_x\mathbf{r}_x)\right\rangle - \left\langle\chi_y^{(-)}(\mathbf{p}_y\mathbf{r}_y)\cdot\varphi_y\left|\left\langle\Psi_B^{ix}\left|V_{(ix)y}\bar{\mathbf{G}}_{C_1}V_{(iy)x}\right|\Psi_A^{iy}\right\rangle\right|\varphi_x\cdot\chi_x^{(+)}(\mathbf{p}_x\mathbf{r}_x)\right\rangle. \tag{22a}$$

A similar expression is found for the term $M_{BA}^{C_2}$:

$$M_{BA}^{C_2} = \left\langle\chi_y^{(-)}(\mathbf{p}_y\mathbf{r}_y)\cdot\varphi_y\left|\left\langle\Psi_B^{jx}\left|V_{(jy)x}\right|\Psi_A^{jy}\right\rangle\right|\varphi_x\cdot\chi_x^{(+)}(\mathbf{p}_x\mathbf{r}_x)\right\rangle - \left\langle\chi_y^{(-)}(\mathbf{p}_y\mathbf{r}_y)\cdot\varphi_y\left|\left\langle\Psi_B^{jx}\left|V_{(jx)y}\bar{\mathbf{G}}_{C_2}V_{(jy)x}\right|\Psi_A^{jy}\right\rangle\right|\varphi_x\cdot\chi_x^{(+)}(\mathbf{p}_x\mathbf{r}_x)\right\rangle. \tag{22b}$$

As a result, the transition operator in (17) transforms to take the following form:

$$\bar{\mathbf{X}}^{BA} = M_{BA}^0 + M_{BA}^{F_1} + M_{BA}^{F_2} + M_{BA}^{F_3} + M_{BA}^{C_1} + M_{BA}^{C_2}, \tag{23}$$

where

$$M_{BA}^0 + M_{BA}^{F_1} = \left\langle\chi_y^{(-)}(\mathbf{p}_y\mathbf{r}_y)\cdot\varphi_y\left|\left\langle\Psi_B^{ij}\left|V_{(ij)y}\right|\Psi_A^{ij}\right\rangle\right|\varphi_x\cdot\chi_x^{(+)}(\mathbf{p}_x\mathbf{r}_x)\right\rangle + \left\langle\chi_y^{(-)}(\mathbf{p}_y\mathbf{r}_y)\cdot\varphi_y\left|\left\langle\Psi_B^{ij}\left|V_{xy}\right|\Psi_A^{ij}\right\rangle\right|\varphi_x\cdot\chi_x^{(+)}(\mathbf{p}_x\mathbf{r}_x)\right\rangle;$$

$$M_{BA}^{F_2} = -\left\langle\chi_y^{(-)}(\mathbf{p}_y\mathbf{r}_y)\cdot\varphi_y\left|\left\langle\Psi_B^{ix}\left|T'_{jy}g_{ix,jy}T'_{ix}\right|\Psi_A^{jy}\right\rangle\right|\varphi_x\cdot\chi_x^{(+)}(\mathbf{p}_x\mathbf{r}_x)\right\rangle;$$

$$M_{BA}^{F_3} = -\left\langle\chi_y^{(-)}(\mathbf{p}_y\mathbf{r}_y)\cdot\varphi_y\left|\left\langle\Psi_B^{jx}\left|T'_{iy}g_{jx,iy}T'_{jx}\right|\Psi_A^{iy}\right\rangle\right|\varphi_x\cdot\chi_x^{(+)}(\mathbf{p}_x\mathbf{r}_x)\right\rangle;$$

$$M_{BA}^{C_1} = \left\langle\chi_y^{(-)}(\mathbf{p}_y\mathbf{r}_y)\cdot\varphi_y\left|\left\langle\Psi_B^{ix}\left|V_{(iy)x}\right|\Psi_A^{iy}\right\rangle\right|\varphi_x\cdot\chi_x^{(+)}(\mathbf{p}_x\mathbf{r}_x)\right\rangle - \left\langle\chi_y^{(-)}(\mathbf{p}_y\mathbf{r}_y)\cdot\varphi_y\left|\left\langle\Psi_B^{ix}\left|V_{(ix)y}\bar{\mathbf{G}}_{C_1}V_{(iy)x}\right|\varphi_x\cdot\Psi_A^{iy}\right\rangle\right|\chi_x^{(+)}(\mathbf{p}_x\mathbf{r}_x)\right\rangle;$$

$$M_{BA}^{C_2} = \left\langle\chi_y^{(-)}(\mathbf{p}_y\mathbf{r}_y)\cdot\varphi_y\left|\left\langle\Psi_B^{jx}\left|V_{(jy)x}\right|\Psi_A^{jy}\right\rangle\right|\varphi_x\cdot\chi_x^{(+)}(\mathbf{p}_x\mathbf{r}_x)\right\rangle - \left\langle\chi_y^{(-)}(\mathbf{p}_y\mathbf{r}_y)\cdot\varphi_y\left|\left\langle\Psi_B^{jx}\left|V_{(jx)y}\bar{\mathbf{G}}_{C_2}V_{(jy)x}\right|\Psi_A^{jy}\right\rangle\right|\varphi_x\cdot\chi_x^{(+)}(\mathbf{p}_x\mathbf{r}_x)\right\rangle.$$

Consider now the physical meaning of every term involved in the expression (23).

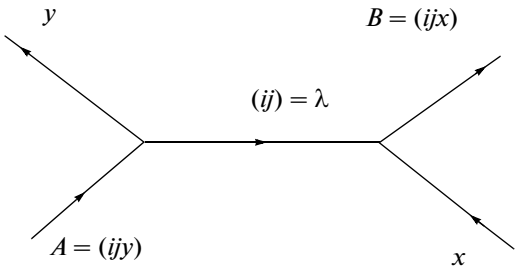

Fig. 2. A pole diagram for $(ij) = \lambda$ cluster transfer.

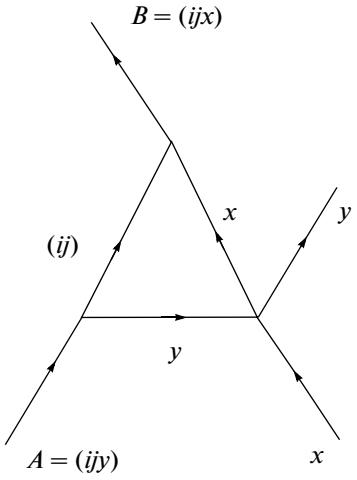

Fig. 3. A triangle diagram of the mechanism of virtual scattering of particles x and y in the field of the cluster $(ij) = \lambda$.

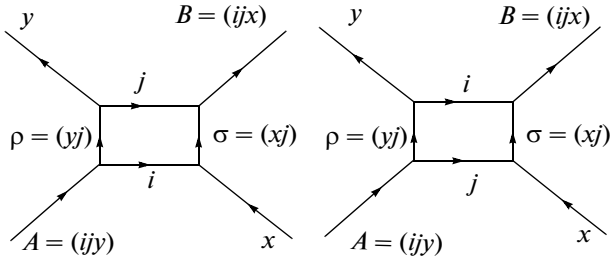

Fig. 4. Quadrangle diagrams of the independent particle transfer mechanism through virtual channel (2,2) and unidirectional internal lines.

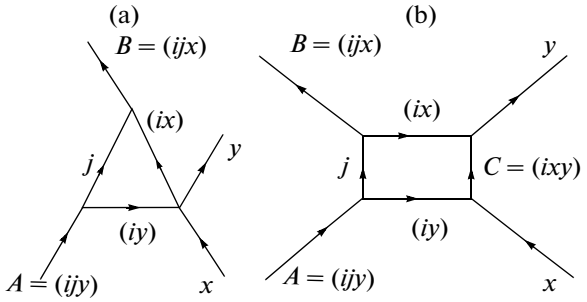

Fig. 5. Diagrams of the particle transfer mechanism through channel $C_1 = (ixy)$.

(1) The first term M^0_{BA} describes the transfer of cluster $\lambda = (ij)$ as a single particle, reduces to a three-particle approximation, is illustrated by a pole diagram shown in Fig. 2, and can be calculated in DWBAFR [4].

(2) The second term $M^{F_1}_{BA}$ describes virtual scattering of clusters x and y in the field of a bound two-particle cluster $\lambda = (ij)$, corresponds to the exchange mechanism, reduces to a three-particle approximation, is illustrated by a triangle diagram shown in Fig. 3, and can be evaluated in DWBAFR [4].

(3) The third and fourth terms $M^{F_2}_{BA}$, $M^{F_3}_{BA}$ contain transitions in the intermediate channel (2,2), correspond to the process of two-step sequential transfer of cluster (i,j), and are illustrated by the quadrangle diagrams in Fig. 4 with unidirectional internal lines.

(4) The terms of type C correspond to the transition through a virtual channel of the type (3,1), describe the rearrangement in a three-particle cluster C without interaction with a fourth particle, and consist of two parts: the first one corresponds to a first order approximation in the interaction and can be considered in DWBAFR [4], while the second one takes into account the terms of a second order in the interaction. In the case of the C_1 channel, these processes are illustrated by the tri- and quadrangle diagrams with multidirectional internal lines shown in Fig. 5. The diagrams for the C_2 channel are obtained by permuting the indices i and j.

The question arises as to what extent it is legitimate to cut off the expansions (10, 16) for the interaction operators and how strong the impact of the remaining terms is. At present, there are calculations of the characteristics of few-nucleon systems (they are discussed in [9]), which demonstrate that for a quasi-Born series similar to (16, 17), first iterations already allow for obtaining a physically significant result. The latter observation is related to the fact that the primary separable part of two-particle $\mathbf{T}_\lambda$-matrices are accounted for in the wave functions of cluster subsystems. As a result, one can do well with an iterative approximation for operators representing a nonseparable reminder of the potential $\mathbf{U}'_{\alpha\beta;C}$ given in (8).

So, the classical AGS and Weinberg–Schmidt methods let the integral equations of a four-body problem be reduced to multichannel equations, which formally coincide with two-particle Lippmann–Schwinger equations and admit iterative methods. The first terms of iterative series correspond to DWBAFR, while the next terms give corrections to the latter, fixed by breakup of virtual two-particle clusters $\lambda = (ij)$.

2. PHYSICAL CRITERIA FOR IMPLEMENTING MECHANISMS THAT INCLUDE INDEPENDENT SEQUENTIAL PARTICLE TRANSFER

Consider second order corrections to DWBAFR due to the breakup of virtual two-particle cluster λ. The terms contain transitions in virtual channel (2,2) and are illustrated by the quadrangle diagrams in Fig. 4 with unidirectional internal lines. Schematically, these processes can be represented as follows:

$$\begin{aligned}&\underbrace{(i,j,y)}_{A}+x\to(j,y)+(x,i)\to\underbrace{(x,i,j)}_{B}+y,\\&\underbrace{(i,j,y)}_{A}+x\to(y,i)+(j,x)\to\underbrace{(x,i,j)}_{B}+y.\end{aligned}\qquad(24)$$

Such type of corrections should be most important in stripping and pickup reactions of two loosely bound fragments, such as nucleons in the reaction (t, p).

The terms of the type $M_{BA}^{C_1}, M_{BA}^{C_2}$ contain transitions in intermediate channel (3,1), are schematically represented as follows:

$$\begin{aligned}&\underbrace{(i,j,y)}_{A}+x\to i+\underbrace{(x,j,y)}_{C_1}\to\underbrace{(x,i,j)}_{B}+y,\\&\underbrace{(i,j,y)}_{A}+x\to j+\underbrace{(x,i,y)}_{C_2}\to\underbrace{(x,i,j)}_{B}+y,\end{aligned}\qquad(25)$$

and are illustrated by the quadrangle diagrams with multidirectional lines (Fig. 5b). Such type of corrections can be important in stripping (pickup) reactions or scattering of composite particles.

The effects that can be interpreted as an indication of the manifestation of mechanisms, related to sequential particle transfer, were first discovered in the experiments [11] on the inelastic deuteron scattering off light nuclei. Afterwards [12-14], physical criteria for implementing such mechanisms, caused by a lack of similarity of the wave functions of transferred particles i and j, both inside a nucleus and in its peripheral region, were formulated. Indeed, if those wave functions are similar, then, they overlap substantially, the transfer of a quasi-bound two-particle cluster takes place and a four-body problem reduces to that of three bodies.

The sequential particle transfer is most likely to occur if the wave functions of particles significantly differ from each other, particularly in the peripheral region of a nucleus. In this case, even at zero orbital angular momentum of the relative motion of particles the wave-function overlap cannot be large, and a correlated two-cluster system is less likely to be constructed. As the behavior of the particle wave functions in the peripheral region of a nucleus is determined by their virtual energies, the energies of transferred particles are required to substantially differ so as to implement two-step mechanisms illustrated by diagrams shown in Fig. 4.

Let us derive an expression for the difference in energies ΔE of virtual particles i and j for the diagram depicted in Fig. 4a. To this end, we write down the energy conservation law at the vertices in the right hand side of a diagram in the laboratory frame:

$$\begin{cases}E_x+\varepsilon_{\sigma\to i+x}+E_i=E_\sigma+E_\sigma^*,\\E_\sigma+E_\sigma^*+\varepsilon_{B\to j+\sigma}+E_j=E_B+E_B^*,\end{cases}\qquad(26)$$

where E_k, $k = x, i, j, \sigma, B$ is the kinetic energy of particles, $\varepsilon_{\sigma\to i+x}(\varepsilon_{B\to j+\sigma})$ denote cluster binding energies in a respective channel of their virtual breakup, defined with a positive sign, $E_\sigma^*\left(E_B^*\right)$ are the energy of the excited state of cluster system σ (nucleus B).

From these equations an expression for the difference in energies "of elementary" particles i and j ΔE_{ij} can be derived:

$$\begin{aligned}\Delta E_{ij}&=E_i-E_j\\&=2E_\sigma+2E_\sigma^*-E_x-E_B-E_B^*-\varepsilon_{\sigma\to i+x}+\varepsilon_{B\to j+\sigma}.\end{aligned}\qquad(27a)$$

In a similar manner, an expression for ΔE_{ij} can be obtained by making use of the energy conservation law at the vertices in the left hand side of the diagram shown in Fig. 4a:

$$\Delta E_{ij}=-2E_\rho-2E_\rho^*+E_y-\varepsilon_{\rho\to j+y}+\varepsilon_{A\to i+\rho}.\qquad(27b)$$

The equality of these quantities gives the total energy conservation law in the reaction.

How are the large values of ΔE_{ij} reached in one or another reaction? In [12] the quantities ΔE_{ij} were analyzed in the stripping (pickup) reactions of loosely bound particles. It was shown that for a small difference in the binding energy of particles i and j a leading contribution to ΔE_{ij} comes from the quantity $2E_\sigma^*$-, which is a twice the energy width of the band formed by all excited states of cluster system σ (or ρ) allowed by the selection rules. Clearly, the maximum width of this band is reached while moving off the magic nuclei, which, for the light nuclei of 1p-shell, corresponds to beryllium and boron isotopes. It is not accidental that the mechanisms illustrated by the quadrangle diagrams were discovered experimentally (and explained theoretically) in the reactions with deuterons and tritons exactly on these nuclei [11–13, 15, 16].

In light heavy-ion reactions [17] the situation can be reversed; i.e., a leading contribution to ΔE_{ij} comes from the difference in binding energies $\left|\varepsilon_{\sigma\to i+x}-\varepsilon_{B\to j+\sigma}\right|\gg 2E_\sigma^*$. If $\varepsilon_{\sigma\to i+x}\geq\varepsilon_{B\to j+\sigma}$, then, the difference ΔE_{ij} decreases with E_σ^* increasing. This means that in light heavy-ion reactions, higher value of ΔE_{ij} is reached for $\varepsilon_{\sigma\to i+x}\geq\varepsilon_{B\to j+\sigma}$ and $\varepsilon_{\sigma\to i+x}\gg$

$2E_\sigma^*$; i.e., to implement mechanism of independent particle transfer highly excited states of cluster σ must be suppressed or strictly forbidden by the selection rules [14].

A contribution of diagrams with multidirectional lines (Fig. 5b) cannot be a priori estimated. It is determined by the structural features of nuclei taking part in reactions.

Theoretical calculations of the angular distributions of reaction products are carried out in [12-14] in rather rough approximations. In the first place, this concerns the usage of the plane wave approximation, Fermi pseudopotentials at interaction vertices, as well as neglect of the recoil effects. Nevertheless, even such a rough calculation showed that the most striking manifestation of two-step mechanisms is the anomalies observed in the angular distributions of reaction products, not related with the orbital angular momentum transfer. From this it follows that if the mechanism of λ cluster system transfer is either suppressed or leads to the shape of the angular distribution that contradicts qualitatively an experiment, then the contribution of two-step mechanism in a specific range of angles can be significant. Another important conclusion which can be drawn from these studies is that a mechanism of sequential particle transfer is not universal and depends critically on the nuclear structure.

In 1975—1977, a number of theoretical investigations in which the cross sections of the reactions with a two nucleon transfer for the nuclei with various atomic weight were evaluated, the distorted wave approximation with a zero interaction radius (DW) were undertaken, and taking into account delay mechanisms illustrated by diagrams shown in Fig. 4 was attempted. These studies can be divided into several groups.

The first of the latter includes [18–20], where an amplitude of the reaction (*t, p*) with stripping off two nucleons was calculated in the framework of DW as a coherent sum of one-step (a pole diagram in Fig. 2) and arbitrarily normalized two-step (the quadrangle diagram in Fig. 4) mechanisms. The calculations showed that a contribution of two-step mechanisms is relatively small except for very small angles of proton emission and varies nonmonotonically with an atomic number of the target nucleus; i.e., depends on the nuclear structure.

In a series of papers [21–24] an amplitude of the reactions with two nucleon transfer was calculated via "exact" function of these nucleons in a final nucleus. Such an approach allows for, in principle, taking into account the contribution of two-step mechanisms. However, additional assumptions, made while evaluating an "exact" function of two nucleons, actually reduced the reaction mechanism to that of the correlated nucleon pair transfer. Indeed, the wave function of interest was found by using a standard WDP-procedure of solving the Schrödinger equation given the binding energy and a number of knots [25]. In [21–23] the binding energy was taken to be equal to that of a two-nucleon cluster, while in [24], to half the binding energy of one or the other nucleon. Under such assumptions the reaction mechanism reduces, by virtue of the similarity of nucleon wave functions, to that of simultaneous stripping off a two-nucleon cluster. Analogously, the transfer of several nucleons in the inelastic scattering of *d*, *t*, ^{3}He was calculated by using the method of coupled channels [26, 27]. It is of no surprise that the corrections related with the two-step mechanisms appeared to be insignificant here as well. In [28, 29] more careful calculations of the "exact function" of two transferred nucleons are performed with introducing various virtual energies of each of them. Nonetheless, these studies also failed to achieve a satisfactory description of experimental angular distributions of protons, though a two-step mechanism of nucleon transfer was to some extent taken into account.

Thus, the physical criteria formulated—impossibility of carrying out simultaneous transfer of a cluster system due to a lack of similarity of the wave functions of transferred "elementary" particles—turn out to be very important for implementing two-step mechanisms. Simplified theoretical approaches that do not take into account the differences in the wave functions of these particles actually reduce the contribution of two-step mechanisms to a minimum. Moreover, none of the theoretical approaches discussed above allows obtaining an absolute value of the experimental cross sections without introducing additional normalization constants.

Nearly all theoretical calculations, which attempted at taking into account a mechanism of independent transfer of virtual particles, were done for the reactions with the transfer of two nucleons. To be able to consider more involved processes, a fundamentally different theoretical apparatus and computational capabilities are required. As a result, neither reactions with sequential nucleon transfer nor with the cluster transfer were studied in recent years.

At present, due to the rapid development of physics of nuclei, which are far away from the stability band, particularly neutron-excess nuclei, interest in the study of their structure and understanding its role in the reactions that take place on such nuclei is steadily growing. The two-nucleon transfer reactions, alongside the elastic scattering, play here a special role, for they permit one to directly examine the neutron periphery of nuclei far from the stability band. As a result, currently the problem of determining the role of mechanisms, which take into account two-step processes in the two-nucleon transfer reactions, once again becomes one of the most important issues in nuclear moderate-energy physics.

In the next section we present a theoretical apparatus that lets the second order corrections to the

DWBAFR amplitude be computed within the framework of modern theoretical models which correctly describe the nuclear structure.

3. GENERAL FORMALISM OF CALCULATING THE REACTION MATRIX ELEMENT WITH TAKING INTO ACCOUNT MECHANISMS THAT INCLUDE SEQUENTIAL PARTICLE TRANSFER

In the on-energy shell approximation of a four-body problem, the operator for transition from A to B channel is defined by the operator given in (23):

$$M_{BA}(\theta_y) = \bar{X}^{BA} \approx M^0_{BA} + M^{F_1}_{BA} + M^{F_2}_{BA} + M^{F_3}_{BA} + M^{C_1}_{BA} + M^{C_2}_{BA},$$

where $M^0_{BA}(\theta_y)$ and $M^{F_1}_{BA}(\theta_y)$ are matrix elements, corresponding to the transfer of cluster $\lambda=(i,j)$ illustrated by pole and triangle diagrams depicted in Figs. 2 and 3, while remaining terms denote matrix elements related with breakup of this virtual system and illustrated by the quadrangle diagrams shown in Figs 4a, 4b, 5b.

Now, let us derive the formulas for calculating all the terms of the matrix element $M_{BA}(\theta_y)$.

3.1. Calculation of the Matrix Element of λ-cluster Transfer

The matrix elements $M^0_{BA}(\theta_y)$ and $M^{F_1}_{BA}(\theta_y)$ of λ-cluster transfer in the three-body approximation can be computed in DWBAFR [3, 4]. Introduce notation J_n (M_n), l_n, s_n for the total angular momenta (their projections), orbital angular momenta and spins of nuclei involved in the reaction ($n = A, B, \lambda, x, y$). The matrix element in DWBAFR in the total momenta transfer representation is given by the expression [4]:

$$\begin{aligned} M^{DWBA}_{BA} &= M^0_{BA} + M^{F_1}_{BA} = (-1)^{2J_x+2J_y-J_1-M_1} \\ &\times \sum_{J_1 J_2 l} \sqrt{(2J_1+1)(2J_2+1)} \langle J_x M_x J_1 M_1 | J_B M_B \rangle \\ &\times \langle J_y M_y J_2 M_2 | J_A M_A \rangle \langle J_1 - M_1 J_2 M_2 | lm \rangle \\ &\times \sum_{\Lambda_1 \Lambda_2} \beta_{\Lambda_1 \Lambda_2 lm}(\theta_y) \cdot \Theta^{J_1 J_2}_{\Lambda_1 \Lambda_2 l}. \end{aligned} \quad (28)$$

In Eq. (28) the quantities $\Theta^{J_1 J_2}_{\Lambda_1 \Lambda_2 l}$ are structure factors associated with reduced decay widths of nuclei A and B, $\beta_{\Lambda_1 \Lambda_2 lm}(\theta_y)$ denote kinematical factors that bear all information on the reaction mechanism and depend on the angle θ_y at which final particles are emitted. By definition

$$\begin{aligned} \beta_{\Lambda_1 \Lambda_2 lm}(\theta_y) &= (-1)^{\mu_1} \langle \Lambda_1 - \mu_1 \Lambda_2 \mu_2 | lm \rangle \\ &\times \int d\mathbf{r}_x d\mathbf{r}_y \chi^{(-)*}_y(\mathbf{k}_y \mathbf{r}_y) \cdot \Psi^*_{\Lambda_1 \mu_1} \\ &\times (V_{y\lambda} + V_{xy}) \cdot \Psi_{\Lambda_2 \mu_2} \cdot \chi_x(\mathbf{k}_x \mathbf{r}_x), \end{aligned} \quad (29)$$

where Λ_1 and Λ_2 are orbital angular momenta of relative motion at the vertices of virtual decay of nuclei B (A) to cluster λ and particle x (y), $\Psi_{\Lambda\mu}$ stand for the respective wave functions of relative motion λ-x (λ-y); $\chi_x(\mathbf{k}_x \mathbf{r}_x)$, $\chi^{(-)*}_y(\mathbf{k}_y \mathbf{r}_y)$ are distorted waves of initial and final reaction channels.

Introduce a form factor of the reaction $A(x, y)B$ for the mechanisms under consideration [3, 4]:

$$\begin{aligned} f_{\Lambda_1 \Lambda_2 lm} &= \sum_{\mu_1 \mu_2} (-1)^{\mu_1} \langle \Lambda_1 \mu_1 \Lambda_2 - \mu_2 | l - m \rangle \\ &\times \Psi^*_{\Lambda_1 \mu_1} \cdot (V_{y\lambda} + V_{xy}) \cdot \Psi_{\Lambda_2 \mu_2} \\ &= \sum_{L'_x L'_y} F^{L'_x L'_y}_{\Lambda_1 \Lambda_2 l} \left\langle L'_x m'_x L'_y m'_y \middle| l - m \right\rangle \cdot Y^*_{L'_x m'_x}(\mathbf{r}) \cdot Y^*_{L'_y m'_y}(\mathbf{r}), \end{aligned} \quad (30)$$

decompose distorted waves over partial components

$$\chi_x(\mathbf{k}_x \mathbf{r}_x) = \frac{4\pi}{k_x r_x} \sum_{L_x m_x} i^{L_x} \cdot \chi_{L_x}(k_x r_x) \cdot Y^*_{L_x m_x}(\mathbf{k}_x) \cdot Y_{L_x m_x}(\mathbf{r}_x),$$

$$\begin{aligned} \chi^{(-)*}_y(\mathbf{k}_y \mathbf{r}_y) &= \chi^{(+)}_y(-\mathbf{k}_y \mathbf{r}_y) \\ &= \frac{4\pi}{k_y r_y} \sum_{L_y m_y} i^{L_y} \cdot \chi_{L_y}(k_y r_y) \cdot \underbrace{Y^*_{L_y m_y}(-\mathbf{k}_y)}_{(-1)^{L_y} Y_{L_y m_y}(\mathbf{k}_y)} \cdot Y_{L_y m_y}(\mathbf{r}_y) \\ &= \frac{4\pi}{k_y r_y} \sum_{L_y m_y} i^{-L_y} \chi_{L_y}(k_y r_y) Y_{L_y m_y}(\mathbf{k}_y) Y_{L_y m_y}(\mathbf{r}_y), \end{aligned}$$

and integrate over the angles $\Omega_{\mathbf{r}_x}$ and $\Omega_{\mathbf{r}_y}$. As a result, we obtain

$$\begin{aligned} \beta_{\Lambda_1 \Lambda_2 lm}(\theta_y) &= \frac{(4\pi)^2}{k_x k_y} \\ &\times \sum_{L_x L_y} (-1)^{\Lambda_1 + \Lambda_2 - l + m} \cdot i^{(L_x - L_y)} \cdot \langle L_x m_x L_y m_y | l - m \rangle \\ &\times Y^*_{L_x m_x}(\mathbf{k}_x) Y_{L_y m_y}(\mathbf{k}_y) \cdot \mathfrak{I}^0_{L_x L_y l}, \end{aligned} \quad (31)$$

$$\mathfrak{I}^0_{L_x L_y l} = \int \chi_{L_x}(k_x r_x) \cdot F^{L_x L_y}_{\Lambda_1 \Lambda_2 l} \cdot \chi_{L_y}(k_y r_y) \cdot r_x \cdot r_y \cdot dr_x \cdot dr_y.$$

Now, choose a reference frame with axis OZ, parallel to the incident beam. Then, taking into account that

$$\begin{aligned}&\langle L_x m_x L_y m_y | l-m\rangle \cdot Y^*_{L_x m_x}(\mathbf{k}_x)\cdot Y_{L_y m_y}(\mathbf{k}_y)\\ &= (-1)^{L_y-m_y}\sqrt{\frac{2l+1}{2L_x+1}}\cdot\langle lmL_y-m|L_x0\rangle\\ &\times\sqrt{\frac{2L_x+1}{8\pi^2}}\cdot P_{L_y-m}(\theta_y),\end{aligned}\qquad(32)$$

$P_{L_y-m}\Rightarrow(-1)^m P_{L_y|m|}$ for $m>0$, and a phase $\Lambda_1+\Lambda_2-l$ is always even (this follows from the presence of the Clebsch–Gordan coefficient with zero projections in the form factor), we finally obtain for the kinematical factors $\beta_{\Lambda_1\Lambda_2 lm}(\theta_y)$:

$$\begin{aligned}\beta_{\Lambda_1\Lambda_2 lm}(\theta_y) &= \frac{4\sqrt{2}\pi}{k_x k_y}\sum_{L_x L_y} i^{L_x+L_y}\sqrt{2l+1}\\ &\times\langle lmL_y-m|L_x0\rangle P_{L_y-m}(\theta_y)\mathfrak{I}^0_{L_x L_y l},\\ \mathfrak{I}^0_{L_x L_y l} &= \int\chi_{L_x}(k_x r_x)(\mathbf{r}_x)F^{L_x L_y}_{\Lambda_1\Lambda_2 l}\cdot\chi_{L_y}(k_y r_y)r_x\cdot r_y\cdot dr_x\cdot dr_y.\end{aligned}$$

As a result, the matrix element DWBAFR is given by the expression

$$\begin{aligned}M^{DWBA}_{BA}(\theta_y) &= (-1)^{2J_x+2J_y-J_1-M_1}\\ &\times\frac{4\sqrt{2}\pi}{k_x k_y}\sum_{J_1 J_2}\sqrt{(2J_1+1)(2J_2+1)(2l+1)}\\ &\times\langle J_x M_x J_1 M_1|J_B M_B\rangle\langle J_y M_y J_2 M_2|J_A M_A\rangle\\ &\times\langle J_1-M_1 J_2 M_2|lm\rangle\sum_{l\Lambda_1\Lambda_2}\sum_{L_x L_y} i^{L_x+L_y}\\ &\times\langle lmL_y-m|L_x0\rangle\cdot P_{L_y-m}(\theta_y)\cdot\mathfrak{I}^0_{L_x L_y l}\cdot\Theta^{J_1 J_2}_{\Lambda_1\Lambda_2 l}.\end{aligned}\qquad(33)$$

The structure factors $\Theta^{J_1 J_2}_{\Lambda_1\Lambda_2 l}$ are found via reduced widths $\tilde\Theta^{B\to\lambda+x}_{\Lambda_1 l_B l_\lambda L_1 l_x s_B s_\lambda s}$ and $\tilde\Theta^{A\to\lambda+y}_{\Lambda_2 l_A l_\lambda L_2 l_y s_A s_\lambda s_y}$ of virtual decay of nuclei B and A. In the shell model with intermediate coupling they are given by the expression [30]:

$$\begin{aligned}\Theta^{J_1 J_2}_{\Lambda_1\Lambda_2 l} &= \sum\tilde\Theta^{B\to\lambda+x}_{\Lambda_1 l_B l_\lambda L_1 l_x s_B s_\lambda s_x}\tilde\Theta^{A\to\lambda+y}_{\Lambda_2 l_A l_\lambda L_2 l_y s_A s_\lambda s_y}\\ &\times(-1)^{J_\lambda+J_2+l_x+l_y+s_x+s_y+I_1+I_2-l}(2I_1+1)(2I_2+1)(2J_\lambda+1)\\ &\times\sqrt{(2J_1+1)(2l_B+1)(2s_B+1)(2L_1+1)(2J_x+1)}\\ &\times\sqrt{(2J_2+1)(2l_A+1)(2s_A+1)(2L_2+1)(2J_y+1)}\\ &\times\begin{Bmatrix}l_\lambda & s_\lambda & J_\lambda\\ L_1 & s_x & I_1\\ l_B & s_B & J_B\end{Bmatrix}\cdot\begin{Bmatrix}l_\lambda & s_\lambda & J_\lambda\\ L_2 & s_y & I_2\\ l_A & s_A & J_A\end{Bmatrix}\\ &\times\begin{Bmatrix}\Lambda_1 & l_x & L_1\\ s_x & I_1 & J_x\end{Bmatrix}\begin{Bmatrix}J_x & \Lambda_1 & I_1\\ J_\lambda & J_B & J_1\end{Bmatrix}\begin{Bmatrix}\Lambda_2 & l_y & L_2\\ s_y & I_2 & J_y\end{Bmatrix}\\ &\times\begin{Bmatrix}J_y & \Lambda_2 & I_2\\ J_\lambda & J_A & J_2\end{Bmatrix}\begin{Bmatrix}J_1 & \Lambda_1 & J_\lambda\\ \Lambda_2 & J_2 & l\end{Bmatrix}.\end{aligned}\qquad(34)$$

For particles x, $y\le\alpha$ $l_x=l_y=0$. In reactions with x, $y\le\alpha$ Eq. (34) gets simplified upon summing up over J_λ and takes the following form:

$$\begin{aligned}\Theta^{J_1 J_2}_{\Lambda_1\Lambda_2 l} &= \sum\tilde\Theta^{B\to\lambda+x}_{\Lambda_1 l_B l_\lambda L_1 l_x s_B s_\lambda s_x}\tilde\Theta^{A\to\lambda+y}_{\Lambda_2 l_A l_\lambda L_2 l_y s_A s_\lambda s_y}\\ &\times(-1)^{-l_B-l_A-l_\lambda-s_\lambda-J_1}\\ &\times\sqrt{(2l_B+1)(2s_B+1)(2l_A+1)(2s_A+1)}\\ &\times\sqrt{(2J_1+1)(2J_2+1)}\\ &\times\begin{Bmatrix}s_\lambda & l_B & J_1\\ J_B & s_x & s_B\end{Bmatrix}\begin{Bmatrix}s_\lambda & l_A & J_2\\ J_A & s_y & s_A\end{Bmatrix}\begin{Bmatrix}l_B & l & l_A\\ \Lambda_2 & l_\lambda & \Lambda_1\end{Bmatrix}\begin{Bmatrix}l_B & l & l_A\\ J_2 & s_\lambda & J_1\end{Bmatrix}.\end{aligned}\qquad(35)$$

3.2. Calculation of the Matrix Element of Sequential Particle Transfer

The matrix elements that take into account breakup of system λ, are related with virtual intermediate channels of type F (2,2) and C (3,1). Let us obtain an expression for the matrix element of the sequential particle transfer mechanism for F-type channels [31]:

$$\underbrace{(i,j,y)}_{A}+x\to\underbrace{(j,y)}_{\rho}+\underbrace{(x,i)}_{\sigma}\to\underbrace{(x,i,j)}_{B}+y.$$

Such a mechanism is illustrated by the quadrangle diagram with unidirectional lines (Fig. 4), while its matrix element is given by the expression (22a):

$$\begin{aligned}&M^{F_2}_{BA}\\ &= -\left\langle\chi^{(-)}_y(\mathbf{p}_y\mathbf{r}_y)\cdot\varphi_y\left|\left\langle\Psi^\sigma_B\left|\mathbf{T}'_\rho g_{\rho\sigma}\mathbf{T}'_\sigma\right|\Psi^\rho_A\right\rangle\right|\varphi_x\cdot\chi^{(+)}_x(\mathbf{p}_x\mathbf{r}_x)\right\rangle.\end{aligned}\qquad(36)$$

The Green's function $g_{\rho\sigma}$ in (36) describes free motion of virtual clusters ρ and σ. In the position representation it is found to be of the following form [32]:

$$\begin{aligned}\langle\mathbf{r}|g_{\rho\sigma}|\mathbf{r}'\rangle &= -\frac{\mu_{\rho\sigma}}{2\pi\hbar^2}\cdot\frac{e^{i\mathbf{k}_{\rho\sigma}|\mathbf{r}-\mathbf{r}'|}}{|\mathbf{r}-\mathbf{r}'|},\\ \frac{e^{i\mathbf{k}_{\rho\sigma}|\mathbf{r}-\mathbf{r}'|}}{|\mathbf{r}-\mathbf{r}'|} &= -4\pi i k_{\rho\sigma}\\ &\times\begin{cases}\sum_{\Lambda=0}^{\infty} j_\Lambda(k_{\rho\sigma}r')h_\Lambda(k_{\rho\sigma}r)\sum_{\mu=0}^{\Lambda}Y_{\Lambda\mu}(\mathbf{r})Y^*_{\Lambda\mu}(\mathbf{r}'), & r>r',\\ \sum_{\Lambda=0}^{\infty} j_\Lambda(k_{\rho\sigma}r)h_\Lambda(k_{\rho\sigma}r')\sum_{\mu=0}^{\Lambda}Y_{\Lambda\mu}(\mathbf{r}')Y^*_{\Lambda\mu}(\mathbf{r}), & r'>r.\end{cases}\end{aligned}\qquad(37)$$

After substituting (37) into (36), an expression for the matrix element $M_{BA}^{F_2}$ assumes the form of the matrix element convolution for two pole mechanisms, appearing upon cutting up the whole quadrangle diagram (Fig. 6) into two independent position spaces: **r** (for the upper pole diagram) and **r'** (for the lower one):

$$M_{BA}^{F_2}(\theta_y) = -2i\frac{\mu_{\rho\sigma}k_{\rho\sigma}}{\hbar^2} \times \sum_{\Lambda}\left\{\int_0^\infty r^2 dr \int_0^r r'^2 dr' M_2^{h_\Lambda} M_1^{j_\Lambda} + \int_0^\infty r'^2 dr' \int_0^{r'} r^2 dr M_2^{j_\Lambda} M_1^{h_\Lambda}\right\}$$

$$M_2^{h_\Lambda} = \int d\mathbf{r}_y d\Omega_{\mathbf{r}} \chi_y^{(-)}(\mathbf{k}_y\mathbf{r}_y)\cdot\varphi_y \times \Psi_B V_{jy}\Psi_\sigma\Psi_\rho h_\Lambda(k_{\rho\sigma}r)Y_{\Lambda\mu}(\mathbf{r})$$
$$M_1^{j_\Lambda} = \int d\mathbf{r}_x d\Omega_{r'} j_\Lambda(k_{\rho\sigma}r')Y_{\Lambda\mu}(\mathbf{r}') \times \Psi_\sigma^*\Psi_\rho^* V_{ix}\Psi_A\cdot\varphi_x\cdot\chi_x^{(+)}(\mathbf{k}_x\mathbf{r}_x) \quad (38)$$

$$M_2^{j_\Lambda} = \int d\mathbf{r}_y d\Omega_{\mathbf{r}} \chi_y^{(-)}(\mathbf{k}_y\mathbf{r}_y)\cdot\varphi_y \times \Psi_B V_{iy}\Psi_\sigma\Psi_\rho j_\Lambda(k_{\rho\sigma}r)Y_{\Lambda\mu}(\mathbf{r})$$
$$M_1^{h_\Lambda} = \int d\mathbf{r}_x d\Omega_{r'} h_\Lambda(k_{\rho\sigma}r')Y_{\Lambda\mu}(\mathbf{r}') \times \Psi_\sigma^*\Psi_\rho^* V_{ix}\Psi_A\cdot\varphi_x\cdot\chi_x^{(+)}(\mathbf{k}_x\mathbf{r}_x)$$

where $M_1^{j_\Lambda}, M_1^{h_\Lambda}(M_2^{j_\Lambda}, M_2^{h_\Lambda})$ correspond to the matrix elements of the lower (upper) part of a whole diagram with replacing the distorted waves in a virtual $\sigma + \rho$ system by the Bessel or Hankel spherical functions with orbital angular momentum Λ. The potentials in (38) provide a system rearrangement at each step of the particle transfer.

The reaction matrix element for the sequential particle transfer mechanism with multidirectional internal lines through the virtual channel (3,1) is found in a similar way.

3.2.1. Matrix element calculation for the lower part of the quadrangle diagram. We use DWBAFR in the representation of the total momentum transfers at each vertex and the total orbital angular momentum transfer to evaluate the matrix elements of both parts of the whole quadrangle diagram shown in Fig. 6. For the sake of systematizing the notation, all the intermediate momenta for the lower part of the diagram in Fig. 6 to be summed over are labeled by the indices (1*n*) or 1; for its upper part, by (2*n*) or 2.

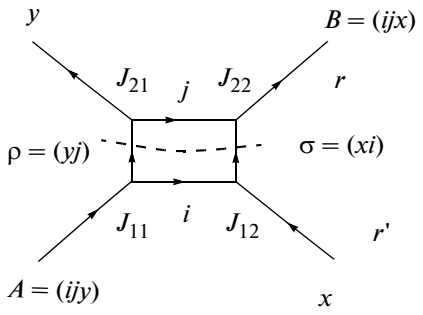

Fig. 6. A quadrangle diagram for the mechanism of independent particle transfer with "cutting" the intermediate virtual states.

Just like in (28), the matrix element $M_1^{j_\Lambda}$ associated with the lower part of the diagram in Fig. 6 will be represented in the form:

$$M_1^{j_\Lambda} = (-1)^{2J_x+2J_\rho-J_{12}-M_{J_{12}}} \times \sum_{J_{11}J_{12}}\sqrt{(2J_{11}+1)(2J_{12}+1)} \times \langle J_x M_x J_{12} M_{12}|J_\sigma M_\sigma\rangle\langle J_\rho M_\rho J_{11} M_{11}|J_A M_A\rangle \times \langle J_{12} - M_{12}\, J_{11}\, M_{11}|l_1\, m_1\rangle \times \sum_{l_1\Lambda_{11}\Lambda_{12}}\beta_{\Lambda_{11}\Lambda_{12}l_1m_1}(\theta_x)\cdot\Theta_{\Lambda_{11}\Lambda_{12}l_1}^{J_{11}J_{12}}, \quad (39)$$

where

$$\beta_{\Lambda_{11}\Lambda_{12}l_1m_1}(\theta_x) = (-1)^{\mu_{11}}\langle\Lambda_{11} - \mu_{11}\,\Lambda_{12}\,\mu_{12}|l_1\,m_1\rangle \times \quad (40)$$
$$\times\int d\mathbf{r}_x d\Omega_{\mathbf{r}'}\chi_x(\mathbf{k}_x\mathbf{r}_x)\cdot\Psi_{\Lambda_{12}}\cdot V_{ix}\cdot\Psi_{\Lambda_{11}}^*\cdot j_\Lambda(k_{\sigma\rho}r')Y_\Lambda^*(\mathbf{r}')$$

An expression for the kinematical factor (40) can be obtained by introducing the invariant form factor $F_{\Lambda_{11}\Lambda_{12}l_1}^{L_x'\Lambda'}$:

$$f_{\Lambda_{11}\Lambda_{12}l_1m_1} = \sum(-1)^{\mu_{12}}\langle\Lambda_{11}\,\mu_{11}\,\Lambda_{12} - \mu_{12}|l_1 - m_1\rangle\Psi_{\Lambda_{12}}V_{ix}\Psi_{\Lambda_{11}}^* = \sum_{L_x'\Lambda'}F_{\Lambda_{11}\Lambda_{12}l_1}^{L_x'\Lambda'}\left\langle L_x'\,m_x'\,\Lambda'\,\mu'\middle|l_1 - m_1\right\rangle \times Y_{L_x'm_x'}^*(\mathbf{r}')Y_{\Lambda'\mu'}^*(\mathbf{r}'). \quad (41)$$

In this case

$$\beta_{\Lambda_{11}\Lambda_{12}l_1m_1}(\theta_x) = (-1)^{\Lambda_{11}+\Lambda_{12}-l_1+m_1} \times \int d\mathbf{r}_x d\Omega_{\mathbf{r}'}\chi_x(\mathbf{k}_x\mathbf{r}_x)\cdot f_{\Lambda_{11}\Lambda_{12}l_1m_1}\cdot j_\Lambda(k_{\sigma\rho}r')\cdot Y_\Lambda^*(\mathbf{r}') \quad (42)$$

Now, decompose the form factor and distorted wave of the initial channel over the partial waves and

integrate (42) over the angular variables. This yields

$$\beta_{\Lambda_{11}\Lambda_{12}\, l_1 m_1}(\theta_x) = \frac{1}{\sqrt{2l_1+1}}\frac{4\pi}{k_x}(-1)^{\Lambda_{11}+\Lambda_{12}-l_1+m_x} \times \sum_{L_x m_x} i^{L_x}\cdot Y^*_{L_x m_x}(\mathbf{k}_x)\left\langle L_x m_x\, \Lambda -\mu \middle| l_1 - m_1\right\rangle \cdot \mathfrak{I}^{L_x\Lambda}_{\Lambda_{11}\,\Lambda_{12}\, l_1}(r'), \tag{43}$$

$$\mathfrak{I}^{L_x\Lambda}_{\Lambda_{11}\Lambda_{12} l_1}(r') = \int \chi_x(k_x r_x)\, F^{L_x\Lambda}_{\Lambda_{11}\Lambda_{12} l_1}(r', r_x) r_x dr_x$$

And the matrix element (39) transforms to take the following form:

$$M_1^{j_\Lambda} = (-1)^{2J_x+2J_\rho-J_{12}-M_{12}}\frac{4\pi}{k_x} \times \sum_{J_{11}J_{12}l_1}\sqrt{(2J_{11}+1)(2J_{12}+1)} \times\left\langle J_x M_x J_{12} M_{12}\middle| J_\sigma M_\sigma\right\rangle\cdot\left\langle J_\rho M_\rho J_{11} M_{11}\middle| J_A M_A\right\rangle \times\left\langle J_{12}-M_{12} J_{11} M_{11}\middle| l_1 m_1\right\rangle \times \sum_{L_x\Lambda_{11}\Lambda_{12}}(-1)^{l_1+m_x}\cdot i^{L_x}\cdot\left\langle L_x m_x \Lambda - m_\Lambda\middle| l_1 - m_1\right\rangle \times \Theta^{J_{11}J_{12}}_{\Lambda_{11}\Lambda_{12}l_1}\cdot \mathfrak{I}^{L_x\Lambda}_{\Lambda_{11}\,\Lambda_{12}\, l_1}(r') j_\Lambda(k_{\sigma\rho}r') Y^*_{L_x m_x}(\mathbf{k}_x). \tag{44}$$

The spectroscopic factors $\Theta^{J_{11}J_{12}}_{\Lambda_{11}\Lambda_{12}l_1}$ are defined by Eq. (34), since both clusters ρ and σ may have their own excited states.

3.2.2. Matrix element calculation for the upper part of the quadrangle diagram. The matrix element for *j* particle transfer in the upper part of the quadrangle diagram with unidirectional lines is calculated in a similar fashion. In the total momentum transfer representation, it looks as follows:

$$M_2^{h_\Lambda} = (-1)^{2J_\sigma+2J_y-J_{22}-M_{22}} \times \sum_{J_{21}J_{22}l_2}\sqrt{(2J_{21}+1)(2J_{22}+1)(2l_2+1)} \times\left\langle J_\sigma M_\sigma J_{22} M_{22}\middle| J_B M_B\right\rangle\cdot\left\langle J_y M_y J_{21} M_{21}\middle| J_\rho M_\rho\right\rangle \left\langle J_{22}-M_{22} J_{21} M_{21}\middle| l_2 m_2\right\rangle \times \sum_{\Lambda_{21}\Lambda_{22}}\beta_{\Lambda_{21}\Lambda_{22}l_2 m_2}(\theta_y)\cdot\Theta^{J_{21}J_{22}}_{\Lambda_{21}\Lambda_{22}l_2}, \tag{45}$$

where

$$\beta_{\Lambda_{21}\Lambda_{22}l_2 m_2}(\theta_y) = (-1)^{\mu_{21}}\frac{1}{\sqrt{2l_2+1}} \times\left\langle \Lambda_{21}-\mu_{21}\Lambda_{22}\mu_{22}\middle| l_2 m_2\right\rangle \times\int\int d\mathbf{r}_x d\Omega_{\mathbf{r}}\ \chi_y(\mathbf{k}_y\mathbf{r}_y)\cdot\Psi_{\Lambda_{22}} V_{jy}\cdot\Psi^*_{\Lambda_{21}}\cdot h_\Lambda(k_{\sigma\rho}r)\cdot Y^*_\Lambda(\mathbf{r}). \tag{46}$$

Over again, introduce the invariant form factor $F^{L'_y L'_\Lambda}_{\Lambda_{21}\Lambda_{22}l_2}$:

$$f_{\Lambda_{21}\Lambda_{22}l_2 m_2} = \sum(-1)^{\mu_{22}} \times\left\langle \Lambda_{21}\mu_{21}\Lambda_{22}-\mu_{22}\middle| l_2 - m_2\right\rangle\cdot\Psi^*_{\Lambda_{21}}\cdot V_{jy}\cdot\Psi_{\Lambda_{22}} = \sum_{L'_y L'_{\sigma\rho}} F^{L'_y L'_{\sigma\rho}}_{\Lambda_{21}\Lambda_{22}l_2}\cdot\left\langle L'_y m'_y \Lambda\mu\middle| l_2 - m_2\right\rangle Y^*_{m'_y m'_{\sigma\rho}}(\mathbf{r}) Y^*_{\Lambda\mu}(\mathbf{r}), \tag{47}$$

decompose the distorted wave of the final channel over the partial waves and integrate (47) over the angles $\Omega_{\mathbf{r}_y}$ and $\Omega_{\mathbf{r}}$. All these manipulations lead to the following expression for the form factor (47):

$$\beta_{\Lambda_{21}\Lambda_{22}l_2 m_2}(\theta_y) = (-1)^{\Lambda_{21}+\Lambda_{22}-l_2+m_2} \times\frac{1}{\sqrt{2l_2+1}}\cdot\frac{4\pi}{k_y}\cdot\left\langle L_y m_y \Lambda\mu\middle| l_2 - m_2\right\rangle, \times Y_{L_y m_y}(\mathbf{k}_y)\mathfrak{I}^{\Lambda L_y}_{\Lambda_{21}\Lambda_{22}l_2}(r)$$

$$\mathfrak{I}^{\Lambda L_y}_{\Lambda_{21}\Lambda_{22}l_2}(r) = \int\chi_y(k_y r_y)\cdot F^{\Lambda L_y}_{\Lambda_{21}\Lambda_{22}l_2}(r, r_y)\cdot r_y\, dr_y \tag{48}$$

while for the matrix element of the upper part of the diagram shown in Fig. 6 we obtain:

$$M_2^{h_\Lambda} = (-1)^{2J_\sigma+2J_y-J_{22}-M_{22}+l_2+m_2} \times\frac{4\pi}{k_y}\sum_{J_{21}J_{22}l_2}\sqrt{(2J_{21}+1)(2J_{22}+1)} \times\left\langle J_\sigma M_\sigma J_{22} M_{22}\middle| J_B M_B\right\rangle\cdot\left\langle J_y M_y J_{21} M_{21}\middle| J_\rho M_\rho\right\rangle \times\left\langle J_{22}-M_{22} J_{21} M_{21}\middle| l_2 m_2\right\rangle \times\sum_{\Lambda_{21}\Lambda_{22}}\left\langle \Lambda\mu L_y m_y\middle| l_2 - m_2\right\rangle\cdot\Theta^{J_{21}J_{22}}_{\Lambda_{21}\Lambda_{22}l_2} \times Y_{L_y m_y}(\mathbf{k}_y)\cdot\mathfrak{I}^{\Lambda L_y}_{\Lambda_{21}\Lambda_{22}l_2}(r)\, h_\Lambda(k_{\sigma\rho}r), \tag{49}$$

where the spectroscopic factors $\Theta^{J_{21}J_{22}}_{\Lambda_{21}\Lambda_{22}l_2}$ are given by Eqs. (34).

3.2.3. Full matrix element calculation for the sequential particle transfer mechanism. In order to completely evaluate the matrix element in (38) it is necessary to multiply (44) and (49), as well as to calculate the sums over intermediate momentum projections in the products of the Clebsch–Gordan coefficients.

Upon multiplying (45) and (50) we obtain

$$M_1^{j_\Lambda} M_2^{h_\Lambda} = (-1)^{2J_x+2J_\rho+2J_\sigma+2J_y-J_{12}-M_{12}-J_{22}-M_{22}} (-1)^{l_2+m_2+l_1+m_1} \cdot i^{L_x-L_y} \times \frac{(4\pi)^2}{k_x k_y} \cdot \sqrt{(2J_{11}+1)(2J_{12}+1)(2J_{21}+1)(2J_{22}+1)} \times \langle J_x M_x J_{12} M_{12} | J_\sigma M_\sigma\rangle \langle J_\rho M_\rho J_{11} M_{11} | J_A M_A\rangle \times \langle J_\sigma M_\sigma J_{22} M_{22} | J_B M_B\rangle \langle J_y M_y J_{21} M_{21} | J_\rho M_\rho\rangle \quad (50)$$

$$\times \langle J_{12} - M_{12} J_{11} M_{11} | l_1 m_1\rangle \langle J_{22} - M_{22} J_{21} M_{21} | l_2 m_2\rangle$$

$$\times \langle L_x m_x \Lambda - m_\Lambda | l_1 - m_1\rangle \langle \Lambda \mu L_y m_y | l_2 - m_2\rangle \times \sum_{\Lambda_{21}\Lambda_{22}} \Theta^{J_{11}J_{12}}_{\Lambda_{11}\Lambda_{12}l_1} \cdot Y^*_{L_x m_x}(\mathbf{k}_x) \cdot \Theta^{J_{21}J_{22}}_{\Lambda_{21}\Lambda_{22}l_2} \cdot Y_{L_y m_y}(\mathbf{k}_y)$$

$$\times \iint \Im^{L_x \Lambda}_{\Lambda_{11}\Lambda_{12}l_1}(r') \cdot \Im^{\Lambda L_y}_{\Lambda_{21}\Lambda_{22}l_2}(r) \times j_\Lambda(k_{\sigma\rho} r') h_\Lambda(k_{\sigma\rho} r) r^2 dr \cdot r'^2 dr'.$$

The next step is to transform the product of the Clebsch–Gordan coefficients.

$$\sum_{M_\sigma} \langle J_x M_x J_{12} M_{12} | J_\sigma M_\sigma\rangle \times \langle J_\sigma M_\sigma J_{22} M_{22} | J_B M_B\rangle = \sum_{J_1 M_1} U(J_x J_{12} J_B J_{22} : J_\sigma J_1) \times \langle J_{12} M_{12} J_{22} M_{22} | J_1 M_1\rangle \langle J_x M_x J_1 M_1 | J_B M_B\rangle; \quad (51a)$$

$$\sum_{M_\rho} \langle J_\rho M_\rho J_{11} M_{11} | J_A M_A\rangle \times \langle J_y M_y J_{21} M_{21} | J_\rho M_\rho\rangle = \sum_{J_2 M_2} U(J_y J_{21} J_A J_{11} : J_\rho J_2) \times \langle J_{21} M_{21} J_{11} M_{11} | J_2 M_2\rangle \langle J_y M_y J_2 M_2 | J_A M_A\rangle. \quad (51b)$$

$$\sum_{M_{12}M_{22}} (-1)^{-J_{12}-M_{12}-J_{22}-M_{22}} \langle J_{12} - M_{12} J_{11} M_{11} | l_1 m_1\rangle \times \langle J_{22} - M_{22} J_{21} M_{21} | l_2 m_2\rangle \langle J_{12} M_{12} J_{22} M_{22} | J_1 M_1\rangle \quad (51c)$$

$$\times \langle J_{21} M_{21} J_{11} M_{11} | J_2 M_2\rangle = \sum_{l m} (-1)^{-M_1-J_1+J_{21}+J_{11}-J_2} \times \sqrt{(2J_1+1)(2J_2+1)(2l_1+1)(2l_2+1)} \times \langle J_1 - M_1 J_2 M_2 | l m\rangle \langle l_1 m_1 l_2 m_2 | l m\rangle \cdot \begin{Bmatrix} J_{12} & J_{11} & l_1 \\ J_{22} & J_{21} & l_2 \\ J_1 & J_2 & l \end{Bmatrix}.$$

$$\sum_\mu (-1)^{l_2+m_2+l_1+m_x} \langle L_x m_x \Lambda - \mu | l_1 - m_1\rangle \times \langle \Lambda \mu L_y m_y | l_2 - m_2\rangle \langle l m_1 l_2 m_2 | l m\rangle = (-1)^{l_2+m+L_x} \sqrt{\frac{(2l_2+1)}{(2L_y+1)}} U(L_x \Lambda l l_2 : l_1 L_y) \times \langle L_x - m_x L_y - m_y | l m\rangle. \quad (51d)$$

As a result, the product of the matrix elements is found to take the form

$$M_1^{j_\Lambda} M_2^{h_\Lambda} = (-1)^{2J_x+2J_\rho+2J_\sigma+2J_y} \frac{(4\pi)^2}{k_x k_y} \times \sqrt{(2J_{11}+1)(2J_{12}+1)(2J_{21}+1)(2J_{22}+1)} \times \sqrt{(2J_1+1)(2J_2+1)(2l_1+1)(2l_2+1)} \times \sqrt{\frac{2l_2+1}{2L_y+1}} i^{L_x-L_y} \times \langle J_x M_x J_1 M_1 | J_B M_B\rangle \langle J_y M_y J_2 M_2 | J_A M_A\rangle \times U(J_x J_{12} J_B J_{22} : J_\sigma J_1) U(J_y J_{21} J_A J_{11} : J_\rho J_2) \times U(L_x \Lambda l l_2 : l_1 L_y) \langle L_x - m_x L_y - m_y | l m\rangle \times \langle L_1 - M_1 L_2 M_2 | l m\rangle (-1)^{-M_1-J_1+J_{21}+J_{11}-J_2+l_2+m+L_x} \times \begin{Bmatrix} J_{12} & J_{11} & l_1 \\ J_{22} & J_{21} & l_2 \\ J_1 & J_2 & l \end{Bmatrix} \sum_{\Lambda_{21}\Lambda_{22}} \Theta^{J_{11}J_{12}}_{\Lambda_{11}\Lambda_{12}l_1} Y^*_{L_x m_x}(\mathbf{k}_x) \times \Theta^{J_{21}J_{22}}_{\Lambda_{21}\Lambda_{22}l_2} Y_{L_y m_y}(\mathbf{k}_y) \Im_{L_x L_y \Lambda}. \quad (52)$$

To transform the product (52) let us rewrite the Racah coefficient $U(L_x \Lambda l l_2 : l_1 L_y)$ as a 6-j-symbol:

$$U(L_x \Lambda l l_2 : l_1 L_y) = (-1)^{L_x+\Lambda+l+l_2} \times \begin{Bmatrix} L_x & \Lambda & l_1 \\ l_2 & l & L_y \end{Bmatrix} \cdot \sqrt{(2l_1+1)(2L_y+1)}.$$

Introduce a generalized spectroscopic factor:

$$\bar{\Theta}^{J_1 J_2}_{l_1 l_2 l} = \sum (-1)^{2J_\rho+2J_\sigma+J_{21}+J_{11}-J_2} \times \sqrt{(2J_{11}+1)(2J_{12}+1)(2J_{21}+1)(2J_{22}+1)} \times (2l_1+1)(2l_2+1) \cdot \Theta^{J_{11}J_{12}}_{\Lambda_{11}\Lambda_{12}l_1} \cdot \Theta^{J_{21}J_{22}}_{\Lambda_{21}\Lambda_{22}l_2} \quad (53)$$

$$\times\ U(J_x J_{12} J_B J_{22} : J_\sigma J_1)$$
$$\times U(J_y J_{21} J_A J_{11} : J_\rho J_2)\cdot \begin{Bmatrix} J_{12} & J_{11} & l_1 \\ J_{22} & J_{21} & l_2 \\ J_1 & J_2 & l \end{Bmatrix}$$

Substituting into (52) relationship (32) and taking into account the definition (53), we obtain that the matrix element in (38) of the mechanism, illustrated by the quadrangle diagram with unidirectional lines, is computed according to the following formula:

$$M_{BA}^{F_2}(\theta_y) = \frac{4\sqrt{2}\pi}{k_x k_y}\sum_{J_1 J_2 l}(-1)^{2J_x+2J_y-M_1-J_1}$$
$$\times\sqrt{(2J_1+1)(2J_2+1)(2l+1)}$$
$$\times\langle J_x M_x J_1 M_1 | J_B M_B\rangle\langle J_y M_y J_2 M_2 | J_A M_A\rangle$$
$$\times\langle J_1 - M_1 J_2 M_2 | l m\rangle\times\sum_{L_x L_y} i^{L_x+L_y}\sum_{\Lambda l_1 l_2}\begin{Bmatrix} L_x & \Lambda & l_1 \\ l_2 & l & L_y \end{Bmatrix} \quad (54)$$
$$\times\langle l m L_y - m | L_x 0\rangle\ \bar\Theta_{l_1 l_2 l}^{J_1 J_2}\ \Im_{L_x L_y \Lambda}\ P_{L_y - m}(\theta_y)$$

$$m = M_x + M_A - M_B - M_y.$$

In (55) a spectroscopic factor is given by the relationship (53), while the multidimensional integral $\Im_{L_x L_y \Lambda}$ is defined as follows:

$$\Im_{L_x L_y \Lambda} = 2i\cdot\mu_{\rho\sigma}k_{\rho\sigma}\cdot(-1)^{\Lambda+1}$$
$$\times\Bigg\{\int_0^\infty r\,dr\cdot\Im^{\Lambda L_y}_{\Lambda_{21}\Lambda_{22}l_2}(r)\cdot h_\Lambda(k_{\rho\sigma}r)$$
$$\times\int_0^r r'dr'\cdot\Im^{L_x\Lambda}_{\Lambda_{11}\Lambda_{12}l_1}(r')j_\Lambda(k_{\rho\sigma}r') \quad (55)$$
$$+\int_0^\infty r'dr'\cdot\Im^{L_x\Lambda}_{\Lambda_{11}\Lambda_{12}l_1}(r')\cdot h_\Lambda(k_{\rho\sigma}r')$$
$$\times\int_0^{r'} r\,dr\cdot\Im^{\Lambda L_y}_{\Lambda_{21}\Lambda_{22}l_2}(r)\cdot j_\Lambda(k_{\rho\sigma}r)\Bigg\}.$$

Combining (33) and (55), we obtain a final expression for calculating the reaction matrix element in DWBAFR with accounting for second order corrections, which correspond to the transfer of virtual clusters separated in time illustrated by the quadrangle diagram with unidirectional internal lines:

$$M_{BA}^{DWBA}(\theta_y) + M_{BA}^{F_2}(\theta_y) = (-1)^{2J_x+2J_y-J_1-M_1}$$
$$\times\frac{4\sqrt{2}\pi}{k_x k_y}\sum_{J_1 J_2}\sqrt{(2J_1+1)(2J_2+1)(2l+1)}$$
$$\times\langle J_x M_x J_1 M_1 | J_B M_B\rangle\langle J_y M_y J_2 M_2 | J_A M_A\rangle \quad (56)$$
$$\times\langle J_1 - M_1 J_2 M_2 | l m\rangle\sum_{l\Lambda_1\Lambda_2}\sum_{L_x L_y} i^{L_x+L_y}\langle l m L_y - m | L_x 0\rangle$$
$$\times P_{L_y-m}(\theta_y)\Bigg(\Theta^{J_1 J_2}_{\Lambda_1\Lambda_2 l}\cdot\Im_{0\Lambda}+\begin{Bmatrix} L_x & \Lambda & l_1 \\ l_2 & l & L_y \end{Bmatrix}\cdot\bar\Theta^{J_1 J_2}_{l_1 l_2 l}\cdot\Im_{L_x L_y}\Bigg).$$

An expression for the matrix element of the process, illustrated by a diagram with multidirectional internal lines, is analogous to (56) up to replacement of summation indices and decay widths of nuclei.

We emphasize that formulas for the reaction matrix element which consider a mechanism of independent virtual cluster transfer are derived for a nonzero radius of particle interaction, without neglecting recoil effects, as well as with consistently taking into account all the states of an intermediate cluster system $\rho + \sigma$ allowed by the selection rules.

3.3. A Brief Description of QUADRO Code

The QUADRO code enables one to compute the matrix elements of independent sequential particle transfer mechanism. The code structure is based on the fact that the desired matrix element is defined as a convolution of those for two pole mechanisms in the DWBAFR approximation. In the course of developing the code, the program OLYMP [33] was heavily used, which implemented a cross section calculation for the reaction with composite particles within the DWBAFR framework.

The QUADRO code consists of four main stages. At the first one, a pole diagram illustrated by the lower part of the quadrangle diagram shown in Fig. 6 is considered. By using a modified version of the OLYMP code on a uniform r'-grid with step h, an array associated with the one-dimensional integral $\Im^{L_x\Lambda}_{\Lambda_{11}\Lambda_{12}l_1}(r') = \int r_x dr_x \chi_{x}(k_x r_x) F^{L_x\Lambda}_{\Lambda_{11}\Lambda_{12}l_1}(r', r_x)$ is calculated and written out.

At the second stage, the reaction $B + y \to \sigma + \rho$, which is inverse to a pole diagram illustrated the upper part of the quadrangle diagram in Fig. 6, is considered by using the OLYMP code. An array associated with the integral $\Im^{\Lambda L_y}_{\Lambda_{21}\Lambda_{22}l_2}(r) = \int r_y\, dr_y\, \chi_{y}(k_y r_y)\ F^{\Lambda L_y}_{\Lambda_{21}\Lambda_{22}l_2}(r, r_y)$ is filled in the manner similar to how this was done at the first stage.

At the third stage, a computation of the part of the desired matrix element $\sum\begin{Bmatrix} L_x & \Lambda & l_1 \\ l_2 & l & L_y \end{Bmatrix}\cdot\bar\Theta^{J_1 J_2}_{l_1 l_2 l}\cdot\Im_{L_x L_y \Lambda}$ is carried out. The reaction parameters and arrays of spectroscopic factors for the lower and upper parts of

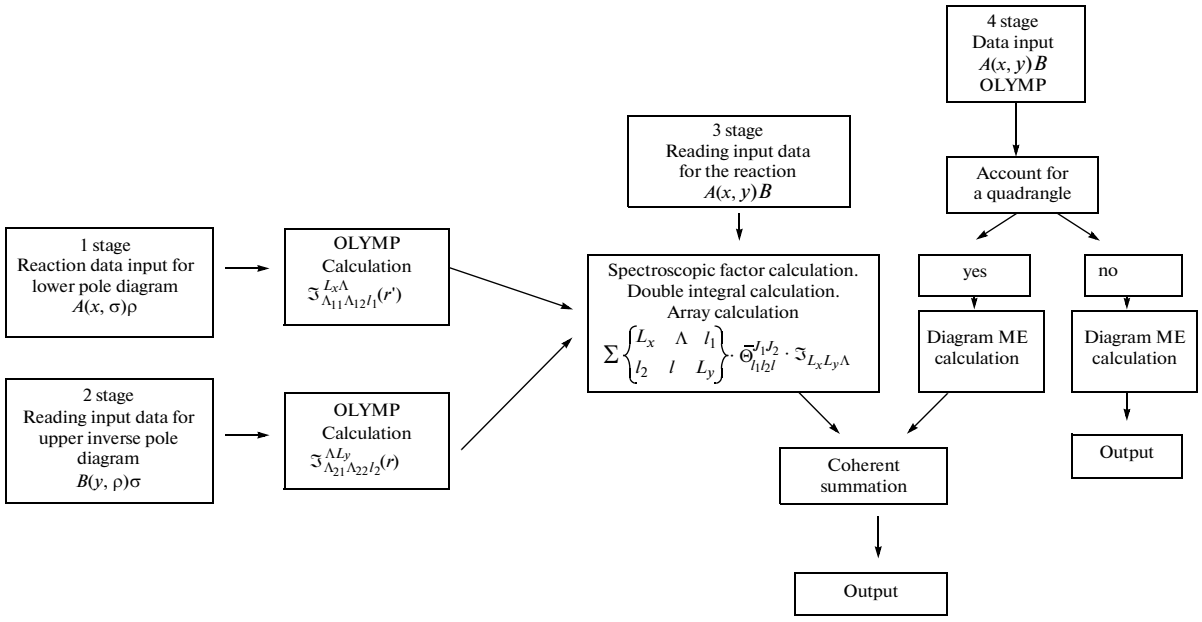

Fig. 7. A flow chart of QUADRO code.

the quadrangle diagram are read from the input data file. The indices and summation limits are defined. A generalized spectroscopic factor $\bar{\Theta}^{J_1J_2}_{l_1l_2l}$ of the reaction is calculated for each term according to Eq. (53). Arrays filled in earlier are used to evaluate a double integral with variable upper limit $\Im_{L_xL_y\Lambda}$:

$$\Im_{L_xL_y\Lambda} = 2i \cdot \mu_{\rho\sigma} k_{\rho\sigma} \cdot (-1)^{\Lambda+1} \frac{4\sqrt{2}\pi}{k_x k_y}$$
$$\times \left\{ \int_0^\infty r\,dr \cdot \Im^{\Lambda L_y}_{\Lambda_{21}\Lambda_{22}l_2}(r) \cdot h_\Lambda(k_{\rho\sigma} r) \right.$$
$$\times \int_0^r r'\,dr' \cdot \Im^{L_x\Lambda}_{\Lambda_{11}\Lambda_{12}l_1}(r') j_\Lambda(k_{\rho\sigma} r')$$
$$+ \int_0^\infty r'\,dr' \cdot \Im^{L_x\Lambda}_{\Lambda_{11}\Lambda_{12}l_1}(r') \cdot h_\Lambda(k_{\rho\sigma} r')$$
$$\left. \times \int_0^{r'} r\,dr \cdot \Im^{\Lambda L_y}_{\Lambda_{21}\Lambda_{22}l_2}(r) \cdot j_\Lambda(k_{\rho\sigma} r) \right\}.$$

All needed summations are performed, and a final array $\sum \begin{Bmatrix} L_x & \Lambda & l_1 \\ l_2 & I & L_y \end{Bmatrix} \cdot \bar{\Theta}^{J_1J_2}_{l_1l_2l} \cdot \Im_{L_xL_y\Lambda}$ is written out to the file.

At the fourth stage, the program calculates, according to Eq. (57), the matrix element, differential cross section of the reaction, and the density matrix of a final nucleus either exclusively for DWBAFR or solely for the mechanism of sequential particle transfer or their coherent sum (optional).

A flow chart for QUADRO code is presented in Fig. 7.

The developed QUADRO code lets the matrix elements of mechanisms of independent sequential particle transfer be calculated as second order corrections to DWBAFR.

The results of differential cross section calculations for various reactions in comparison with experimental data (within the regions where the latter exist) are presented in the next section.

4. CROSS SECTIONS OF SPECIFIC REACTIONS WITH ACCOUNTING FOR THE MECHANISMS THAT INCLUDE SEQUENTIAL PARTICLE TRANSFER

The expression (56) for calculating the reaction matrix element in DWBAFR with taking into account diverse cluster transfer, derived in the previous section, will be used to compute angular distributions of the cross sections for specific reactions. Selection of the reactions is governed by criteria outlined in Sec. 2, whose implementation leads to the contribution of sequential particle transfer expected to be substantial: either the wave functions of particles transferred considerably differ, especially in the peripheral region of a nucleus, or the mechanism of λ cluster system transfer is suppressed by the selection rules. The reactions with neutron-excess light nuclei are considered along with the elastic scattering.

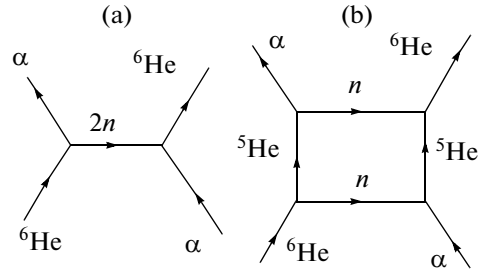

Fig. 8. Diagrams of the exchange mechanisms in elastic α^6He-scattering: (a) dineutron exchange, (b) mechanism of independent neutron transfer.

4.1. Calculation of the Amplitude for the Elastic α^6He-scattering

In the optical model a differential cross section for the elastic scattering of particle x off nucleus A is determined by the scattering amplitude squared $\frac{d\sigma_{\text{упр}}}{d\Omega} = |f(\theta)|^2$ [34]:

$$f(\theta) = f_C(\theta) + \frac{1}{2ik}\sum_{L=0}^{\infty}(2L+1)\,e^{2i\sigma_L}\left(S_L^{opt}-1\right)P_L(\cos\theta),$$

where θ is a scattering angle, k is a wave vector of relative motion of particles x and A, $P_L(\cos\theta)$ are Legendre polynomials, $f_C(\theta), \sigma_L$ denote a Coulomb amplitude and phase, respectively, S_L^{opt} are S-matrix elements, which describe potential scattering in the optical model. As is shown in [4], elastic scattering of composite particles, especially at large angles, is not due to potential scattering alone. It is necessary to account for inelastic processes as well; first of all, the so-called exchange mechanisms, associated with the dissociation of a target nucleus into fragments. In our case, such mechanisms are cluster dineutron exchange and sequential neutron transfer (Fig. 8).

As a result, in addition to the matrix elements of potential scattering S_L^{opt} the total amplitude of elastic scattering of particles x and A will contain exchange coefficients a_L^0 and a_L^1:

$$f(\theta) = f_C(\theta) + \frac{1}{2ik} \times \sum_{L=0}^{\infty}(2L+1)\,e^{2i\sigma_L}\left(S_L^{opt}+a_L^0+a_L^1-1\right)P_L(\cos\theta), \quad (57)$$

which are coefficients of the expansion of amplitudes $\frac{\mu_{xA}}{2\pi\hbar^2}M_{BA}^{\text{DWBA}}$ and $\frac{\mu_{xA}}{2\pi\hbar^2}M_{BA}^{F_2}$ into a series over Legendre polynomials.

The matrix elements M_{BA}^{DWBA} and $M_{BA}^{F_2}$ are defined by formulas (33) and (55), respectively. In the case of elastic scattering $l=0$; $k_x = k_y$; $\Lambda_1 = \Lambda_2$; $J_1 = J_2$; $L_x = L_y = L$. Then,

$$M_{AA}^{\text{DWBA}} = \frac{4\sqrt{2}\pi}{k_x^2} \times \sum_{J_1 M_1}\sqrt{(2J_1+1)}\left\langle J_x M_x J_1 M_1 \middle| J_A M_A\right\rangle^2 \times \sum_{L\,\Lambda_1}(-1)^L\cdot\Theta_{\Lambda_1\Lambda_1 0}^{J_1 J_1}\cdot P_{L0}(\theta_y)\cdot\Im_{LL0}^0, \quad (58)$$

where

$$\Theta_{\Lambda_1\Lambda_1 0}^{J_1 J_1} = \frac{(-1)^{\Lambda_1}\cdot\sum_{l_A s_A}\left(\tilde\Theta_{\Lambda_1 l_A l_\lambda L_2 l_y s_A s_\lambda s_y}^{A\to\lambda+y}\right)^2}{\sqrt{(2\Lambda_1+1)(2J_1+1)}}. \quad (59)$$

Taking into account the normalization of associated Legendre polynomials $P_{L0} = \sqrt{\frac{(2L+1)}{2}}P_L$, as well as the fact that for the elastic α^6He-scattering $J_x = J_A = 0$, we obtain for the coefficients a_L^0 related to a dineutron cluster exchange:

$$a_L^0 = \frac{4\mu_{xA}}{\hbar^2 k} i \times \sum_{\Lambda_1}\frac{(-1)^L}{\sqrt{(2L+1)}}\frac{(-1)^{\Lambda_1}}{\sqrt{(2\Lambda_1+1)}} \times \sum_{l_A s_A}\left(\tilde\Theta_{\Lambda_1 l_A s_A}^{A\to\lambda+y}\right)^2\Im_{LL0}^0. \quad (60)$$

As is seen from (60), additional terms to the amplitude of elastic α^6He-scattering stemming from dineutron cluster transfer, alter the sign as $(-1)^L$. In other words, they have the phase coinciding with that of Legendre polynomials at an angle of 180° and, therefore, cause a cross section of α^6He-scattering to increase at large angles.

Derive now similar expression for the coefficients a_L^1, which define an additional term to the amplitude of elastic scattering associated with independent neutron transfer (Fig. 8b). By using (56), we have for $M_{BA}^{F_2}$:

$$M_{BA}^{F_2}(\theta_y) = \frac{4\sqrt{2}\pi}{k_x^2} \times \sum_{L\Lambda l_1}\bar\Theta_{l_1 l_1 0}^{J_1 J_1}\Im_{LL\Lambda}P_{L-m}(\theta_y)\frac{(-1)^{\Lambda+l_1}}{\sqrt{(2L+1)(2l_1+1)}}, \quad (61)$$

so that the coefficients a_L^1 are given as follows:

$$a_L^1 = \frac{4\mu_{xA}}{\hbar^2 k} i \times \sum_{l_1} \sum_{\Lambda=|l_1-L|}^{l_1+L} \frac{(-1)^{\Lambda+l_1}}{(2L+1)\sqrt{(2l_1+1)}} \bar{\Theta}_{l_1 l_1 0}^{J_1 J_1} \cdot \Im_{LL\Lambda}. \quad (62)$$

Comparing (60) and (62) we can understand, already qualitatively, fundamental differences in the behavior of additional terms to S_L-matrix of elastic scattering related with either dineutron cluster exchange or independent neutron transfer. Indeed, the structure of the coefficients a_L^0 is such that they contain the L-splitting terms additional to the S_L-matrix, thereby providing a sharp rise of the scattering cross section at large angles. The coefficients a_L^1 do not possess such a structure; therefore, a contribution of the process caused by sequential neutron transfer may be substantial at all scattering angles.

Specific calculations of the differential cross section of elastic α^6He-scattering with taking into account additional exchange terms require the spectroscopic factors and potential parameters of nuclear interaction be determined.

The spectroscopic factors were computed according to Eqs. (35), (53), by using information about the structure of wave functions of nuclei ^{6}He and ^{5}He in the conventional nuclear shell model with intermediate coupling [35]. For the two-step mechanism of sequential neutron transfer, the selection rules allow the only state of nucleus ^{5}He, which has $J = 1/2$. At the same time, the ground state of ^{5}He is by 95% the state with $J = 3/2$ [35]. A respective weight factor was accounted for while calculating a reduced decay width of $^6\text{He} \to {}^5\text{He} + n$. We determined the spectroscopic factor of a dineutron (the pole diagram in Fig. 8a) via that of a deuteron in ^{6}Li (it is equal to 1.68 [36]), while the spectroscopic factors of the lower and upper parts of the quadrangle diagram shown in Fig. 8b ($l_1 = 0, 1$) are presented in Table 1.

The following observation can be made about the choice of parameters for α^6He interaction potential. Usually, phenomenological potentials of nuclear interaction with various sets of parameters are used in a specific model to calculate reaction characteristics, which have experimental counterparts. A final parameter set is fixed by optimally matching the calculated and experimental data. The parameters selected in this way depend on a model and compensate its shortcomings. For example, the optical potentials, obtained by fitting the experimental angular distributions in the potential scattering model, take into account the absence of more involved mechanisms in the model, such as channel couplings, additional exchange terms, and so on. Therefore, once the model is changed and extra mechanisms are added, the potential parameter values not only can but should vary within reasonable limits. While taking into account an additional term to the amplitude of elastic scattering, associated with only dineutron transfer [36, 37], we had to use an optical potential of α^6He-interaction too deep and narrow, which did not fully correspond to the physical picture. When, in addition to the dineutron transfer, a two-step mechanism of the neutron transfer [38] is taken into account, best agreement with experiment was achieved with an optical potential of conventional Woods–Saxon form which has physically more reasonable parameters (less depth and greater radius). This circumstance can serve as yet another confirmation of the need to consider the mechanism of independent neutron transfer in elastic α^6He-scattering. Specific parameter values of α^6He optical potential are presented in Table 2.

Table 1. Spectroscopic factors $\bar{\Theta}_{\Lambda_1\Lambda_2 l}^{J_1 J_2}$ for a two-step mechanism in elastic α^6He-scattering ($\Lambda_1 = \Lambda_2 = 1$, $J_1 = J_2$)

J_1 \ l	0	1
1/2	0.04	0.03

The theoretical angular distribution of the cross section for elastic α^6He-scattering was derived according to (58) by coherently summing up the amplitudes of three mechanisms: potential scattering, pole mechanism of dineutron transfer and that of gradual neutron transfer from nucleus ^{6}He to α particle. The calculated differential cross section of elastic α^6He-scattering at $E_{\text{l.f.}} = 19.6$ MeV ($E_{\text{cms}} = 11.76$ MeV) is compared with experimental data (Fig. 9).

As is seen from the figure, the contributions of all three mechanisms under consideration are comparable in magnitude, and there are both constructive and destructive (around 60°) interferences. The shape of the calculated curve matches the experimental one without introducing any additional factors that normalize the contributions coming from individual mechanisms.

The angular distribution for the angles around 50° is governed by the potential scattering. Within this angular range the contribution coming from the two-step mechanism of neutron transfer exceeds that of the dineutron transfer mechanism. Moreover, as was expected, the contribution of this mechanism to the cross section of elastic scattering is substantial for all angles, which the scattered particles are emitted at. At large angles, the contribution of mechanisms of dineutron and independent neutron transfers become dominant.

Dineutron transfer takes place in the peripheral region of a nucleus, which is equivalent to attenuation of the absorption of this cluster in the inner region of a

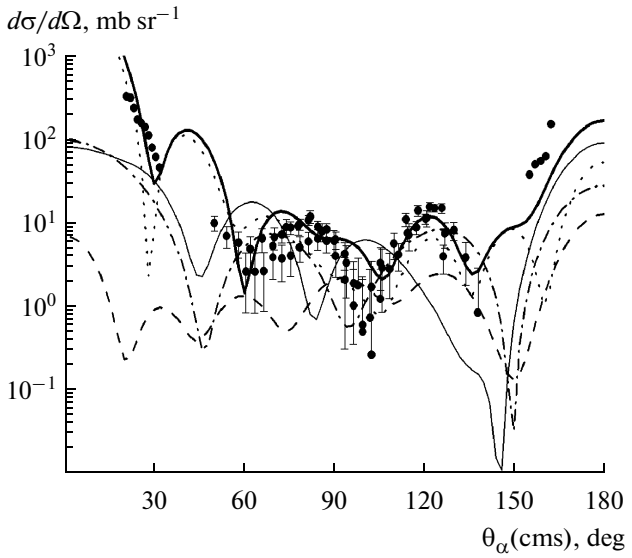

Fig. 9. Differential cross section of elastic α^6He-scattering: dotted curve—cross section of potential scattering, dashed one—dineutron transfer, dash-dotted—independent neutron transfer, solid thin one—coherent summation of contributions coming from two mechanisms of neutron transfer, solid thick curve—coherent summation of contributions coming from all mechanisms, data points—experimental data [37].

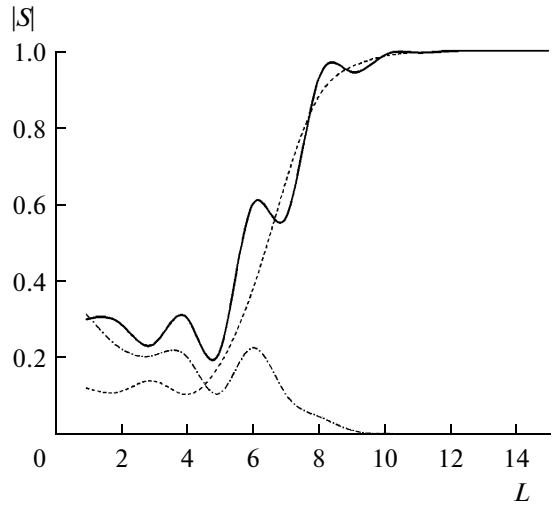

Fig. 10. Reflection coefficient as a function of L for elastic α^6He-scattering: solid curve—total η_L, dotted one—η_L^{opt}, dash-dotted one—additional component due to exchange processes $\left|a_L^0\right|$.

nucleus. In various phenomenological approaches such an attenuation is introduced in some model dependent way. All phenomenological models lead to the S-matrix nonmonotonically depending on L in the surface region of a nucleus [4]. An alternative method of taking into account dineutron transfer has these nonmonotonicities to appear microscopically.

To illustrate the nonmonotonic resonant nature of the S-matrix dependence on L, the total $\eta_L = \left|S_L^{opt} + a_L^0\right|$ and optical $\eta_L^{opt} = \left|S_L^{opt}\right|$ reflection coefficients are given in Fig. 10 along with additional terms $\left|a_L^0\right|$ associated with dineutron transfer [36].

As is seen from the figure, consideration of the dineutron transfer leads to considerable nonmonotonicity of the S-matrix both at small L and at the boundary of a nucleus for $L \sim 5$–6. The total reflection coefficient reveals a sharp change in approaching unity which is not the case for its potential counterpart. We noted that the addition terms alter the sign as $(-1)^L$; i.e., the phenomenological model with L-splitting potential can also be reproduced by adding to the

Table 2. Shape and parameters of the optical potential for elastic α^6He-scattering, as well as for entrance and exit channels in the reactions ^{9}Be$(d, p)^{10}$Be, ^{10}B$(t, p)^{12}$B, ^{13}C$(d, \alpha)^{11}$B, ^{13}C$(^3$He, $\alpha)$, ^{12}C$(0^+, 2^+)$

Channel	V, MeV	r_V, fm	a_V, fm	W, MeV	r_W, fm	a_W, fm	WD, MeV	r_{WD}, fm	a_{WD}, fm	V_{SO}, MeV	r_{S0}, fm	a_{S0}, fm	r_c, fm
$\alpha + {}^6$He	150.00	2.10	0.610				15.00	1.98	0.54				1.40
$d + {}^9$Be	73.00	1.200	0.870	14.00	1.650	0.410							1.30
$p + {}^{10}$Be	58.66	1.220	0.620				16.00	1.35	0.63				1.09
$t + {}^{10}$B	174.00	1.140	0.490	19.40	1.530	1.070							1.24
$p + {}^{12}$B	53.00	1.240	0.630	10.40	1.380	0.320							1.30
$d + {}^{13}$C	98.90	1.050	0.880				10.70	1.76	0.44	4.00	1.00	0.81	1.30
$\alpha + {}^{11}$B	212.10	1.360	0.520	15.00	1.700	0.563							1.34
^{3}He + ^{13}C	128.40	1.125	0.771	17.36	1.508	0.938							1.07
$\alpha + {}^{12}$C	199.10	1.262	0.650	42.17	1.262	0.680							1.25

Note: $V(r) = -V \cdot f(x_V) - i\left[W \cdot f(x_W) - 4WD \cdot \frac{df(x_{WD})}{dr}\right] + 2V_{SO} \cdot \frac{1}{r} \cdot \frac{df(x_{SO})}{dr} \cdot (\mathbf{L} \cdot \mathbf{S})$; $f(x_i) = \left[1 + \exp\left(\frac{r - r_{0i}}{a_i}\right)\right]^{-1}$.

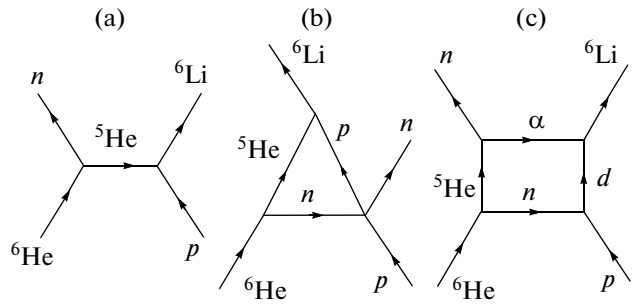

Fig. 11. Diagrams of the mechanisms for heavy particle stripping (a), exchange (b), and sequential transfer of cluster ^{5}He (c) in the reaction $p(^6\mathrm{He}, n)^6\mathrm{Li}(0^+)$.

S-matrix the term that describes dineutron transfer. In other words, introduction of the additional term a_L^0 to potential scattering allows obtaining, in the context of a unified theoretical approach, a detailed description of the features pertaining to the reflection coefficients postulated in various phenomenological models.

On the other hand, none of the phenomenological models can provide us with rich physical information about behavior of the *S*-matrix near the nuclear surface (and, thus, the cross section behavior at large angles) comparable with that obtained within a microscopic approach which is associated with taking into account dineutron transfer.

The behavior of the *S*-matrix in the surface region of a nucleus allows estimating $R_{\alpha-2n}$ in an independent way. A boundary value of $L \cong 5$ corresponds to that of $R_{\alpha-2n} \cong 4.4$ fm at energies ~ 10 MeV in a center-of-mass frame.

4.2. Differential Cross Section Calculation for the Charge Exchange Reaction p(⁶He, n)⁶Li (0⁺)

The reaction $p(^6\mathrm{He}, n\gamma)^6\mathrm{Li}$ is an example of those which are extremely important in understanding the mechanism of light element formation in the universe. During nucleosynthesis a large cross section of the reactions with loosely bound nuclei (^{6}He, ^{9}Li, ^{7}Be, etc.) can alter a chain of β-decays, leading to formation of various elements [40], and, therefore, a whole scenario of nucleosynthesis.

While calculating a differential cross section of the charge exchange reaction $p(^6\mathrm{He}, n)^6\mathrm{Li}$ (0^+, 3.56 MeV), the mechanisms of ^{5}He heavy cluster stripping, virtual neutron exchange by proton in the field of ^{5}He cluster, and sequential transfer of a neutron and α-particle, illustrated by the diagrams shown in Fig. 11, are taken into account.

Since there is a lack of experimental data on this reaction in the energy range of ~ 10 MeV/nucleon, results obtained for the differential cross section of this reaction are predictive in nature.

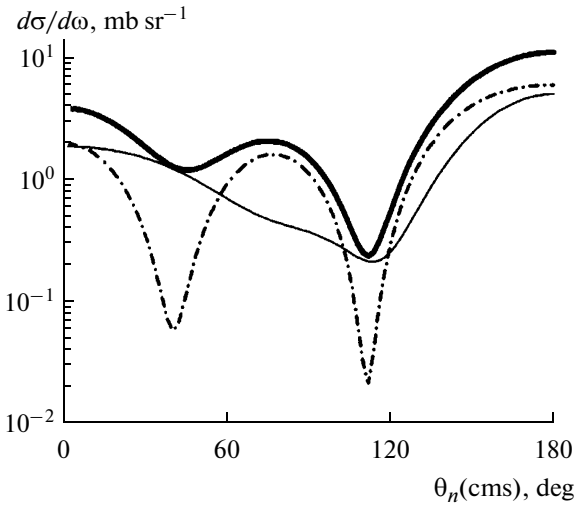

Fig. 12. Differential cross section of the reaction $p(^6\mathrm{He})^6\mathrm{Li}(0^+)$; solid thin curve—contribution from the mechanisms of heavy particle stripping and exchange, dashed one—sequential transfer of clusters, solid one—the total cross section.

The cross section calculations of the reaction $p(^6\mathrm{He}, n)^6\mathrm{Li}(0^+)$ at $E_{\mathrm{cms}} = 9$ MeV done by us within the framework of HMS method (Hybrid Monte Carlo Simulation) [41], showed that the angular distribution of neutrons in this reaction, produced in pre-equilibrium processes, is concentrated within the range of angles of up to 10° at which neutrons are emitted. Neutron production at larger angles occurs due to direct mechanisms.

The optical potentials used in the calculations are defined in the context of a global potential [42], implemented by using the package EMPIRE [43]. We took these potentials "as-is". Specific values of their parameters are presented in Table 2. The coefficients of ^{6}Li (0^+; 3.56 MeV, $T = 1$) wave function expansion, carried out over the basis of *LS*-coupling, necessary for the calculation of spectroscopic factors, are taken from [35]. A spectroscopic factor for the mechanism of heavy particle stripping and exchange was found to be $\Theta^{J_1=1 J_2=1}_{\Lambda_1=1 \Lambda_2=1 l=0} = 0.693$. The spectroscopic factor values for the quadrangle diagram are given in Table 3.

The calculated contributions coming from every individual mechanism and the total differential cross section as a function of a neutron emission angle are shown in Fig. 12.

The cross sections of all mechanisms under consideration are comparable in magnitude. A coherent contribution of the heavy stripping and exchange mechanisms is almost isotropic up to angles of $\theta_n \sim 120°$. However, at larger angles it increases. A contribution of the independent cluster transfer mechanism is of oscillating nature, featuring the main maximum located at large angles. A total differential cross section of the

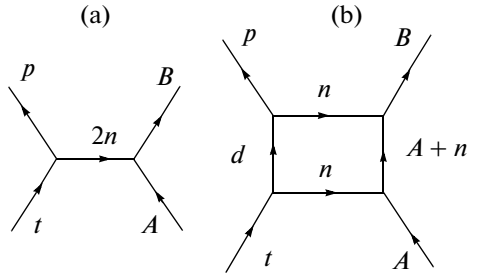

Fig. 13. Diagrams of the mechanisms for dineutron cluster transfer in the reaction $A(t, p)B$: (a) dineutron pickup; (b) sequential transfer of neutrons.

charge exchange reaction with all three mechanisms taken into account has a weak oscillatory dependence on θ_n with a maximum at $\theta_n = 180°$. A total cross section of the reaction is found to be ≈ 0.56 b.

4.3. Differential Cross Section Calculation for the Reaction ^{7}Li(t, p)^{9}Li

We calculated a differential cross section of the reaction ^{7}Li$(t, p)^9$Li at tritium energy $E_{\text{cms}} = 9$ MeV within the framework of the mechanisms of dineutron pickup and sequential neutron transfer (respective diagrams are shown in Fig. 13).

The parameters of calculation (optical potentials and structure factors) are defined in the same way as for the charge exchange reaction. The coefficients of ^{7}Li ground state wave function expansion over the basis of *LS*-coupling are taken from [35]. The ground state of ^{9}Li has a total spin $J = 3/2$, orbital angular momentum $L = 1$, and isospin $T = 3/2$. This means that two excess neutrons in ^{9}Li occupy a free subshell of $1p_{3/2}$ shell. The structure factor values in the reaction ^{7}Li$(t, p)^9$Li are presented in Table 4, while a calculated differential cross section of the reaction is given in Fig. 14.

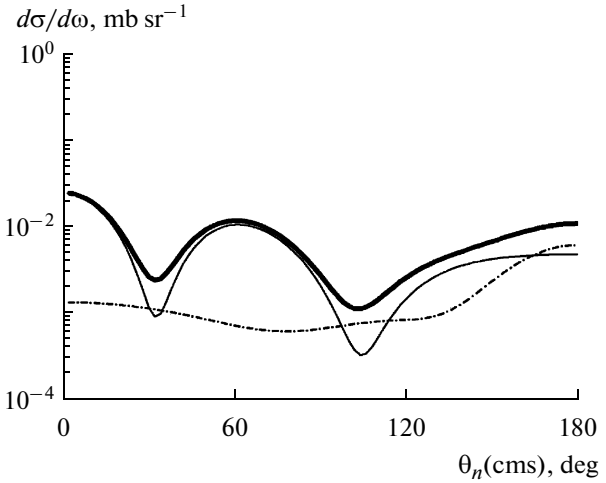

Fig. 14. Differential cross section of the reaction ^{7}Li$(t, p)^9$Li: solid thin curve—contribution from the dineutron transfer mechanism, dash-dotted one—independent neutron transfer mechanism, solid one—their coherent sum.

As is seen from the figure, a leading contribution to the total cross section comes from the dineutron cluster transfer mechanism. Nevertheless, the independent neutron transfer mechanism noticeably smoothes out the angular distribution minima and its contribution is comparable with that coming from the mechanism of dineutron cluster transfer at large angles. This fact indicates that in the reaction (t, p) both possible two-neutron configurations of nucleus ^{9}Li should appear.

Table 3. Spectroscopic factors $\Theta^{J_{n1}J_{n2}}_{\Lambda_{n1}\Lambda_{n2}l_n}$ for each stage of the two-step mechanism in the reaction ^{6}He$(p, n)^6$Li(0^+) ($l_n = 1$, $J_{n2} = 0$, $\Lambda_{n2} = 0$)

Mechanism's stage	J_{n1}	Λ_{11}	Λ_{21}
		1	2
Lower part of diagram	1/2	0.521	
Upper part of diagram	1		−0.666
	0		

Table 4. Spectroscopic factors $\Theta^{J_1J_2}_{\Lambda_1\Lambda_2 l}$ for direct mechanisms of dineutron cluster pickup and heavy particle exchange ($J_2 = \Lambda_2 = 0$), $\Theta^{J_{n1}J_{n2}}_{\Lambda_{n1}\Lambda_{n2}l_n}$ for each stage of the two-step mechanism in the reaction ^{7}Li$(t, p)^9$Li ($l_1 = l_2 = 1$, $J_{12} = J_{22}$, $\Lambda_{12} = \Lambda_{22} = 0$, $\Lambda_{11} = \Lambda_{21} = 1$)

		J_1 \ Λ_1	0	2
Mechanisms of dineutron pickup and heavy particle exchange		0	0.205	
		2		0.145
Stages of two-step mechanism	lower part of diagram $n = 1$	J_{11} \ J_{22}	1/2	3/2
		1	−0.077	−0.155
	upper part of diagram $n = 2$	J_{21} \ J_{22}	1/2	3/2
		1	0.050	−0.099

4.4. Differential Cross Section Calculation for the Reaction ^{9}Be(d, p)^{10}Be

In the reaction ^{9}Be(d, p)^{10}Be two pole mechanisms are possible, which describe the processes of direct deuteron interaction with nucleus ^{9}Be: neutron stripping (a pole diagram in Fig. 15a) and exchange by a heavy cluster ^{8}Li (a pole diagram in Fig. 15b). Analysis of the results of correlated measurements in the reaction ^{9}Be(d,p)^{10}Be carried out in [44, 45] showed high sensitivity of the characteristics to the structure of the wave functions and demonstrated necessity of accounting for the multistep reaction mechanisms. This conclusion drawn in [44, 45] does not look surprising, as it is the experiments on inelastic scattering of deuterons off nucleus ^{9}Be [10], where the effects, which can be interpreted as a manifestation of two-step mechanisms, were for the first time discovered. Therefore, in the reaction^{9}Be(d,p)^{10}Be we considered the additional mechanism of sequential neutron and dineutron (the quadrangle diagram shown in Fig. 15c) transfer.

The mechanism of neutron and dineutron transfer in the four-body approximation corresponds to the initial channel (2,2). To evaluate the matrix element of this mechanism we considered a diagram in Fig. 15c, as well as that shown in Fig. 6, as a convolution of two pole mechanisms, which arise upon cutting up a whole quadrangle diagram into two independent position spaces. By using the convolution method described in Sec. 3, an expression for the matrix element, coinciding with (55) up to phase and normalization factors, was obtained. In addition, an expression for the matrix element gets greatly simplified, as the orbital angular momenta transferred are zero at decay vertices in the right hand side of the diagram shown in Fig. 15c, and the total momenta of dineutron, p, n, d, and t are equal to their spins.

For the mechanisms corresponding to quadrangle diagrams with multi directional lines, similarity of the wave functions of transferred virtual particles is independent of their energies [12, 13]. The contribution to the cross section of the reaction ^{9}Be(d, p)^{10}Be coming from the two-step mechanism is mainly due to the structural features of nuclei that take part in the reaction: the values of transferred spins and orbital angular momenta, reduced widths at decay vertices and so on.

The matrix elements of the pole mechanisms were calculated in DWBAFR [4] according to Eq. (31). The reduced widths were computed by using the shell model with intermediate coupling [35]; the structure factors, in the representation of transferred total J and orbital angular l momenta and spin s [30]. For the neutron stripping in the reaction ^{9}Be(d, p)^{10}Be the structure factor $\Theta^{l=1}_{s=1/2\,J=3/2}$ has a single value of 0.769. The matrix element of ^{8}Li heavy cluster stripping turned out to be irrelevant due to the smallness of recoil effects and was not taken into account. The structure

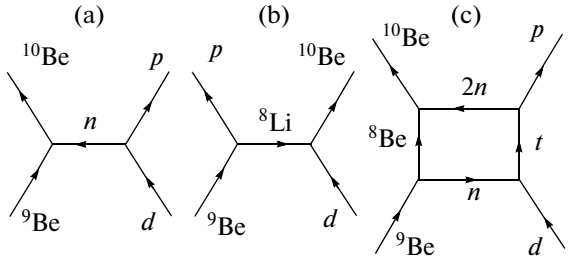

Fig. 15. Diagrams of the mechanisms for the reaction ^{9}Be(d, p)^{10}Be: (a) neutron stripping, (b) stripping of heavy cluster ^{8}Li, (c) two-step mechanism of sequential neutron pickup and dineutron stripping.

factor for a quadrangle diagram was determined through those of the neutron pickup and dineutron stripping. Here $l_1 = 1$, and the orbital angular momentum l_2, which is equal to the spin of intermediate nucleus ^{8}Be, can take the values 0 or 2, because of two $1p$-neutrons transferred in the upper part of the diagram in Fig. 15c during decay of a final nucleus. In the case of $l_2 = 0$ the structure factor has a single value of 0.280, with the total orbital angular momentum l transfer equal to unity.

While calculating the structure factor for $l_2 = 2$ the following circumstance should be kept in mind. ^{8}Be nucleus in the state 2^+ is an unbound system and cannot be interpreted in the context of the shell model. Therefore, the wave functions of relative motion of ^{8}Be + $2n$ with extended asymptotic are less than the shell ones in the inner region of nucleus ^{10}Be. As a result, shell values of the reduced widths for such systems are deliberately overestimated and should be normalized. Such normalization was carried out in [44] as well. Specific values of the structure factor $\bar{\Theta}^{J_1 J_2}_{l_1 l_2 l}$ (with a normalization coefficient of 0.5 for $l_2 = 2$) are given in Table 5.

As is seen from this table, the total orbital angular momentum l transfer can take the values from 1 to 3. Angular dependence of the matrix element of the independent particle transfer mechanism results from the vector addition of the momentum l with both the momenta of partial components of distorted waves in the initial and final reaction channels and the momentum Λ, which defines an expansion of the Green's

Table 5. Spectroscopic factors $\bar{\Theta}^{J\,s}_{l_1 l_2 l}$ in the reaction ^{9}Be(d, p)^{10}Be for the mechanism of independent neutron and dineutron transfer ($J = 3/2$, $l_1 = 1$, $s = 1/2$)

l_2 \ l	1	1	2	3
0	0.27995			
2		0.08173	−0.00002	0.00001

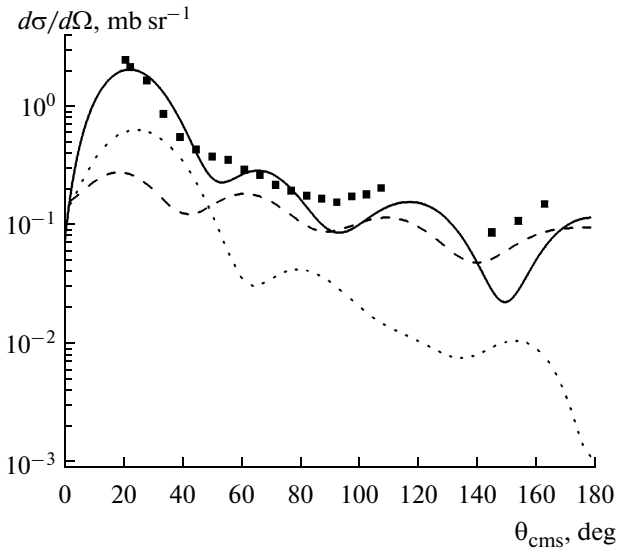

Fig. 16. Angular distribution of protons in the reaction ^{9}Be(d, p)^{10}Be at E_d = 15 MeV: squares—experimental cross section [44], solid thick curve—overall angular distribution with accounting for all mechanisms, dashed one—cross section of the stripping mechanism, dotted one—cross section corresponding to the mechanism of sequential neutron pickup and dineutron stripping .

function of virtual intermediate system $t + {}^8$Be. Therefore, it is nearly impossible to predict the shape of an angular distribution of protons for the mechanism of independent transfer of a neutron and dineutron without doing specific calculations.

For the reaction ^{9}Be(d,p)^{10}Be we calculated differential cross sections for the mechanisms of neutron stripping and sequential transfer of a neutron and dineutron, along with a total differential cross section defined as a coherent sum of the amplitudes of these two mechanisms. The optical potential parameters for $d + {}^9$Be and $p + {}^{10}$Be in the initial and final reaction channels somewhat differ from those which were used in [44, 45]; they are presented in Table 2.

The results of calculations for the angular distribution of protons—the products in this reaction—are shown in Fig. 16. As is seen from this figure, both mechanisms of neutron stripping and independent transfer of a neutron and dineutron give comparable contributions to the cross section of the reaction ^{9}Be(d,p)^{10}Be throughout an entire angular range of proton emission. The cross section of neutron stripping mechanism unlike respective experimental data has an oscillating shape for all angles, since it is fixed by a single value of the momentum transfer $l = 1$. The cross section of the two-step mechanism for relatively small angles of proton emission has wider maximum (its value at $\theta_p \approx 20°$ even somewhat exceeds that of the cross section for the neutron stripping mechanism) and smoother angular dependence at larger angles. An overall curve describes the experiment quite satisfactorily, if it is remembered that no extra normalization constants were introduced during calculations and the wave function of ^{10}Be was not varied as it was done in [44] in the context of the method of coupled channels.

4.5. Differential Cross Section Calculation for the Reaction $^{10}B(d, p)^{11}B$

Correlated measurements in the reaction ^{10}B(d, p)^{11}B at E_d = 15.3 MeV with formation of nucleus ^{11}B in the ground ($3/2^-$) and two lower $1/2^-$ (2.125 MeV) and $5/2^-$ (4.445 MeV) excited states [46] yielded angular and energy dependences of the differential cross sections of this reaction.

Theoretical analysis of experimental results [46] made it possible to estimate a contribution to the mechanism of the reaction ^{10}B(d, p)^{11}B coming from the processes more involved that the neutron stripping: firstly, collective excitation of nonspherical nuclei of boron was considered by using the coupled channel method (CCM) [47]; secondly, effects of second order in perturbation theory by two-step mechanisms [31]. Of particular interest is the formation of a final nucleus in the state $1/2^-$ (2.125 MeV). The latter state cannot be formed by stripping a neutron (at the momentum transfer $l = 1$), whereas in the experiment it is excited quite intensively, and the angular distribution of the differential cross section is observed to rise at small angles, which is characteristic of a direct process.

The reactions with ^{10}B are traditionally difficult for a theoretical interpretation of their mechanism. On the one hand, nucleus ^{10}B resides in the middle of 1p-shell and it is hard to describe its stationary characteristics by various models. In particular, in the shell model the wave function of the ground state of nucleus ^{10}B [35] contains two different components with the same values of the quantum numbers of this model (an orbital angular momentum, spin, etc.), so that for a complete description of these components one is forced to introduce additional quantum numbers of SU_3 scheme. The latter circumstance means that the shell model cannot provide us with correct spectroscopic factors for various channels of ^{10}B decay, and a nucleus itself in the ground state has a considerable static deformation. On the other hand, since the total spin J of the ground state of ^{10}B is anomalously large ($J = 3$), many components, differing in the total and orbital angular momenta and spins transfers, contribute to the reaction amplitude.

CCM and its implementation in the program CHUCK [47], which is adapted for producing an output containing the spin-tensor components of the density matrix for a final nuclei ^{12}B*, were used to take into account collective excitation of boron nuclei. The sets of parameters for the Woods–Saxon optical potentials used in CCM calculations are given in Table 2.

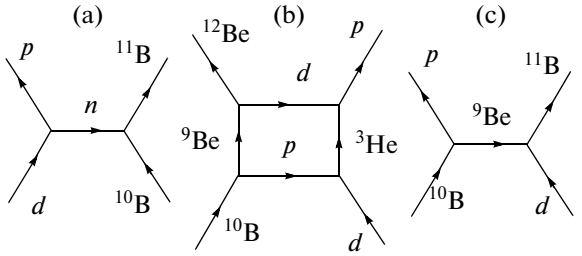

Fig. 17. Diagrams of the mechanisms: neutron stripping (a), two-step particle transfer (b), and heavy particle stripping (c), in the reaction ^{10}B $(d, p)^{11}$B.

There are three mechanisms describing the processes of direct interaction between deuterons and nucleus ^{9}Be that are possible in the reaction ^{10}B$(d, p)^{11}$B: neutron stripping (a pole diagram in Fig. 17a); its second order correction, two-step mechanism of particle transfer (the quadrangle diagram shown in Fig. 17b); and a pole mechanism of heavy cluster transfer (Fig. 17c). The contribution of the latter mechanism turned out to be small and was not taken into account.

The matrix element of the reaction was calculated according to Eq. (57). The contributions from the first two mechanisms are summed up coherently. During calculations, the optical potential parameters are taken to be the same as in those carried out within the CCM framework (Table 2). The spectroscopic factors for various mechanisms of this reaction were evaluated in the context of the shell model with intermediate coupling [35]. Because of their overwhelming number, a corresponding table will not be presented here.

The results of calculations for the differential cross sections of the reaction ^{10}B$(d, p)^{11}$Bwith formation of nucleus ^{11}B in the ground and $1/2^-$ (2.125 MeV) states are given in Fig. 18.

Both DWBAFR (without a nuclear deformation taken into account) and CCM are in good agreement with experiment for the transition to the ground state of a final nucleus (Fig. 18a). Since formation of the state $1/2^-$ (2.125 MeV) of nucleus ^{11}B in the reaction ^{10}B$(d, p_1)^{11}$B in the frame of the neutron stripping mechanism is forbidden by the selection rules, the matrix element for this state was calculated for the two-step mechanism (Fig. 18b) according to Eq. (55). The contribution of the two-step mechanism to the angular distribution of protons with formation of ^{11}B ($1/2^-$, 2.125 MeV) without any additional normalizations is shown in Fig. 18b. The states $3/2^-$ (0.0 MeV), $5/2^-$ (2.429 MeV), and $7/2^-$ (6.76 MeV) of virtual nucleus ^{9}Be were all accounted for in the calculations. As is seen form the figure, a decisive role is played by the two-step mechanism with formation of virtual nucleus ^{9}Be in the states $3/2^-$ and $7/2^-$. This latter mechanism, along with the pole one of heavy particle stripping (a diagram in Fig. 17c), satisfactorily

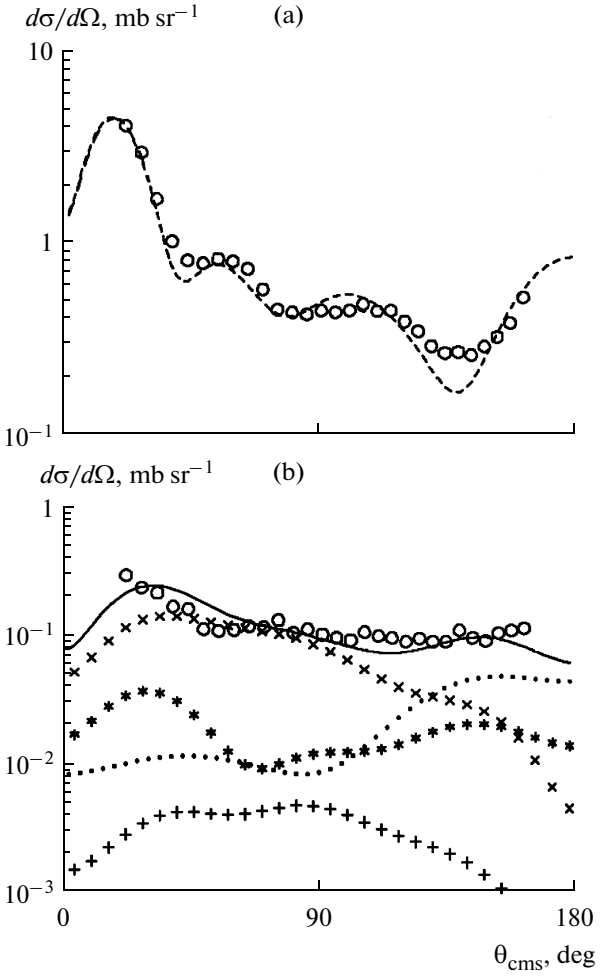

Fig. 18. Angular dependences of differential cross section of the reaction ^{10}B$(d, p)^{11}$B at $E_d = 15.3$ MeV with formation of a final nucleus in the ground ($3/2^-$) (a) and excited ($1/2^-$) (b) states. Experimental results are shown with circles. Statistical uncertainties do not exceed a circle size. Curves are results of calculations for various reaction mechanisms assumed: dashed one—neutron stripping according to CCM with parameters of deformation $\beta = -0.55$ and $\beta = 0.4$; dotted one—heavy particle stripping. The mechanism which takes into account delay is represented by curves corresponding to different states of intermediate nucleus ^{9}Be: $3/2^-$ (×), $5/2^-$ (+), and $7/2^-$ (*). A solid curve corresponds to the sum of contributions from all mechanisms.

describe experimental data over almost the entire angular range.

Analysis of the angular and energy dependences of the differential cross section for the (d, p)-reaction on nucleus ^{10}B with formation of the states $3/2^-$ (0.0 MeV) and $1/2^-$ (2.125 MeV) of a final nucleus showed that taking into account the two-step mechanisms naturally explains intense excitation of the state $1/2^-$ (2.125 MeV) of a final nucleus in the reaction considered.

Table 6. Spectroscopic factors $\bar{\Theta}^{J\,s}_{l_1 l_2 l}$ in the reaction ^{10}B(t, p)^{12}B for the mechanism of independent neutron transfer ($l_1 = l_2 = 1$)

J	2		3
l \ s	0	1	1
1		−0.0968	
2	0.8256	0.2806	0.1597

4.6. Differential Cross Section Calculation for the Reaction $^{10}B(t, p)^{12}B$

The reaction ^{10}B(t, p)^{12}B has attracted the attention of the researchers, both theoreticians and experimenters, for the past several decades. For this reaction, the spin values of initial and final nuclei are such that for the dineutron cluster stripping mechanism an orbital angular momentum transferred to the nucleus ^{12}B can have a single value $l = 2$. Meanwhile, an experimental angular distribution of protons [48] is sufficiently smooth, has no pronounced diffraction structure, characteristic of the cluster stripping mechanism, and does not exhibit a maximum associated with such an angular momentum transfer for the proton emission angles appreciably different from zero. Such a behavior of the differential cross section gives us a reason to believe that in the reaction ^{10}B(t, p)^{12}B a significant role should be played by the sequential neutron transfer mechanism.

This mechanism in the reaction ^{10}B(t, p)^{12}B with formation of virtual intermediate system $d + {}^{11}$B was earlier considered in [11] at a qualitative level (plane wave and zero-interaction-range approximations were used with introduction of normalization factors). Nevertheless, even in these approximations it is such a mechanism that explained the fact that the shape of an angular distribution of protons was not determined by the angular momentum transfer, allowed by the selection rules for the dineutron cluster stripping mechanism.

We have already noted in Sec. 2 dependence of the contribution of two-step mechanism on a lack of similarity between the wave functions of transferred particles. In the reaction ^{10}B(t, p)^{12}B this lack of similarity between the wave functions of transferred neutrons is ensured by the large difference in virtual energies of neutrons (Eq. (27)), as well as structural features of nuclei.

In [49], we calculated the cross section of the reaction ^{10}B(t, p)^{12}B with taking into account the pole mechanisms of dineutron stripping, as well as the mechanism of sequential transfer of two neutrons (Fig. 13). It was shown that the contribution coming from the mechanism of heavy cluster stripping contributes is small and can be neglected.

The matrix element calculation for the dineutron cluster stripping (a pole diagram shown in Fig. 13a) was performed in DWBAFR [4]. The structure factors were calculated in the representation of the total J and orbital angular l momenta and spin s transfers [30]. As the dineutron spin $s = 0$, the orbital angular l and total J momenta appear to be equal to each other so that in the reaction ^{10}B(t, p)^{12}B the structure factor $\bar{\Theta}^{l=2}_{s=1/2J=2}$ has a single value equal to 0.811.

The matrix element for the two-step mechanism of neutron transfer illustrated by the quadrangle diagram shown in Fig. 13b with unidirectional lines was calculated according to Eq. (55).

For the reaction ^{10}B(t, p)^{12}B $l_1 = l_2 = 1$, $s_1 = s_2 = 1/2$, the total momentum J transfer can take the values 2, 3, 4, while the orbital angular one $l = 1, 2$. In Table 6, the spectroscopic factors are presented for all combinations of l, s, J allowed by the selection rules.

As is seen from this table, the components of $\bar{\Theta}^{J_1 J_2}_{l_1 l_2 l}$ with $l = 2$ are the dominant ones for the mechanism of sequential neutron transfer.

The cross section calculation for the reaction (t, p) was carried out according to Eq. (57) by coherently summing up the matrix elements of both mechanisms considered. The optical potential parameters in the initial and final channels are taken the same as in [49] (Table 2).

The calculated angular distribution of protons, which are the products of the reaction ^{10}B(t, p)^{12}B, is shown in Fig. 19. The calculated cross sections for each of the mechanisms under consideration turned out to be sufficiently robust to small variations in the parameters of optical potentials. The dineutron stripping mechanism gives a leading contribution to the cross section, though an angular distribution of protons for this one has a more pronounced diffraction structure in comparison to experiment than was expected. A contribution to the total cross section coming from the mechanism of sequential neutron transfer is considerably smaller than that of the two-step mechanism in the reaction ^{9}Be(d, p)^{10}Be. Nonetheless, at small proton emission angles it is comparable with a contribution coming from the stripping mechanism, which leads to an increase of the cross section at small θ_p and has the latter raised at the first minimum in the angular distribution. An overall curve obtained by coherently summing up the amplitudes of both mechanisms is in good agreement with experiment and reproduces all of its characteristic features.

Thus, we showed that taking into account the corrections which come from the two-step mechanisms dramatically improves the agreement between theoretical angular distributions of the products obtained

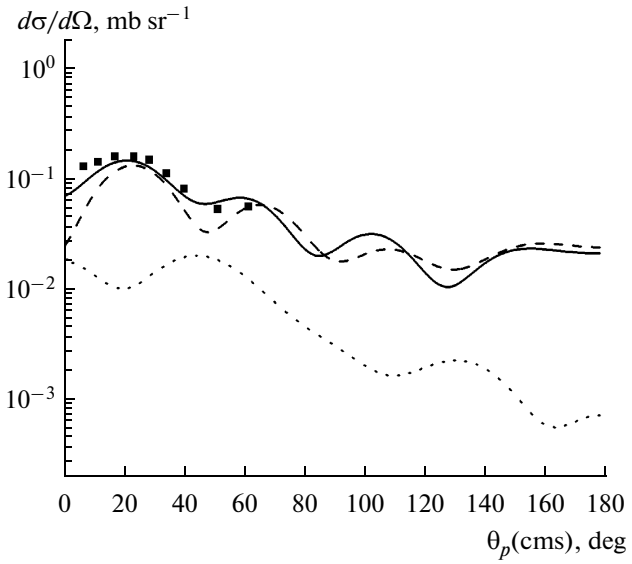

Fig. 19. Angular distribution of protons in the reaction $^{10}B(t, p)^{12}B$ at $E_t = 21$ MeV: squares—experimental cross section [48]. Designations of theoretical curves are the same as in Fig. 16.

in the reactions with light nuclei and corresponding experimental data.

5. NEUTRON PERIPHERY OF LIGHT NEUTRON-EXCESS NUCLEI

The study of light neutron-excess nuclei in reactions with radioactive beams has recently become one of the topical problems in modern nuclear physics, primarily due to discovery of nuclei with extended nucleon periphery, the so-called halo nuclei. Detailed experimental studies of the spectroscopy of hydrogen and lithium isotopes with large (about 4–5) excess of neutrons were undertaken in [50–56]. In the experiments [50–53], conducted in an inverse geometry, certain shapes of spatial distribution of the nucleons in neutron-excess nuclei were identified by using complex correlation techniques. However, even the lightest nuclei with two excess neutrons are still not well understood both in terms of their spectroscopy and the topology of spatial distribution of neutrons, which form an outer halo, and the remaining nuclear core.

The nuclei of 1p-shell with two excess neutrons can have two spatial configurations, differing in neutron location relative to the core (Fig. 20). The first one (a dineutron configuration) features the neutrons located very close to each other with their center of mass far from the core. The second (cigarlike) configuration consists of uncorrelated neutrons located on opposite sides of the core. The existence of such configurations together with an estimate of their relative contribution to the nuclear periphery was experimentally confirmed and investigated in some detail both theoretically [57–62] and experimentally [57, 63, 64] in the most studied neutron-excess nucleus ^{6}He.

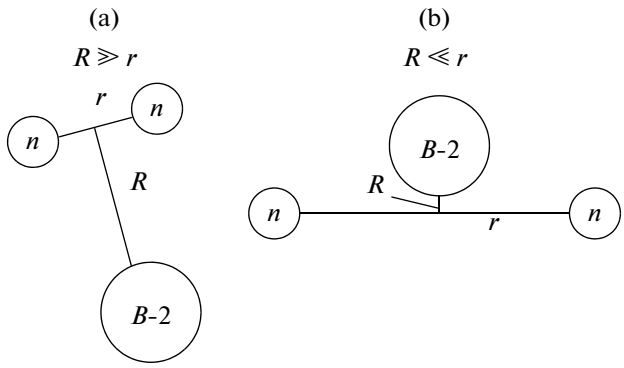

Fig. 20. Possible spatial configurations of two excess neutrons in light nuclei: (a) dineutron, (b) cigarlike.

We used the analysis of angular distributions of the cross sections in the reactions with formation of such nuclei and taking into account one- and two-step mechanisms, for the method capable of detecting each of two spatial configurations of a neutron-excess nucleus. Description of experimental data on the reaction cross sections throughout the entire angular range allowed us to correctly estimate the contribution coming from each of the mechanisms, reconstruct the wave function of relative motion of excess neutrons and a core-nucleus, and study the configuration of neutron periphery.

5.1. The Structure of ^{6}He Nucleus Manifested in the Elastic α^6He Scattering

Theoretical works that address an issue of the wave function configuration in a neutron-excess nucleus ^{6}He in the context of the three-body model [58] and K-harmonic method (with $K = K_{min}$, $K_{min} + 2$) [59] predict the presence of two different spatial configurations: dineutron and cigarlike ones (Fig. 20). A quite satisfactory description of the experimental cross section for α^6He-scattering obtained for all angles and with taking into account various mechanisms (see previous section) allows reconstructing of the wave function of relative motion of an α-particle and a dineutron, just like that of a neutron and α-particle and a neutron and ^{5}He in the ground state of ^{6}He. We obtained desired wave functions by applying the WDP-procedure [25], which consists of choosing the depth of respective potentials, setting the nuclear binding energy according to decay channels, the number of nodes of desired functions, and the geometrical parameters of potentials.

The rms radii for each of the configurations calculated with these functions are almost identical and equal to $\cong$4.2 fm, which is consistent with theoretical estimates [58, 59]. Presence of dineutron cluster con-

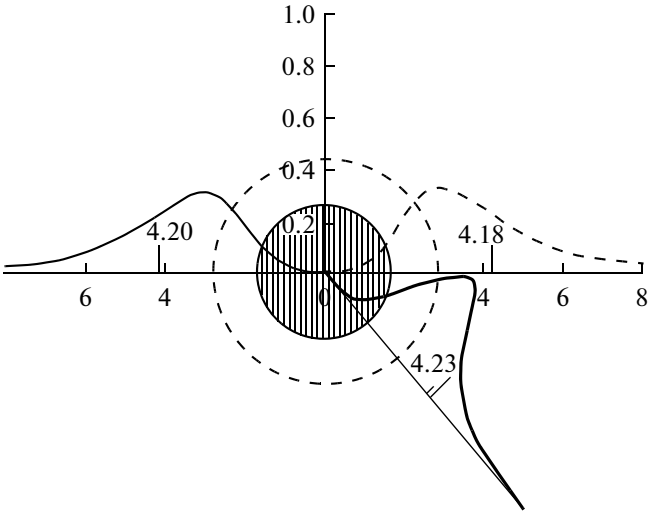

Fig. 21. A schematic diagram of the neutron peripheral structure for ^{6}He, reproduced in elastic α^6He-scattering. A central shaded circle denotes α-particle (R = 1.67 fm [66]), while a dashed circumference corresponds to the radius of ^{6}He (R = 2.9 fm [37, 55, 57–59, 66]). Curves stand for the probability densities of various two-neutron configurations: solid thick one—dineutron $2n - \alpha$ (R = 4.44 fm), solid thin one—single-neutron $n_1 - {}^5$He (R = 4.20 fm), dashed curve—single-neutron $n_2 - \alpha$ (R = 4.18 fm).

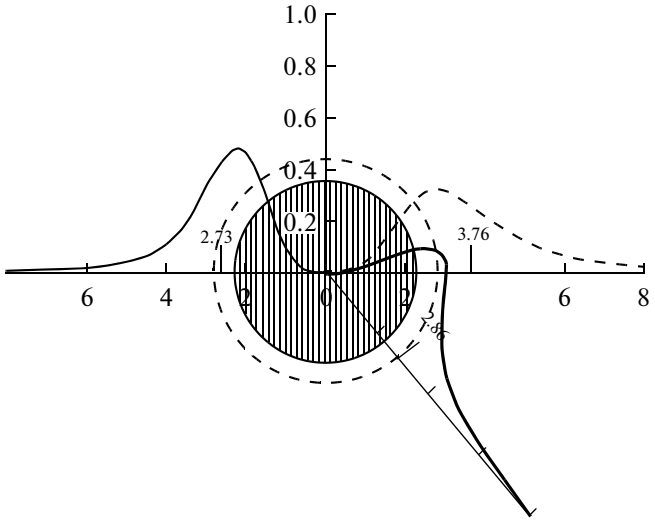

Fig. 22. A schematic diagram of the neutron peripheral structure for the ^{10}Be nucleus. A central shaded circle denotes ^{8}Be nucleus (R = 2.2 fm [66]), while a dashed circumference corresponds to the radius of ^{10}Be (R = 2.8 fm [66]). Curves stand for the probability densities of various two-neutron configurations: solid thick one—dineutron $2n - {}^8$Be (R = 2.86 fm), solid thin one—single-neutron $n_1 - {}^9$Be (R = 2.73 fm), dashed curve—single-neutron $n_2 - {}^8$Be (R = 3.76 fm).

figuration in the wave function of the ground state of ^{6}He is a prerequisite for describing the inverse maxima of the cross section for elastic α^6He-scattering. Another possible n_1–α–n_2 "cigarlike" spatial configuration of ^{6}He actualizes the two-step mechanism of neutron transfer, which contributes noticeably at all particle emission angles. Despite the differing weights in the wave function of ^{6}He nucleus, they are important for describing the cross sections of elastic α^6He-scattering. Thus, a neutron periphery of ^{6}He nucleus manifests itself as a well-formed two-neutron halo, since the radius of each configuration is more than twice as large as that of the core, which is nucleus ^{4}He (1,67 fm [66]), and 1.3 times larger than the radius of ^{6}He nucleus (2,9 fm [37, 55, 57–61, 66]). The neutron periphery structure of ^{6}He nucleus, shown in Fig. 21, demonstrates the presence of both halo components sufficiently far from the core (an α-particle).

It might be expected that such a structure of the ^{6}He nucleus will manifest itself in the reactions of a fragmentation of this nucleus by heavy nuclei. Indeed, a dineutron configuration gives a leading contribution to the cross section of ^{6}He fragmentation reaction with energy of 20–60 MeV on photoemulsion stacks [63, 64]. A cigarlike configuration is likely to manifest itself in the reactions of ^{6}He fragmentation on heavy nuclei at larger energies (0.8 GeV/nucleon) [67]. Let us emphasize that in the elastic α^6He-scattering a two-neutron halo of ^{6}He displays both dineutron and cigarlike configurations.

5.2. The Structure of a Neutron Halo in Nuclei ^{10}Be and ^{12}B

Determining the contributions to the cross section of the reaction ^{9}Be$(d,p)^{10}$Be (^{10}B$(t, p)^{12}$B) coming from various mechanisms, done in the previous section, allows us to reconstruct (in the context of the WDP-procedure) the wave function of relative motion of ^{8}Be (^{10}B) and a dineutron, as well as ^{8}Be (^{10}B) and both neutrons in the ground state of ^{10}Be (^{12}B).

Consider the behavior of the wave functions obtained separately for each nucleus.

The neutron periphery structure of ^{10}Be nucleus in the ground state is presented in Fig. 22. A ^{8}Be nucleus is shown in the figure by a shaded central circle. Various curves show the probability densities for the wave functions (quantities $(r\Psi_l(r))^2$) of relative motion of a dineutron and ^{8}Be, as well as each of the neutrons and the respective nuclear core. The rms radii (indicated by arrows) calculated for possible configurations of neutron periphery in ^{10}Be substantially differ from each other. While calculating the rms radius of relative motion of a dineutron and ^{8}Be it is necessary to take into account that for this system the orbital angular momentum $l_2$can take the values 0 and 2. However, as a reduced decay width for $^{10}\text{Be} \to {}^8\text{Be} + 2n$ with $l_2 = 0$ is

considerably larger than that with $l_2 = 2$ (see Table 5), we defined the rms radius of such a configuration to be equal to 2.86 fm. The rms radii for both neutron configurations are given by the probability densities with orbital momentum $l = 1$; their values are found to be R (^{8}Be + n_1) = 3.76 fm, R (^{9}Be + n_2) = 2.73 fm. As is seen form the figure, this structure significantly differs from the neutron periphery of nucleus ^{6}He (Fig. 21).

The neutron periphery structures in these nuclei differ in the first place in the behavior of a dineutron configuration: while in the elastic α^6He-scattering it is the configuration that forms a neutron halo, in the reaction ^{9}Be(d, p)^{10}Be it manifests itself only near the surface of nucleus ^{10}Be ($R_{^{10}\mathrm{Be}} \cong 2.8$ fm); i.e., represents a dineutron "skin". The one-neutron configurations of ^{10}Be, formed in this reaction, cannot be regarded as cigarlike since they are not symmetric; their rms radii differ by more than 1 fm. This difference in radii leads to the observation that if one of the neutrons is located almost on the surface of ^{10}Be, abutting on a dineutron "skin", then the second one (a decay product of virtual ^{9}Be nucleus) is noticeably far from the core-nucleus and forms a faint halo. Furthermore, in ^{6}He the halo radius is about 1.5 times larger than that of ^{6}He. In ^{10}Be such a ratio for the configuration ^{8}Be + n_1 is $\approx$1.3 (for all remaining configurations it is less than unity). Such a structure of the neutron periphery explains significant probability for ^{9}Be nucleus to be dissociated, and, thus, the magnitude of the contribution coming from the mechanism of sequential particle transfer in the reaction ^{9}Be(d, p)^{10}Be.

The neutron periphery of nucleus ^{12}B is presented in Fig. 23. A central shaded circle denotes the ^{10}B nucleus. The curves show the probability densities for the wave functions of relative motion of a dineutron and ^{10}B with $l = 2$ and relative n_1–^{11}B, n_2–^{10}B motion with l_1, $l_2 = 1$ found by analyzing the cross sections of the reaction ^{10}B(t, p)^{12}B. The respective rms radii (indicated by arrows) considerably differ from each other and have the following values: for $2n$–^{10}B-configuration—2.96 fm, for n_1–^{11}B-configuration—2.78 fm, and for n_2–^{10}B-configuration—2.21 fm. If one takes note of the fact that the radius of ^{12}B nucleus is 2.84 fm [66], then, it can be argued that, in this reaction, a neutron halo in nucleus ^{12}B is actually seen as a dineutron "skin" on its surface, with a ratio of the radius of the latter to that of ^{12}B $\approx$ 1.

The analysis showed significant difference between the two-neutron peripheries in nuclei ^{6}He, ^{10}Be, and ^{12}B. If a first nucleus this halo exists in both dineutron and "cigarlike" configurations, which gives a cross section of the elastic α^6He-scattering, then such a halo in nuclei ^{10}Be and ^{12}B in the reaction (t, p) is actually not observed.

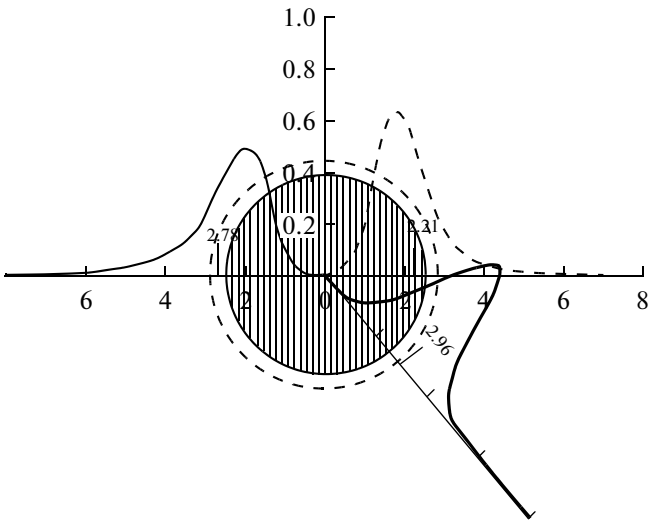

Fig. 23. A schematic diagram of the neutron peripheral structure for the ^{12}B nucleus. A central shaded circle denotes ^{10}B nucleus (R = 2.84 fm [66]), while a dashed circumference corresponds to the radius of ^{12}B (R = 2.84 fm [66]). Curves display the probability densities of various configurations: solid thick one—dineutron $2n$ – ^{10}B (R = 2.96 fm), solid thin one—single-neutron n_1 – ^{11}B (R = 2.78 fm), dashed curve—single-neutron n_2 – ^{10}B (R = 2.21 fm).

6. EFFECT OF INDEPENDENT PARTICLE TRANSFER MECHANISM ON THE CHARACTERISTICS OF ORIENTED NUCLEI

6.1. Generalities

Those nuclear systems, in which an isotropy of the spatial spin distribution of particles is violated, are called the oriented ones. In this section we shall consider the effect of the mechanisms, associated with independent two-step particle transfer, exerted on the characteristics of oriented nuclei formed in nuclear reactions.

The main characteristic of an oriented system is a density matrix or its statistical tensors [30, 68]. Consider the binary reaction $A(x, y)B^*$ with unpolarized particles. The density matrix for the final state of a system is determined via that of the initial state and the matrix element of transition operator:

$$\begin{aligned}\rho\left(M_B M'_B; M_y M'_y; \theta_y\right) &= \sum_{M_x M'_x M_A M'_x} \rho_{J_x}(M_x M'_x)\cdot \rho_{J_A}(M_A M'_A) \\ &\times M_{BA}\left(M_x M_A M_y M_B; \theta_y\right) \\ &\times M^*_{BA}\left(M'_x M'_x M'_y M'_B; \theta_y\right),\end{aligned} \tag{63}$$

where $\rho_{J_x}(M_x M'_x)$ and $\rho_{J_A}(M_A M'_A)$ are a spin density matrix of incident particles and a target nucleus,

respectively. For unpolarized beams and targets these matrices are defined as follows:

$$\rho_{J_x}(M_x M'_x) = \frac{\delta_{M_x M'_x}}{2J_x+1}, \qquad \rho_{J_A}(M_A M'_A) = \frac{\delta_{M_A M'_A}}{2J_A+1} \tag{64}$$

and have a trace equal to unity.

If no polarization of particle y is detected in experiment, then the density matrix given in (63) can be reduced by using the following relation [30, 69]:

$$\rho_{J_B}\left(M_B M'_B;\theta_y\right) = \sum_{M_y M'_y} \rho\left(M_B M'_B; M_y M'_y;\theta_y\right), \tag{65}$$

where $\rho_{J_B}\left(M_B M'_B;\theta_y\right)$ is a reduced density matrix describing orientation characteristics of nucleus $B^*(J_B, M_B)$ only.

The spin-tensors of the density matrix for nucleus $B^*(J_B, M_B)$, which are formed in the binary reaction $A(x, y)B^*$ with unpolarized particles, are expressed through the matrix element of the reaction [30]:

$$\rho_{k\kappa}(J_B;\theta_y) = \frac{\mu_{xA}\ \mu_{yB}}{4\pi^2\hbar^4}\cdot\frac{k_x}{k_y}\cdot\frac{\sqrt{2J_B+1}}{(2J_x+1)(2J_A+1)} \times \sum_{M_B M'_B}(-1)^{J_B-M'_B}\left\langle J_B M'_B J_B - M_B \middle| k\kappa\right\rangle \times \sum_{M_x M_A M_y} M_{BA}(M_B;\theta_y)\cdot M^*_{BA}(M'_B;\theta_y). \tag{66}$$

Normalization in (66) is chosen in such a way that

$$\rho_{00}(J_B;\theta_y) = \mathrm{Sp}\left[\rho_{J_B}\left(M_B M'_B;\theta_y\right)\right] = \frac{d\sigma}{d\Omega}(\theta_y). \tag{67}$$

The method of correlation studies presented in [30] allows the quantities $A_{k\kappa}(J_B)$ to be recovered on the base of measurement of the angular correlation functions coinciding with the spin-tensors of nucleus B^* up to some factor [70]:

$$A_{k\kappa}(J_B) = \rho_{k\kappa}(J_B)R_k(LL'J_BJ_0), \quad R_k(LL'J_BJ_0) = (-)^{1+J_B-J_0+L'-L-k} \times\sqrt{(2J_B+1)(2L+1)(2L'+1)} \times\left\langle L1L'-1\middle|k0\right\rangle W(J_BJ_BLL':kJ_0), \tag{68}$$

where L, L' are multipolarities of gamma radiations that remove the excitation of a final nucleus $J_B \xrightarrow{L, L'} J_0$.

Knowing the spin-tensors of the density matrix, one can calculate the characteristics of oriented systems, such as polarization tensors and populations of spin sublevels [30, 71, 72]. In a reference frame with axis Z, perpendicular to the reaction plane formed by vectors $\mathbf{k}_x$ and $\mathbf{k}_y$, and axis X, which is parallel to $\mathbf{k}_B$, the polarization tensors are given by the expression:

$$\left\langle T_{k\kappa}(\theta_y)\right\rangle = \frac{1}{\sqrt{((2J_B+1))(2k+1)}}\cdot\frac{\rho_{k\kappa}(\theta_y)}{\rho_{00}(\theta_y)}. \tag{69}$$

Populations of magnetic sublevels are determined by the diagonal elements of the density matrix in this reference frame.

The polarization tensors have a more profound physical meaning than the spin-tensors or spin density matrix elements, because for any rank they are expressed in terms of spherical components of the angular momentum operator and characterize asymmetry in the distribution of spin components of the B^* nucleus relative to its symmetry axis and a reaction plane. Thus, by taking into account the second order corrections, caused by the sequential particle transfer in the calculations of the reaction matrix element, one can evaluate the orientation characteristics of a final nucleus, confront them with experimental data, and assess an effect exerted upon them by the two-step transfer mechanism.

The formalism given so far was used to analyze the orientation characteristics of nuclei ^{11}B* and ^{12}C*—the products of the reaction ^{13}C(d, α)^{11}B*and ^{13}C(^{3}He, α)^{12}C(0^+; 2^+, 4.443 MeV) at energies of incident particles ≅7–10 MeV per nucleon.

6.2. Calculation of the Differential Cross Sections for the Reaction ^{13}C(d, α)^{11}B at E_d = 15.3 MeV and statistical tensors of the ^{11}B(5/2$^-$ nucleus)*

Experimental differential cross sections for this reaction with production of ^{11}B in the ground and three lowest excited states are obtained in [73, 74]. The theoretical analysis of experimental results enabled determination of a contribution to the cross section of the reaction, studied from the more involved mechanisms than just a deuteron cluster pickup. These mechanisms are associated, firstly, with the collective excitation of nonspherical nucleus ^{11}B [47], and, secondly, with the pole transfer of a heavy cluster and its correction caused by the independent two-step particle transfer mechanism. A contribution of this mechanism to the cross section of the reaction ^{13}C(d, α)^{11}B* is expected to be substantial, since the energy difference ΔE between a virtual neutron and ^{8}Be for the heavy particle stripping mechanism (Eq. (27)) is considerable because of wide band ΔE*of

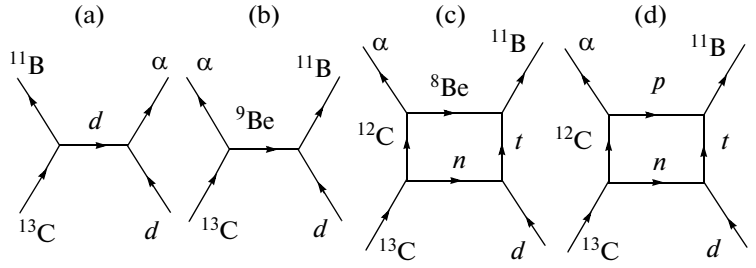

Fig. 24. Diagrams of the reaction mechanisms for ^{13}C($\alpha m\, d$)^{11}B: (a) deuteron pickup; (b) heavy cluster exchange; (c) two-step cluster transfer, (d) two-step transfer of light particles.

levels for a virtual nucleus ^{12}C allowed by the selection rules.

The theoretical cross sections are calculated [73, 74] assuming direct mechanisms represented by the diagrams in Fig. 24 to take place, along with the mechanism of compound nucleus formation [75–77]. A dineutron cluster pickup both for $3/2^-$ (the ground state) and $5/2^-$ (levels of the ^{11}B nucleus) were calculated by taking into account the collective excitation of rotational band in the ^{11}B nucleus, based on the ground ($3/2^-$) state. Optimal agreement between theoretical and experimental angular dependences was achieved for the parameter of quadrupole deformation $|\beta_2| = 0.4$.

Initial values of the optical potential parameters were taken from [78] in the entrance $d + {}^{13}$C channel for the energy of 15 MeV and exit $\alpha + {}^{11}$B channel for the energy 22.5 MeV. While calculating the cross sections, some parameter values for the optical potentials were slightly varied (within 10%) to achieve better agreement between theory and experiment. The final sets of optical potential parameters, used to compute all the reaction mechanisms, are given in Table 2. The structure factors for different reaction mechanisms are evaluated in a standard way according to Eqs. (34), (53) in the framework of the shell model with intermediate coupling [35] by using the representation of the total J and orbital angular l momenta and spin s transfers [30].

The corresponding structure factors for the pole mechanisms of deuteron pickup (Fig. 24a) and heavy ^{9}Be cluster stripping (Fig. 24b) are given in Table 7. The structure factors for the mechanism illustrated by

Table 7. Spectroscopic factors $\Theta^{J_1 J_2}_{\Lambda_1 \Lambda_2 l}$ for the mechanisms of deuteron pickup and heavy cluster stripping in the reaction ^{13}C(d, α)^{11}B(J_B) ($J_2 = 1$) ($J_2 = 1$)

Reaction mechanism	J_B	E^*, MeV	J_1 \ 1	0			2					
deuteron pickup ($\Lambda_2 = 0$)	3/2	0	1	−0.082			−0.152					
			2				0.352					
	1/2	2.13	1	−0.061			−0.179					
	5/2	4.44	2				−0.155					
			3				0.130					
	3/2	5.03	1	−0.080			0.232					
			2				−0.146					
heavy cluster transfer ^{9}Be	J_B	E^*, MeV	l	0		1	2				3	
			Δ_2	0	2	2	2	0	2	2	2	2
			J_1 \ Λ_1	0	2	2	0	2	2	4	2	4
	3/2	0	1	0.100	−0.139	−0.071						
	1/2	2.13	1	−0.084	0.050	0.056						
			3			0.063	−0.057	0.107	0.102	0.023		
	5/2	4.44	3			0.060	−0.013	−0.068	0.020			
	3/2	5.03	1	−0.031	0.035	0.028						
			3				0.001	0.059	−0.004	0.045		
			5					0.046	−0.015	0.029	0.033	−0.020

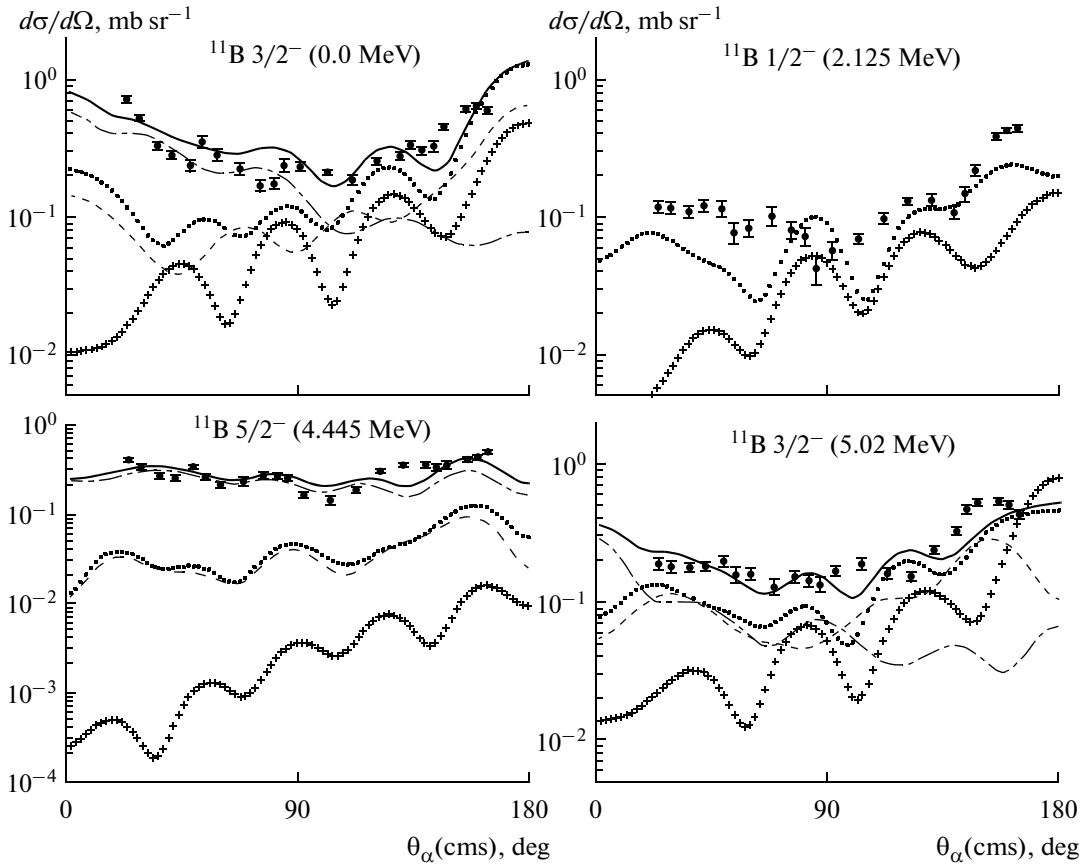

Fig. 25. Angular dependences of differential cross section for the reaction $^{13}C(d, a)^{11}B$ at $E_d = 15.3$ MeV. Circles denote experimental data [73]. Statistical uncertainties are shown when they exceed circle size. Curves are results of calculations for various reaction mechanisms assumed: dashed-dotted one—deuteron pickup when collective excitation of ^{11}B nucleus is taken into account; dashed one—heavy particle stripping, crosses—two-step cluster transfer, dotted curve—coherent sum of two last mechanisms, and a solid curve corresponds to an overall calculated curve.

a quadrangle diagram are not presented because of their great number.

A comparison of experimental and calculated reaction cross sections for various states of final nucleus ^{11}B is shown in Fig. 25. The calculation results showed that for all transitions studied, a contribution to the differential cross section from the mechanism of compound nucleus formation was small and, therefore, was further neglected. A contribution of the independent neutron and proton transfer mechanism (Fig. 24d) also turned out to be insignificant. Apparently, this can be explained by large values of the binding energies at the two decay vertices $^{12}C \rightarrow {}^{11}B + p$ and $\alpha \rightarrow p + t$.

As it follows from Fig. 25, the mechanism of deuteron cluster pickup for ^{11}B formation in the ground and $1/2^-$ (2.125 MeV) states dominates at angles in the forward hemisphere θ_α. A contribution of this mechanism to the angular distribution of α-particles with formation of ^{11}B in $5/2^-$ state was found to be leading for all angles. This mechanism is leading in the forward hemisphere, along with that of heavy particle stripping, for the state $3/2^-$ (5.02 MeV) as well.

For all states of ^{11}B the mechanism of ^9Be stripping yields a substantial contribution at angles in the backward hemisphere. The mechanism of two-step sequential transfer of cluster ^8Be and neutron (Fig. 24c) is only visible for angles $\theta_\alpha > 60°$. Since the amplitudes of the heavy particle stripping and sequential particle transfer mechanisms were coherently summed up, both constructive and destructive interferences were observed. Taking into account those interferences noticeably modified the shape of calculated curves and improved agreement with experiment. Overall, theoretical angular distributions are in good agreement with the experimental ones throughout an entire angular range. Agreement in absolute values of calculated and experimental cross sections is achieved without introducing additional normalization factors.

Calculated angular dependences of some components of the statistical tensors for ^{11}B ($5/2^-$, 4.445 MeV) nucleus, formed in the reaction $^{13}C(d, \alpha\gamma)^{11}B$ [74]

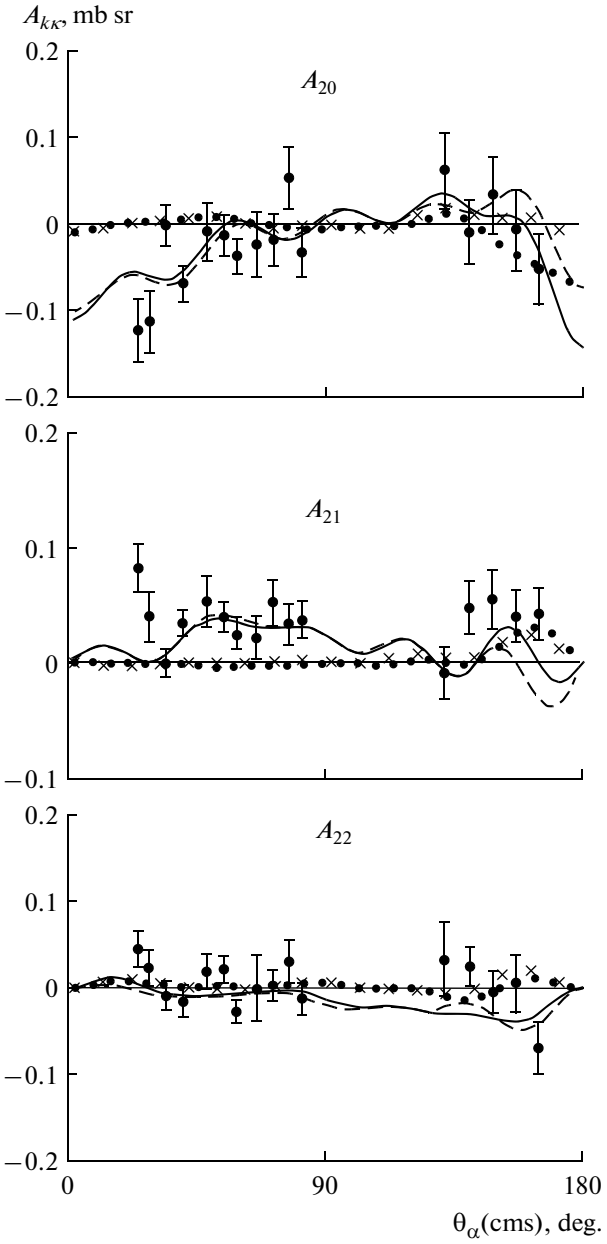

Fig. 26. Angular dependences of spin-tensor components $A_{k\kappa}(\theta_\alpha)$. Experimental data are borrowed from [74]. Curves—calculations for various reaction mechanisms assumed: dashed one—deuteron pickup in CCM, crosses—heavy particle stripping, dotted curve—coherent sum of mechanisms of heavy particle stripping and sequential cluster transfer, solid one—sum of all mechanisms.

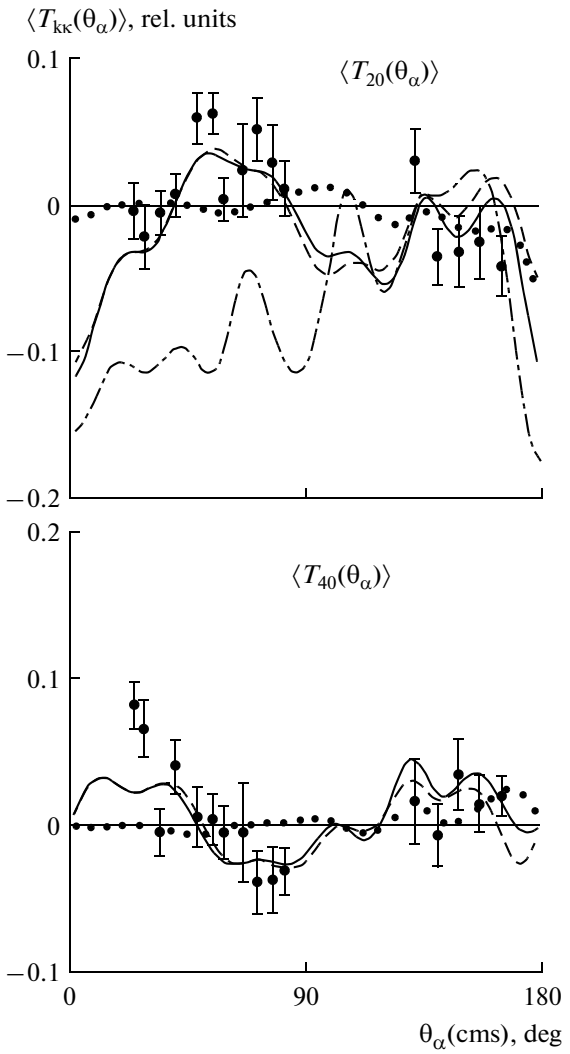

Fig. 27. Angular dependences of orientation tensor components for quadrupole and hexadecapole momenta of nucleus ^{11}B ($5/2^-$, 4.445 MeV). Experimental data are borrowed from [74]. Designations of curves are the same as in Fig. 25. A dash-dotted curve corresponds to the component of $\langle T_{20}(\theta_\alpha)\rangle$ for $\beta_2 = -0.4$.

with taking into account three mechanisms discussed above, are displayed in Fig. 26.

As might be expected, the mechanism of deuteron pickup with collective excitations of ^{11}B taken into account turned out to be the leading one in the forward hemisphere of the angles θ_α, while the mechanisms of ^{9}Be stripping and sequential cluster transfer yield a considerable contribution in the backward hemisphere. Agreement between the overall theoretical curves and experiment is for the most part qualitative, since the calculation does not provide us with a detailed description of $A_{k\kappa}(\theta_\alpha)$ at all θ_α angles studied.

The orientation tensor components (72) of the quadrupole moment ($k = 2$) of the ^{11}B($5/2^-$) nucleus are shown in Fig. 27. The calculation satisfactorily describes general behavior of the experimental angular dependence of these components, although quantitative agreement is not observed here either.

Not only the magnitude but also the sign of the static quadrupole deformation parameter β_2 of the ^{11}B nucleus was refined as a result of the sensitivity of calculated results to the static deformation parameter of

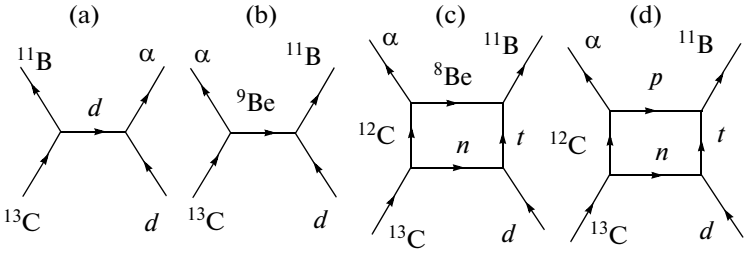

Fig. 28. Diagrams of the reaction mechanisms for ^{13}C(^{3}He, α)^{12}C: (a) neutron pickup; (b) exchange by a heavy cluster ^{9}Be, (c) two-step transfer of a virtual neutron and ^{8}Be.

a final nucleus. Figure 27 shows that when the sign is altered, the theoretical dependences of $\langle T_{2\kappa}(\theta_\alpha)\rangle$ get dramatically modified both in shape and magnitude, with the preference for a positive sign of the quadrupole deformation being evident, which cannot be said while analyzing the angular dependence of the cross section alone.

6.3. Calculation of Differential Cross Section for the reaction ^{13}C(^{3}He, α)^{12}C and Statistical Tensors of Nuclei ^{12}C(2^+, 4.443 MeV)

The orientation characteristics of nucleus ^{12}C(2^+, 4.443 MeV), formed in the reaction ^{13}C(^{3}He, α)^{12}C, were studied in [79].

Measurement of double differential cross sections of the reaction ^{13}C(^{3}He, α)^{12}C(0^+; 2^+, 4.443 MeV) has allowed reconstructing the statistical tensors $\rho_{k\kappa}(\theta_\alpha)$ of the density matrix for the ^{12}C nucleus in the state 2^+ (4.443 MeV). The most interesting of the obtained results turned out to be that concerning relatively large values of the rank $k = 4$ components, which, for the mechanism of neutron pickup with angular momentum transfer, $l = 1$ must be identically zero according to [30]. In [80] the quantities $\rho_{k\kappa}(\theta_\alpha)$ obtained at emission angles of α-particles in the forward hemisphere were calculated for the mechanism of neutron pickup in CCM [47], where collective nature of nucleus ^{12}C was taken into account, thereby eliminating the constraint imposed upon the angular momentum l transfer. The computation allowed one to produce a qualitative description of experimental values for $\rho_{k\kappa}(\theta_\alpha)$ in the forward hemisphere, although detailed agreement with experiment was not achieved. In [81] we evaluated differential cross sections of the reaction ^{13}C(^{3}He, α)^{12}C(0^+; 2^+, 4.443 MeV) and statistical tensors $\rho_{k\kappa}(\theta_\alpha)$ for the mechanisms of neutron pickup and exchange by a heavy cluster ^{9}Be.

The diagrams that illustrate various mechanisms of the reaction ^{13}C(^{3}He, α)^{12}C(0^+; 2^+, 4.443 MeV) are presented in Fig. 28. The first (Fig. 28a) corresponds to the process of direct pickup of a neutron with $l = 1$. The last two diagrams illustrate the process of exchange transfer of heavy cluster ^{9}Be in the pole approximation (Fig. 28b) and two-step transfer of virtual cluster ^{8}Be and neutron (the quadrangle diagram in Fig. 28c).

How important is it to take into consideration a two-step mechanism in the matrix element calculation for the reaction ^{13}C(^{3}He, α)^{12}C(0^+; 2^+, 4.443 MeV), which takes into account independent particle transfer? For the reaction under study, the energy difference ΔE of virtual particles transferred (Eq. (27)) is large because of high binding energy ε at the vertex $n + {}^3\mathrm{He} \to \alpha$ and wide band ΔE^* of levels of virtual nucleus ^{12}C allowed by the selection rules. As a result, the wave functions of virtual ^{8}Be and neutron overlap slightly, and the probability of their transfer to a target nucleus separately in time should be high. These considerations suggest that a priori the contributions coming from the one-step pole and two-step sequential transfer mechanisms should be comparable in the reaction ^{13}C(^{3}He, α)^{12}C.

We calculated the neutron pickup matrix element in the reaction ^{13}C(^{3}He, α)^{12}C by DWBAFR in the pole approximation according to Eq. (33). By using Eq. (57) the matrix element of heavy cluster ^{9}Be transfer was determined as a sum of the pole and sequential neutron and heavy cluster ^{8}Be transfers.

The differential cross sections and statistical tensors of the density matrix for the ^{12}C nucleus formed in the reaction ^{13}C(^{3}He, α)^{12}C(2^+) were evaluated.

In Table 8 we present maximal values of spectroscopic factors for various mechanisms of the reaction ^{13}C(^{3}He, α)^{12}C(0^+, 2^+) that were calculated according to Eqs. (34), (53) [81]: neutron pickup ($^{13}\mathrm{C} \to n +$ ^{12}C(0^+, 2^+)), exchange by a heavy cluster ^{9}Be ($^{13}\mathrm{C} \to$ $^{9}\mathrm{Be} + \alpha$), ditto with ^{8}Be ($^{12}\mathrm{C}(0^+, 2^+) \to {}^{8}\mathrm{Be} + \alpha$). As is seen from the table, these factors for each state of final nucleus ^{12}C are the quantities of the same order, so that it can be expected in advance that the contributions to the reaction cross section from all three mechanisms will be substantial.

The calculated differential cross sections for the reaction ^{13}C(^{3}He, α)^{12}C at incident helium ion energies of 18 MeV with formation of ground and excited 2^+ states of nucleus ^{12}C are presented in Fig. 29 for various reaction mechanisms. As is seen from this figure,

Table 8. Spectroscopic factors $\Theta^{J_1 J_2}_{\Lambda_1 \Lambda_2 l}$ for the mechanisms of deuteron pickup and ^{9}Be heavy cluster stripping, and $\Theta^{J_1 J_2}_{\Lambda_1 \Lambda_2 l}$ in the case of ^{8}Be heavy cluster stripping—second stage of the two-step mechanism in the reaction ^{13}C(^{3}He, α)^{12}C(0^+; 2^+, 4.443 MeV)

Reaction mechanism	J_B	J_1	J_2	Λ_1	Λ_1	l	Spectroscopic factors
Neutron pickup	2^+	1/2	3/2	0	1	1	–0.34247
	0^+	1/2	1/2	0	1	1	–0.26350
Heavy cluster exchange ^{9}Be	2^+	3	1	3	0	1	0.05603
		3	1	3	2	1	0.06735
		5	1	5	2	3	–0.07866
	0^+	1	1	1	0	1	–0.10461
				1	2	1	0.18604
Heavy cluster exchange ^{8}Be (upper part of quadrangle diagram in Fig. 28c.)	2^+	2	2	0	0	0	0.06425
				2	2	0	0.20966
				2	2	1	0.11483
				2	2	4	0.07739
	0^+	0	0	0	0	0	0.47602
				2	2	0	0.33028
				4	4	0	0.20129

the neutron stripping mechanism dominates in the forward hemisphere, while the exchange one with ^{9}Be heavy cluster transfer determines a cross section in the backward hemisphere.

A contribution of the two-step mechanism, which takes into account the delay, is significant at all α-particle emission angles. Moreover, while forming ^{12}C in the ground state, this mechanism significantly increases a cross section of the exchange mechanism in the forward hemisphere, thus improving on agreement between theoretical and experimental cross sections [79, 80] at all angles without introducing additional normalizations. In other words, to correctly describe experimental cross sections of the reaction ^{13}C(^{3}He, α)^{12}C(0^+, 2^+) it is necessary to account for the two-step mechanism of heavy cluster transfer.

The statistical tensors make it possible to estimate the orientation of various multipole moments of nucleus ^{12}C(2^+). The lowest rank polarization tensors possess a clear physical meaning: the tensor $\langle T_{10} \rangle$ is proportional to the polarization vector and characterizes an induced polarization of a system in the plane perpendicular to that of the reaction. The tensors $\langle T_{20} \rangle$ and $\langle T_{22} \rangle$ coincide to a normalization with longitudinal and transverse components of the alignment tensor.

Figure 30 demonstrates the contributions to some of the polarization tensors of an oriented nucleus ^{12}C(2^+) coming from various reaction mechanisms. As is seen from the figure, the pole mechanism of neutron stripping is important for the appearance of the induced polarization of a nucleus. The higher rank polarization tensors are associated with the heavy cluster transfer mechanism, with the impact of the sequential transfer mechanism most significant at moderate emission angles.

Thus, the role of various mechanisms in forming an oriented final nucleus is demonstrated with examples of various characteristics of the reactions ^{13}C(d, α)^{11}B(3/2$^-$, 5/2$^-$, 4.443 MeV) and ^{13}C(^{3}He, α)^{12}C(0^+; 2^+, 4.443 MeV) (a differential cross section of elastic and inelastic scattering, statistical tensors of the density matrix, induced vector and tensor polarizations). The results obtained show the importance of taking into account the mechanism of sequential virtual cluster transfer illustrated by a quadrangle diagram.

7. A SIMPLIFIED CALCULATION METHOD FOR THE TWO-STEP MECHANISM AMPLITUDES

An expression (56) was used in previous sections to calculate the matrix elements of quadrangle mechanisms. This expression is analytically obtained in the case of the four-body approximation for the channels (3,1). There are reactions that do not fit into the considered channel scheme for a four-body problem and for which the mechanism of sequential particle transfer illustrated by a quadrangle diagram is a natural extension of a perturbation series. In this case we used a visual method of convolution of two amplitudes in

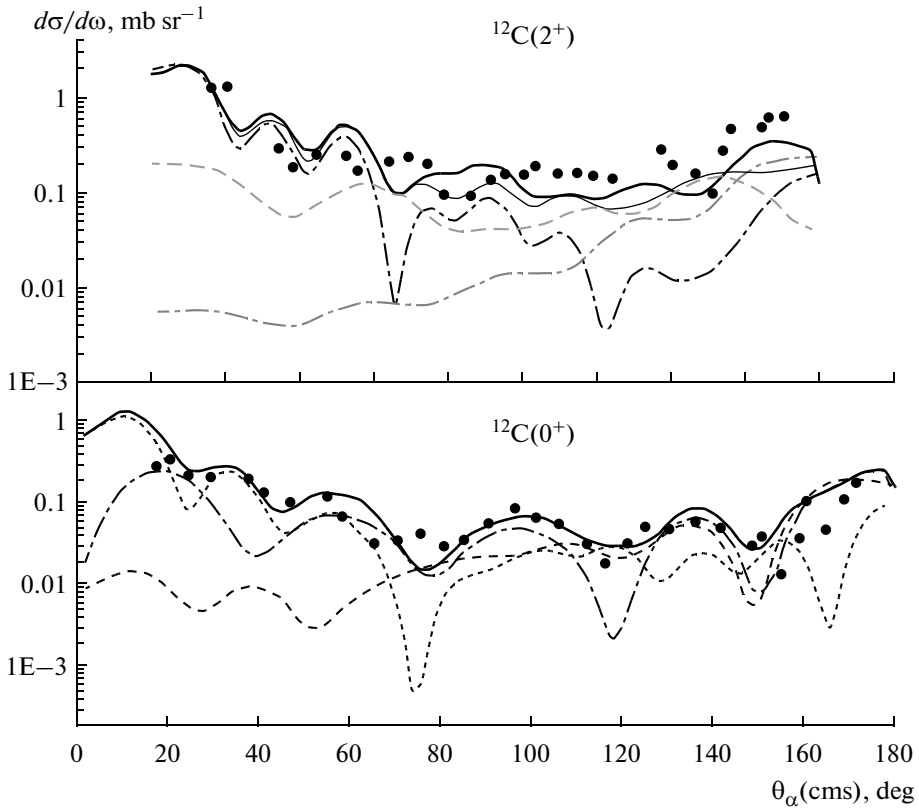

Fig. 29. Calculated differential cross sections of the reaction $^{13}C(^3He, \alpha)^{12}C$ at $E_{He} = 18$ MeV for the ground and excited 2^+ states of ^{12}C nucleus for various reaction mechanisms: dotted curve—cross section of neutron stripping, dotted one—^9Be heavy cluster transfer, dash-dotted one—^9Be cluster transfer with both pole and quadrangle diagrams taken into account, solid curve—total cross section for the reaction with all mechanisms taken into account. Experimental data are borrowed from [79].

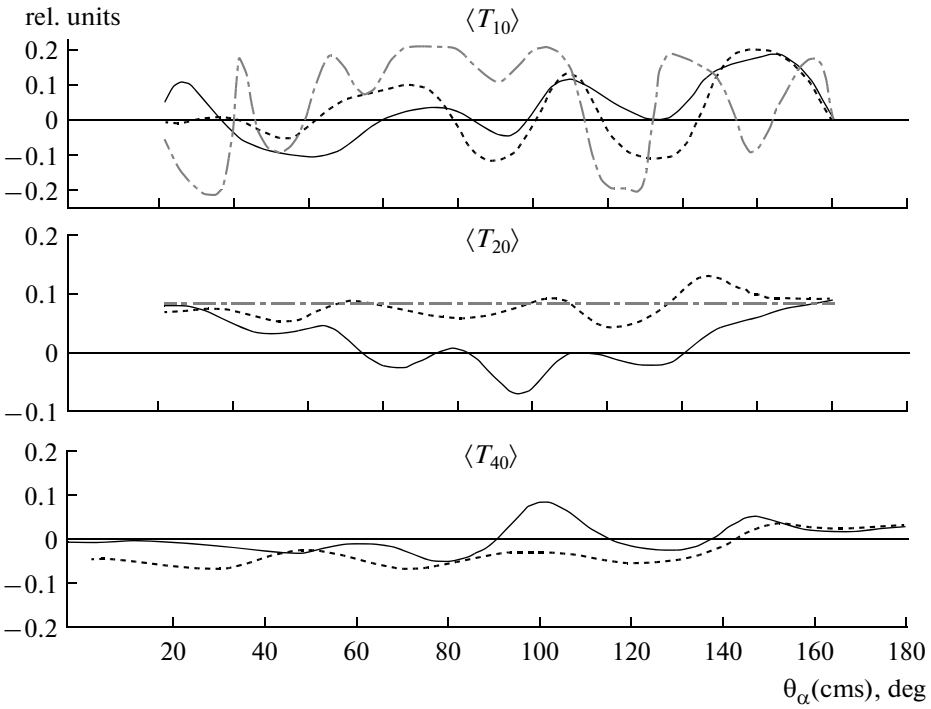

Fig. 30. Polarization tensors of oriented nucleus $^{12}C(2^+)$ for various reaction mechanisms. Curve designations are the same as in Fig. 29. Experimental data are borrowed from [80].

DWBAFR, which is based on a graphical representation, and showed that the expression obtained this way coincides with (56), up to phase factors and normalization. Expression (56) contains coherent summations over the momenta of an intermediate system. Any simplification of the general formulas for calculating the matrix elements of such mechanisms is highly desirable. Let us analyze possible simplifications of the formula related with analytical summation done over the intermediate momenta, without losing physical aspects of the two-step mechanisms.

Let the reaction $A(x, y)B$ proceed through a virtual $(\sigma\rho)$ state. Consider the case when a cluster $\sigma \le 4$ has a zero internal orbital angular momentum. We obtain an expression for the matrix element of the quadrangle diagram in the form of a convolution of two pole mechanisms (Fig. 6) and sum it up over all states of ρ cluster allowed by the selection rules, similar to what was done in [82].

Let us use DWBAFR in the representation of the total spin J, orbital angular momentum l, and spin s transfers to calculate the matrix elements of the reaction $A(x, y)B$ for each of the pole mechanisms [30].

As an example, consider the reaction ^{9}Be(^{3}He, d)^{10}B illustrated by a diagram in Fig. 31. In the four-body approximation (^{8}Be, n, d, p) this reaction corresponds to the transition from channel (2,2) to the final one (2,2) via the virtual state of channel (3,1): (^{8}Be, n) + (d, p) $\to$ ^{8}Be + (n, d, p) $\to$ (^{8}Be, d) + (n, p). A diagram in Fig. 31 illustrates a second order correction to the proton pickup mechanism.

7.1. Matrix Element for Lower Part of the Quadrangle Diagram in Fig. 31

The lower part of the diagram describes the neutron pickup mechanism. Following [30] the matrix element of such a mechanism without integration over radial variables and without considering the constant normalization factors has the following form:

$$\begin{aligned} M_1 &= \langle l_A m_A s_A \zeta_A | J_A M_A \rangle \\ &\times \langle l_\rho m_\rho s_\rho \zeta_\rho | J_\rho M_\rho \rangle \langle l_\rho m_\rho l_1 m_1 | l_A m_A \rangle \\ &\times \langle s_\rho \zeta_\rho S_1 \zeta_1 | s_A \zeta_A \rangle \langle s_x \zeta_x S_1 \zeta_1 | s_\sigma \zeta_\sigma \rangle \\ &\times \sqrt{(2l_1+1)} \times \beta_{\Lambda L_x l_1 m_1}(k_{\rho\sigma} r') \Theta_{l_1 S_1}^{A\to l+\rho} \Theta_{S_1}^{\sigma\to l+x}, \end{aligned} \tag{70}$$

where l_1, S_1 (S_2) are orbital angular momentum transfer and spin at the decay vertices of nucleus A (σ), kinematical factors $\beta_{\Lambda L_x l_1 m_1}(k_{\rho\sigma} r')$ are given by Eq. (32), and $\Theta_{l_1 S_1}^{A\to n+\rho}$ $\left(\Theta_{S_1}^{x\to n+\sigma}\right)$ denote reduced decay widths for nucleus A (a particle x), which include coefficients a_{LS}, arising in the decomposition of the wave functions of nuclei A and σ done over the basis functions of LS-coupling.

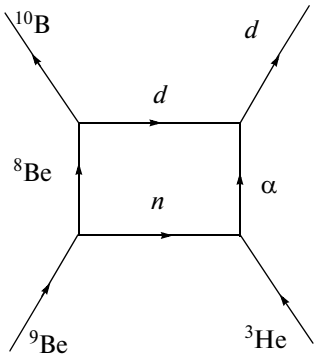

Fig. 31. A diagram of the sequential particle transfer mechanism in the reaction ^{9}Be(^{3}He, d)^{10}B.

7.2. Matrix Element for Upper Part of the Quadrangle Diagram in Fig. 31

The upper part of the diagram in Fig. 31 corresponds to the particle stripping mechanism. The matrix element of the latter M_2 (without considering the constant normalization factors) has the form similar to the expression given in (74) for the lower part of a whole diagram, up to replacement of the decay widths for respective nuclei:

$$\begin{aligned} M_2 &= \langle l_B m_B s_B \zeta_B | J_B M_B \rangle \\ &\times \langle l'_\rho m'_\rho s'_\rho \zeta'_\rho | J_\rho M_\rho \rangle \langle l'_\rho m'_\rho l_2 m_2 | l_B m_B \rangle \\ &\times \langle s'_\rho \zeta'_\rho S_2 \zeta_2 | S_B \zeta_B \rangle \langle S_2 \zeta_2 s_y \zeta_y | s'_\sigma \zeta'_\sigma \rangle \\ &\times \sqrt{(2l_2+1)} \beta_{\Lambda L_y l_2 m_2}(k_{\sigma\rho} r; \theta_y) \Theta_{l_2 S_2}^{B\to d+\rho} \Theta_{S_2}^{\sigma\to d+y}. \end{aligned} \tag{71}$$

7.3. Matrix Element Simplification for the Mechanisms Accounting for Delay

In order to derive a full matrix element of the mechanism that takes into account delay, it is necessary to multiply the matrix elements (70), (71) and, according to (56), integrate over the radial variables. However, a general idea of how a full matrix element can be simplified can be grasped without doing all these rigorous procedures.

If, in a specific reaction the binding energies ε are large at nuclear decay vertices, with an excitation energy band $\Delta E_\rho^* \ll \varepsilon$, then dependence of the wave function of cluster ρ on ΔE^* can be neglected in the matrix elements (70), (71) and summation over ΔE_ρ^* and J_ρ can be performed analytically. Such a simplification of general formulas was done earlier [14] in the plane wave approximation. We did the same [83] in a general case as well by assuming that in a specific reaction these approximations hold.

1. *Summation over* ΔE^*_ρ. By virtue of orthogonality [35] of the intermediate coupling coefficients a_{LS} for each state of cluster ρ with spin J_ρ, summation over ΔE^*_ρ can be carried out by using the following relation:

$$\sum_{\Delta E^*_{\rho\,\rho}} a_{L_\rho s_\rho}(J_\rho) a_{L'_\rho s'_\rho}(J_\rho) = \delta_{L_\rho L'_\rho}\delta_{s_\rho s'_\rho}. \quad (72)$$

2. *Summation over momentum* J_ρ:

$$\sum_{J_\rho M_\rho} \langle L_\rho\, \mu_\rho s_\rho\, \varsigma_\rho | J_\rho\, M_\rho\rangle \left\langle L_\rho\, \mu'_\rho s_\rho\, \varsigma'_\rho \middle| J_\rho\, M_\rho \right\rangle = \delta_{\mu_\rho \mu'_\rho}\delta_{\varsigma_\rho \varsigma'_\rho}. \quad (73)$$

3. *Transformation of the Clebsch–Gordan coefficients that contain spins of particles and nuclei*:

$$1)\quad \langle s_\rho \zeta_\rho S_1 \zeta_1 | s_A \zeta_A\rangle \langle s_\rho \zeta_\rho S_2 \zeta_2 | s_B \zeta_B\rangle = (-1)^{2S_1+\zeta_1+S_A-S_\rho}\sum\sqrt{\frac{(2s_A+1)}{(2s_\rho+1)}}U(s_A S_1 s_B S_2 : s_\rho S) \langle S_1 \zeta_1\, S_2 - \zeta_2 | S\zeta\rangle \langle s_A \zeta_A S\zeta | s_B \zeta_B\rangle; \quad (74)$$

$$2)\quad \sum(-1)^{2S_1+\zeta_1}\langle S_2 \zeta_2\, s_y \zeta_y | s_\sigma \zeta_\sigma\rangle \times \langle s_x\zeta_x\, S_1\zeta_1 | s_\sigma\zeta_\sigma\rangle \langle S_1 - \zeta_1\, S_2\, \zeta_2 | S\zeta\rangle = \sum(-1)^{2S_1+S_2-\zeta}\sqrt{\frac{(2s_\sigma+1)}{2s_y+1)}}\,U(s_x S_1 s_y S_2 : s_\sigma S). \quad (75)$$

4. *Transformation of the Clebsch–Gordan coefficients that contain the orbital angular momenta of nuclei and those transferred*:

$$\sum \langle L_\rho\, \mu_\rho\, l_1 m_1 | L_{\mathbf{A}}\, \mu_{\mathbf{A}}\rangle \cdot \langle L_\rho\, \mu_\rho\, l_2\, m_2 | L_{\mathbf{B}}\, \mu_{\mathbf{B}}\rangle = (-1)^{2l_1+m_1-L_\rho+L_{\mathbf{A}}}\sqrt{\frac{(2L_{\mathbf{A}}+1)}{(2L_\rho+1)}} \times U(L_{\mathbf{A}} l_1\, L_{\mathbf{B}} l_2 : L_\rho l)\cdot \langle l_1 - m_1\, l_2\, m_2 | l\, m\rangle \times \langle L_{\mathbf{A}}\, \mu_{\mathbf{A}}\, l\, m | L_{\mathbf{B}}\, \mu_{\mathbf{B}}\rangle. \quad (76)$$

5. *Summation over projections of the orbital angular momenta and spins of nuclei A and B*:

$$\sum \langle l_A\, \mu_A\, s_A\, \zeta_A | J_A\, M_A\rangle \langle l_B\, \mu_B\, s_B\, \zeta_B | J_B\, M_B\rangle \times \langle l_A\, \mu_A\, l\, m | l_B\, \mu_B\rangle \langle s_A\, \zeta_A\, S\, \zeta | s_B\, \zeta_B\rangle = \sum \begin{pmatrix} l_A & s_A & J_A \\ l & S & J \\ l_B & s_B & J_B \end{pmatrix} \langle J_A\ M_A\ J\ M | J_B\ M_B\rangle \times \langle l\ \mu\ S\ \zeta | J\ M\rangle. \quad (77)$$

6. *Isolation of the Clebsch–Gordan coefficients and phases, depending on the orbital angular momenta, in the expression for kinematical factors, and summation over projection of* m_Λ:

$$\sum_{m_\Lambda}(-1)^{\mu_x+2l_1+m_l+m_2}\langle L_x\, \mu_{\mathbf{x}}\, \Lambda\, m_\Lambda | l_1 - m_1\rangle \times \langle \Lambda\, m_\Lambda\, L_y\, \mu_{\mathbf{y}} | l_2 - m_2\rangle \langle l_1 m_1 l_2 m_2 | l\, m\rangle = (-1)^{\Lambda+l_1+l_2+l}\sqrt{(2l_1+1)(2l_2+1)} \times W(L_x l_1\, L_y l_2 : \Lambda l)\langle L_x\, \mu_{\mathbf{x}}\, L_y\, \mu_y | l\, m\rangle. \quad (78)$$

As a result of all these transformations, a simplified matrix element assumes the following form:

$$M^{simp}_{BA} = \sqrt{(2l+1)(2S+1)} \times \langle J_A M_A\, J\, M | J_B\, M_B\rangle \langle s_y\, \zeta_y\, S\, \zeta | s_x\, \zeta_x\rangle \times \langle l\, m\, S\, \zeta | J\ M\rangle \sum_{l_1 l_2}\bar{\Theta}^{l\,S\,J}_{l_1 l_2} \times \sum_{L_x L_y \Lambda} i^{L_x+L_y}\ \langle l - m\, L_y\, m | L_x 0\rangle \cdot \times \begin{Bmatrix} L_x & \Lambda & l_1 \\ l_2 & l & L_y \end{Bmatrix}\cdot P_{L_y|m|}(\theta_y)\cdot \mathfrak{I}_{L_x L_y \Lambda}, \quad (79)$$

where *l, S, J* are an orbital angular momentum, spin, and total spin transferred, l_1, l_2 denote orbital angular momentum transfers for the upper and lower parts of the diagram, a multidimensional integral $\mathfrak{I}_{L_x L_y \Lambda}$ is given by Eq. (56), while $\bar{\Theta}^{l\,S\,J}_{l_1 l_2}$ stand for structure factors written as follows

$$\bar{\Theta}^{l\,S\,J}_{l_1 l_2} = (-1)^{s_A-s_\rho+l_A-l_\rho+2S_1+S_2+2S-J} \times \sqrt{\frac{(2s_A+1)(2l_A+1)(2s_\sigma+1)}{(2S+1)(2s_\rho+1)(2l_\rho+1)(2s_x+1)}} \times U(l_A l_1 l_B l_2 : l_\rho l)\ U(s_A S_1 s_B S_2 : s_\rho S) \times U(s_x S_1 s_y S_2 : s_\sigma S)\begin{Bmatrix} l_A & s_A & J_A \\ l & S & J \\ l_B & s_B & J_B \end{Bmatrix} \times (-1)^{\Lambda+l_1+l_2}\,\Theta^{A\to\rho+n}_{l_1 S_1}\Theta^{\rho\to B+d}_{l_2 S_2}\Theta^{x\to\sigma+n}_{S_1}\Theta^{\sigma\to d+y}_{S_2}. \quad (80)$$

Formulas (79), (80) together with expression (56), which define a multidimensional integral for second order mechanisms associated with independent parti-

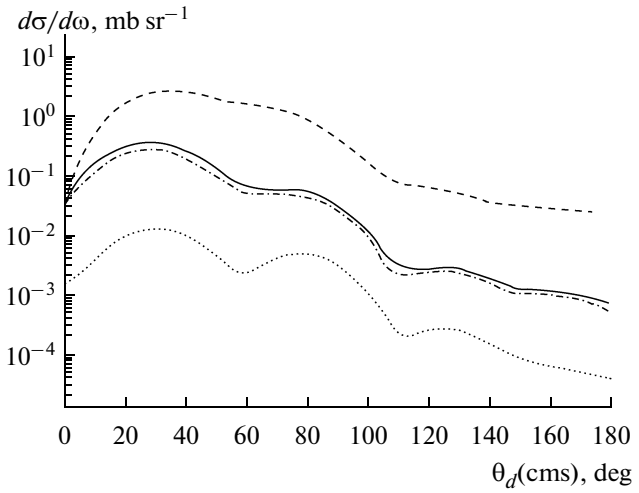

Fig. 32. Angular distribution of deuterons in the reaction ^{9}Be(^{3}He, d)^{10}B: solid thick curve—simplified calculation for the two-step mechanism, dotted one—exact calculation for the level 0^+ of virtual nucleus ^{8}Be, dash-dotted one—for the level 2^+ of virtual nucleus ^{8}Be, solid thin curve—their coherent sum, thick dotted one—simplified calculation with a normalization coefficient ~0.8.

cle transfer, were used [83] to estimate a contribution from such mechanisms in the reaction ^{9}Be(^{3}He, d)^{10}B.

For the two-step mechanism in this reaction, all conditions necessary for usage of the approximate formulas are met: binding energies of a neutron in ^{9}Be, as well as a deuteron in ^{10}B, are substantially less than that of a neutron in α-particle, and since the selection rules allow only the first two states of ^{8}Be (0^+ and 2^+) to be excited, ΔE^* does not exceed 3 MeV.

A differential cross section of deuterons calculated for this mechanism with the matrix element (83), obtained in the approximation of analytical summation over all possible states of the ^{8}Be nucleus (76, 77), is shown by a dashed curve in Fig. 32. For the sake of comparison, differential cross sections, evaluated by using exact Eqs. (57) for 0^+ and 2^+ levels of the ^{8}Be nucleus, are shown by dotted and dash-dotted curves, respectively, while their coherent sum is given by a solid one. As is seen form the figure, the calculation done with an approximate formula reproduces a shape of the deuteron angular distribution, overestimating, as might be expected, the value of the cross section. The cross section of this reaction computed by using approximate formulas with a normalization factor of 0.8 is shown by a thick dotted curve. It is seen that upon introducing a normalization factor the theoretical curves evaluated according to exact and simplified formulas virtually coincide. Thus, the usage of a simplified approach makes it possible to correctly estimate a contribution of independent particle transfer mechanisms with a significant reduction in the computing power.

CONCLUSIONS

The cluster structure of nuclei enables one to consider reactions on 1p-shell light nuclei with moderate energy particles (up to 10 MeV/nucleon) in the three- and four-body approximations and use an appropriate theoretical formalism, developed in [2, 5, 7–9], to describe them. The clusters in a nucleus are virtual entities, and the probability of existence is determined by the nuclear structure. The proposed theoretical approach to dealing with reactions is based on effective fusion of the apparatus of integral equations for a few-body problem with the models that take into account a nuclear structure.

In this review, we developed the formalism for calculating the cross sections of nuclear reactions on light nuclei, based on the integral equation apparatus for a four-body problem in the Alt–Grassberger–Sandhas (AGS) approach. We showed that the one-step mechanisms in DWBAFR correspond to the first terms of iterative series of the integral equations for a four-body problem. Subsequent terms of iterative series give second order corrections to DWBAFR, which represent mechanisms of independent two-step cluster transfer.

A physical criterion to be judged as a manifestation of two-step mechanisms is the energy difference of virtual clusters transferred: if it is large then their wave functions overlap slightly and it can a priori be expected that the two-step mechanisms will substantially contribute to the characteristics of a nuclear reaction.

In the review we present a theoretical formalism that allows deriving in analytical form the expressions for the matrix elements of two-step reaction mechanisms illustrated by quadrangle diagrams. The decomposition of the Green's function of a virtual cluster system over spherical functions corresponds to cutting up a whole quadrangle diagram into two coordinate spaces. As a result, the matrix element of the two-step transfer mechanism is found to be a convolution of those in DWBAFR for the upper and lower parts of a quadrangle diagram. In order to implement this formalism, the QUADRO code is developed, which calculates matrix elements of independent sequential particle transfer mechanisms.

We have calculated the cross sections for a number of reactions on light nuclei of 1p-shell, where the two-step mechanisms, according to physical criteria we found, should be appreciable. In fact, we showed for the first time that an angular distribution of α-particles in elastic ^{6}He-scattering, as well as that of protons, which are produced in the reactions ^{9}Be(d, p)^{10}Be, ^{10}B(d, p)^{11}B($1/2^-$) and ^{10}B(t, p)^{12}B, can be reconciled with experiment by taking into account second order corrections to the pole mechanisms. The structure factors that give a contribution of one- and two-step mechanisms in these reactions are the quantities of the same order; for both mechanisms a leading contribution to the cross section comes from the components

with nonzero orbital angular momentum transfer. A coherent sum of the matrix elements of both mechanisms makes it possible to reconcile theoretical angular distributions with experimental ones, whose distinctive feature is a maximum at small proton emission angles and the absence of a pronounced diffraction structure.

We predicted angular dependences of the differential cross sections and magnitudes of the total cross sections for the charge exchange reactions $p(^6\mathrm{He}, n)^6\mathrm{Li}$ (0^+, 3.56 MeV) and reaction $^7\mathrm{Li}(t, p)^9\mathrm{Li}$. These calculations were also carried out by taking into account second order corrections to the mechanisms of stripping (pickup) and the nucleon-exchange process in neutron-excess nuclei.

The cross section calculations for two-nucleon transfer reactions allowed us to reconstruct the structure of neutron periphery in the light neutron-excess nuclei. Its analysis showed a significant difference in two-neutron periphery in the nuclei ^{6}He, ^{10}Be, and ^{12}B: while for the first one it is a halo in both dineutron and "cigarlike" configurations that defines a cross section of elastic ^{6}He-scattering, for the nuclei ^{10}Be and ^{12}B in the reaction (t, p) such a halo is not actually seen. This can partially be explained by the large binding energy between the core and α-particle in ^{6}He so that both a dineutron and two uncorrelated neutrons can move around far enough from the core. The neutron peripheries in the nuclei ^{10}Be and ^{12}B differ from each other as well. In ^{10}Be a faint halo, composed of just a single neutron, is formed. On the contrary, in ^{12}B a dineutron forms a "skin" on its surface, while both nucleons are likely to reside rather inside a nucleus. It can also be noted that a cigarlike configuration of the periphery in all nuclei is asymmetric, and this asymmetry depends on the way a nucleus was formed. The nature of asymmetry is associated with the four-body (rather than three-body) approximation used. In this approximation the initial, final, and virtual channels of the reaction are various cluster combinations. Therefore, recoil effects can be different when one of the neutrons gets isolated from the rest of a cluster system. Such a behavior of the neutron periphery suggests a complex structure the 1p-shell nuclei possess, in which it is hard to tell apart a "skeleton" and neutrons moving relative to the latter, and, therefore, to observe the existence of a neutron halo inside them.

Finally, within the framework of the theoretical formalism developed, we interpreted experimental results obtained for oriented nuclei, found physical characteristics of such nuclei, and estimated an impact of the mechanisms associated with independent particle transfer exerted upon these characteristics.

The role of various mechanisms in forming an oriented final nucleus is exemplified by various characteristics of the reactions $^{13}\mathrm{C}(d, \alpha)^{11}\mathrm{B}(3/2^-, 5/2^-$, 4.443 MeV) and $^{13}\mathrm{C}(^3\mathrm{He}, \alpha)^{12}\mathrm{C}$ (0^+; 2^+, 4.443 MeV) (a differential cross section of elastic and inelastic scattering, statistical tensors of the density matrix, induced vector and tensor polarizations). The results obtained stress the importance of taking into account the mechanism of sequential transfer of virtual clusters already in the cross section calculations for elastic and inelastic scattering. Polarization characteristics change qualitatively when a two-step mechanism is taken into consideration, particularly at moderate angles of α-particle emission. This fact once again emphasizes the complexity of the mechanism of nuclear reactions involving α-particles, its distinction from the pole mechanisms of stripping or pickup. In the reactions $^{13}\mathrm{C}(d, \alpha)^{11}\mathrm{B}(5/2^-$, 4.443 MeV) and $^{13}\mathrm{C}(^3\mathrm{He}, \alpha)^{12}\mathrm{C}(2^+$, 4.443 MeV) only taking into account all considered mechanisms allowed us to describe a large set of characteristics for the oriented nuclei $^{11}\mathrm{B}(5/2^-)$ and $^{12}\mathrm{C}(2^+)$ produced in the reactions.

At last, we proposed a simplified method of calculating the cross sections of two-step mechanisms for the reactions, in which the specific relations hold between the binding energies at decay vertices of two- or three-body clusters and energy bandwidth of excited states of virtual clusters, allowed by the selection rules over all intermediate angular momenta. We showed that using a simplified approach allows one to quite correctly estimate a contribution of independent particle transfer mechanisms with a significant reduction in the computing power.

REFERENCES

1. V. G. Neudatchin and Yu. F. Smirnov, *Nucleon Associations in Light Nuclei* (Nauka, Moscow, 1969) [in Russian].
2. L. D. Faddeev, *Mathematical Aspects of Three Body Problem in Quantum Scattering Theory* (Daniel Davey, New York, 1965).
3. N. Austern, R. M. Drisko, E. C. Halbert, and G. R. Satchler, "Theory of Finite-Range Distorted Waves Calculations," Phys. Rev. B **133**, 3–16 (1964).
4. N. S. Zelenskaya and I. B. Teplov, *Exchange Processes in Nuclear Reactions* (Mosk. Gos. Univ., Moscow, 1985) [in Russian].
5. O. A. Yakubovskii, "On the Integral Equations in the Theory of N Particle Scattering," Sov. J. Nucl. Phys. **5**, 937 (1967).
6. C. Lovelas, "Practical Theory of Three-Particle States. 1. Nonrelativistic," Phys. Rev. B **135**, 1225–1249 (1964).
7. P. Grassberger and W. Sandhas, "Systematical Treatment of the Non-Relativistic N-Particle Scattering Problem," Nucl. Phys. B **2**, 181–206 (1967).
8. S. Weinberg, "Systematical Solution of Multi-Particle Scattering Problems," Phys. Rev. B **133**, 232–256 (1964).
9. E. Shmid and Kh. Tsigel'man, in "Problem of Three-Body in Quantum Mechanics" (Nauka, Moscow, 1979), pp. 151–154 [in Russian].

10. E. O. Alt, P. Grassberger, and W. Sandhas, "Derivation of the DWBA in Exact Three-Body Theory," Nucl. Phys. A **139**, 209–229 (1969).
11. E. A. Edakova, V. G. Neudatchin, and E. A. Romanovskii, "Possible Manifestation of a Second-Order Process in Deuteron Inelastic Scattering by Nuclei," Sov. Phys. JETP **11**, 180 (1960).
12. I. Bang, N. S. Zelenskaya, E. Zh. Makzumov, et al., "Manifestation of Mechanisms Described by Qaudrangle Diagram in the (t,p) (^{3}He,p) Reactions in Nuclei of 1p-Shell," Sov. J. Nucl. Phys. **4**, 688 (1966).
13. V. G. Neudatchin, N. S. Zelenskaya, E. G. Magsumov, et al., "Quadrangle Diagrams in the (p, p'), (d,d'), (t, p) – (^{3}He, p) Reactions in Some Nuclei of p-Shell and Simple Method for Calculating Their Angular Distributions," Phys. Lett. B **27**, 490–493 (1968).
14. N. S. Zelenskaya, "Manifestation of Mechanisms, Described by Quadrangle Diagram in the Reactions with Heavy Ions Stripping (Pickup)," Sov. J. Nucl. Phys. **13**, 417 (1971).
15. R. Middleton and D. J. Pullen, "A Study of Some (t, p) Reactions. Method and Results for ^{7}Li, ^{10}B and ^{11}B," Nucl. Phys. A **51**, 50–62 (1964).
16. J. H. Towle and B. E. F. Macefield, "A Study of ^{9}Be(^{3}He,n)^{11}C Reaction," Nucl. Phys. A **66**, 65–79 (1965).
17. M. C. Taylor and G. C. Phyllips, "A Study of the Reaction ^{9}Be(^{3}He,^{6}Li) ^{6}Li," Nucl. Phys. A **126**, 615–627 (1969).
18. J. Bang and S. A. Wollesen, "A Two-Step Process on Two-Particle Transfer Reactions," Phys. Lett. D **33**, 395–399 (1970).
19. N. B. de Tacassy, "On the Contribution from a Two-Step Mechanism, Involving the Sequential Transfer of Two Neutrons, to the Calculation of (t, p) Reaction Cross Sections," Nucl. Phys. A **231**, 243–256 (1974).
20. N. Hashimoto and M. Kawai, "The (*p-d-t*) Process in Strong (*p*, *t*) Transitions," Phys. Lett. B **59**, 243–256 (1975).
21. R. L. Jaffe and W. J. Gerace, "Formfactors for Two-Nucleon Transfer Reactions," Nucl. Phys. A **125**, 1–27 (1969).
22. B. F. Bayman and A. Kallio, "Relative-Angular-Momentum-Zero Part of Two-Nucleon Wave Functions," Phys. Rev. **156**, 1121–1128 (1967).
23. P. J. Iano and W. T. Pinkston, "Aspects of Two-Nucleon Transfer Reactions," Nucl. Phys. A **237**, 189–214 (1975).
24. J. Bang and F. A. Gareev, "Wave Functions and Particle Transfer Formfactors of ^{42}Ca and ^{18}O," Nucl. Phys. A **232**, 45–57 (1974).
25. N. Austern, *Direct Nuclear Reaction Theories* (Wiley-Intersci., New York, 1970)).
26. W. R. Coker, T. Udagava, and H. H. Wolter, "Coupled-Reaction-Channels Study of (h, p) Reactions," Phys. Rev. C **7**, 1154–1165 (1973).
27. R. O. Nelson and N. R. Robertson, "The Evidence of Two-Step Process in the Spherical-Nuclei-Reactions," Phys. Lett. B **43**, 389–393 (1973).
28. R. H. Ibarra, "Nuclear Overlaps in Two-Particle Transfer Reactions," Nucl. Phys. A **211**, 317–322 (1973).
29. R. H. Ibarra, M. Vallieres, and D. H. Fang, "Extended Basis Shell-Model Study of Two-Nucleon Transfer Reactions," Nucl. Phys. A **256**, 21–26 (1976).
30. N. S. Zelenskaya and I. B. Teplov, *Properties of Excited Nuclear States and Angular Correlations in Nuclear Reactions* (Energoatomizdat, Moscow, 1995) [in Russian].
31. L. I. Galanina and N. S. Zelenskaya, "Delayed Mechanism Accounting in Direct Nuclear Reactions on Nuclei of 1p-Shell," Izv. Akad. Nauk, Ser. Fiz. **64**, 496–499 (2000).
32. S. Sunakawa, *Quantum Scattering Theory* (Iwanami Shote, Tokyo, Japan, 1977; Mir, Moscow, 1979).
33. T. L. Belyaeva, P. N. Zaikin, N. S. Zelenskaya, A. M. Sokolov, and I. B. Teplov, *OLYMP Calculation Program for Reaction Cross-Sections with Complex Particles by the Distorted-Wave Method with Finite Interaction Radius* (Mosk. Gos. Univ., Moscow, 1981) [in Russian].
34. A. G. Sitenko, *Theory of Nuclear Reactions* (Energoatomizdat, Moscow, 1983) [in Russian].
35. A. N. Boyarkina, *Structure of ^{1}p-Shell Nuclei* (Mosk. Gos. Univ., Moscow, 1973) [in Russian].
36. L. I. Galanina and N. S. Zelenskaya, "Manifestations of a Dineutron Cluster in Elastic α^6He Scattering," Phys. At. Nucl. **65**, 1282 (2002).
37. R. Raabe, L. I. Galanina, N. S. Zelenskaya, et al., "2n-Transfer Contribution in the ^{4}He(^{6}He, ^{6}He)^{4}He Cross Section at $E_{c.m.} = 11.6$ MeV," Phys. Rev. C **67**, 044602 (2003).
38. L. I. Galanina and N. S. Zelenskaya, "Mechanism of Independent Neutron Transfer in Elastic α^6He Scattering and Structure of the ^{6}He Nuclear Wave Function," Phys. At. Nucl. **70**, 283 (2007).
39. R. Raabe, A. Piechaczek, A. Andreev, et al., "Elastic 2n-Transfer in the ^{4}He(^{6}He,^{6}He)^{4}He Scattering," Phys. Lett. B **458**, 1–7 (1999).
40. Yu. A. Penionzhkevich, "Nuclear Astrophysics," Phys. At. Nucl. **73**, 1460 (2010).
41. M. Blann and M. B. Chadwick, "New Precompound Model: Angular Distributions," Phys. Rev. C **57**, 233–243 (1998).
42. A. J. Koning and J. P. Delaroche, "Global Potential," Nucl. Phys. A **713**, 231 (2003).
43. M. Herman, www.nds.iaea.org/empire/.
44. V. M. Lebedev, N. V. Orlova, and A. V. Spasskii, "Multistep Processes in ^{9}Be(d, pγ)^{10}Be Reaction at E_d = 12.5 MeV," Phys. At. Nucl. **61**, 1493 (1998).
45. N. S. Zelenskaya et al., "Correlation Features of the Reaction ^{9}Be(d, pγ)^{10}Be at $E_d = 15.3$ MeV and Structure of the ^{10}Be Nucleus," Phys. At. Nucl. **64**, 1909 (2001).
46. L. I. Galanina et al., "Investigation of the ^{10}B(d, pγ)^{11}B Reaction Mechanism at $E_d = 15.3$ MeV by the Method of Angular pγ Correlations," Phys. At. Nucl. **68**, 1957 (2005).
47. P. D. Kunz, http://spot.colorado.edu/~kunz/ Home.html.
48. F. Ajsenberg-Selove, E. R. Flynn, and O. Hansen, "(t, p) Reaction on ^{4}He, ^{6}Li, ^{7}Li, ^{9}Be, ^{10}B, ^{11}B and ^{12}C," Phys. Rev. C **17**, 516–521 (1978).

49. L. I. Galanina and N. S. Zelenskaya, "The Role of Various Mechanisms in the Formation of the ^{12}B Nucleus in the ^{10}B(t, p)^{12}B Reaction," Izv. Akad. Nauk SSSR, Ser. Fiz. **72**, 331–335 (2008).

50. A. A. Korsheninnikov, "Analysis of Three-Particle Decay Properties of Nuclei with $A = 12$ and 16 in K-Harmonics Method," Sov. J. Nucl. Phys. **52**, 827 (1990).

51. A. A. Korcheninnikov and T. Kobayashi, "Main Mechanisms in Fragmentation of Exotic Nucleus," Nucl. Phys. A **567**, 97–110 (1994).

52. A. A. Korcheninnikov, D. Yochida, D. A. Aleksandrov, et al., "Spectroscopy of ^{12}Be and ^{13}Be Using a ^{12}Be Radioactive Beam," Phys. Lett. B **343**, 53–58 (1995).

53. A. A. Korcheninnikov, E. Yu. Nikolskii, T. Kobayashi, et al., "Spectroscopy of the Halo Nucleus ^{11}Li by Experimental Study of ^{11}Li + p Collisions," Phys. Rev. C **53**, 537–550 (1996).

54. M. G. Gornov, Yu. B. Gurov, and V. A. Pechkurov, "Excited States of ^{11}Li," Phys. Rev. Lett. **81**, 4325–4328 (1998).

55. Yu. B. Gurov, S. V. Lapushkin, B. A. Chernyshov, and V. G. Sandunovskii, "Search for Superheavy Hydrogen Isotopes in Pion Absorption Reactions," Phys. Part. Nucl. **40**, 558 (2009).

56. Yu. B. Gurov et al., "Spectroscopy of the ^{10}Li Isotope in Stopped Pion Absorption Reactions on a ^{14}C Radioactive Target," Izv. Akad. Nauk, Ser. Fiz. **75**, 495–498 (2011).

57. A. A. Korsheninnikov, "Nuclear Exotics near and above the Stability Boundary," Doctoral Dissertation in Physics and Mathematics (Moscow, 1996).

58. V. I. Kukulin, V. M. Krasnopol'sky, V. T. Voronchev and P. V. Sazonov, "Detailed Study of the Cluster Structure of Light Nuclei in Three-Body Problem. (II). The Spectrum of Low-Lying States of Nuclei with A = 6," Nucl. Phys. A **453**, 365–388 (1986).

59. B. V. Danilin and M. V. Zhukov, "Resonance $3\to3^-$ Scattering and Structure of the Excited States of A = 6 Nuclei," Phys. At. Nucl. **56**, 460 (1993).

60. S. N. Ershov and B. V. Danilin, "Breakup Reactions of Two-Neutron-Halo Nuclei," Phys. Part. Nucl. **39**, 835 (2008).

61. S. N. Ershov and B. V. Danilin, "Excitation of Two-Neutron-Halo Nuclei in a Continuum," Phys. At. Nucl. **72**, 1704 (2009).

62. E. T. Ibraeva, M. A. Zhusupov, and O. Imambekov, "Structure of Light Neutron-Rich Nuclei and Mechanism of Elastic Proton Scattering," Phys. At. Nucl. **74**, 1595 (2011).

63. V. P. Zavarzina, E. S. Konobeevskii, and A. V. Stepanov, "The Role of Configurations of Neutron Halo in the Formation of the Model Vertex Function for Description of the Two-Neutron Transfer Reaction," Izv. Akad. Nauk, Ser. Fiz., No. 3, 845–856 (2008).

64. G. E. Belovitskii et al., "Quasifree Proton Scattering on Halo Nuclei as a Tool for Studying the Neutron-Halo Structure," Phys. At. Nucl. **72**, 1714 (2009).

65. L. I. Galanina and N. S. Zelenskaya, "Neutron Periphery in Light Nuclei," Phys. At. Nucl. **72**, 1695 (2009).

66. TsDFE. http://cdfe.sinp.msu.ru

67. G. M. Ter-Akopian, A. M. Rodin, A. S. Fomichev, et al., "Two-Neutron Exchange Observed in the ^{6}He+^{6}He Reaction Search for the "Di-Neutron" Configuration of ^{6}He," Phys. Lett. B **426**, 251–256 (1998).

68. Fergyusson

69. L. I. Galanina and N. S. Zelenskaya, "Statistical Tensors of Complex Systems," Izv. Akad. Nauk, Ser. Fiz. **70**, 1627–1632 (2006).

70. L. S. Bidenharn and M. E. Rose, "Theory of Angular Correlation of Nuclear Radiations," Rev. Mod. Phys. **25**, 729–777 (1953).

71. K. Blum, *Density Matrix Theory and Applications (Physics of Atoms and Molecules)* (Springer, New York, 1996; Fizmatlit, Moscow, 1959).

72. L. I. Galanina and N. S. Zelenskaya, "Calculation of the Properties of Binary Nuclear Reactions with consideration of the Spin-Orbit Interaction," Izv. Akad. Nauk, Ser. Fiz. **64**, 954–959 (2000).

73. L. I. Galanina et al., "Investigation of the ^{13}C(d, α)^{11}B Reaction Mechanism at $E_d = 15.3$ MeV," Bull. Russ. Acad. Sci., Phys. **73**, 806–809 (2009).

74. L. I. Galanina et al., "Study of Orientation Characteristics of ^{11}B($5/2^-$, 4.445 MeV) Nucleus the in ^{13}C(d, $\alpha\gamma$)^{11}B Reaction at $E_d = 15.3$ MeV," Bull. Russ. Acad. Sci., Phys. **74**, 447 (2010).

75. W. Hauser and H. Feschbach, Phys. Rev. **87**, 336 (1952).

76. H. Feschbach and V. I. Weisskopf, Phys. Rev. **76**, 1550 (1949).

77. T. L. Belyaeva, N. S. Zelenskaya, and N. V. Odintsov, "Computation of Correlation Characteristics of Nuclear Reactions Induced by Semi-Heavy Ions," Comp. Phys. Commun. **73**, 161–169 (1992).

78. S. V. Perrey and F. G. Perrey, Atom. Data Nucl. Data Tables **17**, 1-1-1 (1976).

79. O. I. Vasil'eva et al., "Determination of the Spin-Tensor Components of Density Matrix for 4.43 MeV(2^+) State of ^{12}C Nucleus in (^{3}He, $\alpha\gamma$) Reaction," Izv. Akad. Nauk SSSR, Ser. Fiz. **48**, 1959–1964 (1984).

80. V. M. Lebedev, N. V. Orlova, and A. V. Spasskii, "Determination of the Deformation of the ^{12}C Nucleus from Angular Correlations in the ^{11}B(α, tγ)^{12}C and ^{13}C(^{3}He, $\alpha\gamma$)^{12}C Reactions," Phys. At. Nucl. **62**, 1455 (1999).

81. L. I. Galanina and N. S. Zelenskaya, "Role of Various Mechanisms in the Formation of a ^{12}C Nucleus in the ^{13}C(^{3}He, α)^{12}C Reaction," Phys. At. Nucl. **70**, 848 (2007).

82. N. S. Zelenskaya et al., "General Features of Multi-Nucleon Transfer Reaction on Nuclei of 1p Shell," Sov. J. Nucl. Phys. **6**, 47 (1967).

83. L. I. Galanina and N. S. Zelenskaya, "Simplified Method to Calculate Amplitudes of Delay-Involving Mechanisms," Izv. Akad. Nauk, Ser. Fiz. **69**, 1741–1745 (2005).